Molecular characterization of protein-dependent lipid transport during mitochondrial biogenesis

Dissertation

for the award of the degree
“Doctor rerum naturalium” (Dr. rer. nat.)
of the Georg-August-Universität Göttingen

within the doctoral program Biomolecules: Structure-Function-Dynamics
of the Georg-August University School of Science (GAUSS)

submitted by

Fereshteh Sadeqi

from
Kabul, Afghanistan

Göttingen, 2022

Members of the Thesis Advisory Committee

Prof. Dr. Michael Meinecke (first reviewer)
Heidelberg University Biochemistry Center, Germany

Prof. Dr.Andreas Janshoff (second reviewer)
Institute of Physical Chemistry, University of Göttingen

Prof. Dr. Silvio Rizzoli
Department of Neuro- and Sensory Physiology, University Medical Center, Göttingen

Further members of the Examination Board

Prof. Dr. Kai Tittmann
Department of Molecular Enzymology, University of Göttingen

Prof. Dr. Ralph Kehlenbach
Department of Molecular Biology, University Medical Center Göttingen

Dr. Alexander Stein
Membrane Protein Biochemistry, Max Planck Institute for Biophysical Chemistry, Göttingen

Date of oral examination: 28.03.2022

-to my mother and father-

-to my siblings-

Acknowledgements

First of all, I would like to thank my supervisor **Prof. Dr. Michael Meinecke** for giving me the opportunity to work on such an exciting project. Thank you for introducing me to so many collaborators and for always inspiring me to expand my scientific knowledge and skills. Most of all, I want to thank you for all of your support, for always encouraging me and especially for your great guidance.

Moreover, I am grateful to **Prof. Dr. Andreas Janshoff** and **Prof. Dr. Silvio Rizzoli** for being members of my thesis advisory committee. Thank you for your helpful suggestions and advices during the committee meetings. I would also like to thank Prof. Dr. Andreas Janshoff for his collaborative work on this project. I am also grateful to my extended committee members **Prof. Dr. Kai Tittmann, Dr. Alexander Stein, Prof. Dr. Ralph Kehlenbach**.

I would also like to thank:

- **Dr. Marian Vache** for providing RIfS Data and his valuable time and help.
- **Kai Stroh** for providing MD simulations and for many helpful discussions and **Prof. Herre Jelger Risselada** for all the suggestions and advices.
- **Prof. Dr. Ivo Feussner** and his group. Especially, **Sabine Freitag** for teaching me TLC and **Dr. Cornelia Herrfurth** for helping me with the quantification of the GC/FID data.
- **Dr. Dietmar Riedel** and **Gudrum Heim** for providing all TEM images.
- my colleagues and former members from the **Meinecke lab**. Special thanks to **Indrani Mukherjee, Mausumi Ghosh, Barbora Knotková** and **Tanja Gall** for all of your support, for being amazing lab mates and good friends.
- All members from the group of **Prof. Dr. Peter Rehling**, people from the **Entwicklungsbiologie** and members from the **group of Prof. Dr. Kai Tittmann**. Thank you all for creating a very pleasant working atmosphere.
- The **GGNB** and the **Biomolecules** program for your amazing support.

Last but not least, I am very grateful to **my family**. Thank you for your unlimited support, your unconditional love, your precious time and for always believing in me and all of my decisions.

Table of Contents

List of Figures

List of Tables

List of Abbreviations

%	Percentage
µL	Microliter
µm	Micrometer
µM	Micromolar
°C	Degree celsius
AGPAT	1-acyl-glycerol-3-phosphate acyltransferases
ALPS	Amphipathic Lipid Packing Sensor
APS	Ammonium persulfate
ATP	Adenosinetriphosphate
BAR	Bin/Amphysin/Rvs
BAR	Bennett Acceptance Ratio
BN-PAGE	Blue native polyacrylamide gel electrophoresis
BSA	Bovine serum albumin
cDNA	Complementary DNA
CDP-DAG	cytidine diphosphate-diacylglycerol
CJ	Cristae junctions
CL	Cardiolipin
CM	Cristae membranes
cm	Centimetre
DAG	diacylglycerol
DHAP	dihydroxyacetone phosphate
DNA	Desoxyribonucleic acid
Dnase I	Deoxyribonuclease I
dNTP	Desoxyribonucleoside triphosphate
ECL	Enhanced chemiluminescence
E. coil	Escherichia coli
EDTA	Ethylene diamine tetra acetic acid
ENTH	Epsin N-terminal homology
EM	Electron microscope or electron microscopy
ER	Endoplasmic reticulum
ERMES	ER-mitochondria encounter structure
EtBr	Ethidium Bromide

FRET	Förster (fluorescence) resonance energy transfer
g	Gram
G3P	glycerol-3-phosphate
Gep1	genetic interactor of prohibitin protein 1
GPAT	G3P acyltransferase
GTPase	Guanosin triphosphate hydrolase
GUV	Giant unilamellar vesicle
h	Hour
H_2O	Water
HCl	Hydrogenchloride
His	Histidine
His-Trap	Histidine affinity chromatography column
HRP	Horseradish peroxidase
IBM	Inner boundary membrane
IMM	Inner mitochondrial membrane
IMAC	Immobilised metal ion affinity chromatograhy
IMS	Intermembrane space
IPTG	Isopropyl β-D-1-thiogalactopyranoside
ITO	Indium tin oxide
KDa	Kilodalton
L	Litre
LB	Lysogeny broth
LPA	lyso-phosphatidic acid
LTP	lipid transfer protein
LUV	Large unilamellar vesicle
mA	Milliampere
mg	Milligram
MAMs	Mitochondrial associated ER membranes
MES	2-(N-morpholino)ethanesulfonic acid
Mgm1	Mitochondrial genome maintenance
Mdm35	mitochondrial distribution and morphology protein 35
MIA	Mitochondrial IMS import and assembly machinery
MICOS	Mitochondrial contact site and cristae organizing system

min	Minute
mL	Milliliter
mM	Millimolar
mm	Millimeter
mol	Mole
MLCL	monolysocardiolipin
NaCl	Sodiumchloride
ng	Nanogram
nM	Nanomolar
nm	Nanometer
OD	Optical density
OMM	Outer mitochondrial membrane
OPA1	Optic atrophy 1
PA	Phosphatidic acid
PBS	Phosphate-buffered saline
PC	Phosphatidylcholine
PCR	Polymerase chain reaction
PE	Phosphatidylethanolamine
PG	Phosphatidylglycerol
PGP	phosphatidylglycerol phosphate
PI	Phosphatidylinositol
PITP	phosphatidylinositol transfer proteins
PL	glycerophospholipids
PLD	phospholipase D
PMSF	Phenylmethylsulfonyl fluoride
POPA	1-palmitoyl-2-oleoyl-sn-glycero-3-phosphatidic acid
POPC	1-palmitoyl-2-oleoyl-sn-glycero-3-phosphocholine
POPE	1-palmitoyl-2-oleoyl-sn-glycero-3-phosphatidylethanolamine
PS	Phosphatidylserine
PVDF	Poly vinylidene difluoride membrane
Rhodamine PE	L-α-PE-N-(lissamine rhodamine B sulfonyl) (Ammonium Salt)

rpm	Rounds per minute
PRELI	protein of relevant evolutionary and lymphoid interest
PRELI1	protein of relevant evolutionary and lymphoid interest 1
PRELI2	protein of relevant evolutionary and lymphoid interest 2
SAM	Sorting and assembly machinery
S. cerevisiae (S.c)	Saccharomyces cerevisiae
SD	Standard deviation
SDS	Sodium dodecyl sulfate
SDS-PAGE	Sodium dodecyl sulfate polyacrylamide gel electrophoresis
sec	Second
SEM	Standard error of mean
SLMO1	slowmo homologue 1
SLMO2	slowmo homologue 2
SMP	synaptotagmin-like mitochondrial lipid-binding protein
StAR	stereoidogenic acute regulatory protein
START	(StAR)-related lipid transfer domain
TAE	Tris-acetate-EDTA buffer
TGA	triacylglycerols
TBS	Tris-buffered saline
TBS-T	Tris-buffered saline with Tween
TCA	Trichloroacetic acid
TEMED	Tetramethylethylenediamine
TIM	Translocase of the inner membrane
TOM	Translocase of the outer membrane
TRIAP1	TP53-regulated inhibitor of apoptosis 1
TULIP	tubular lipid-binding protein
U	Unit
Ups	unprocessed
Ups1	unprocessed 1
Ups2	unprocessed 2
V	Volt
w/w	Wet weight
xg	Times

Abstract

Mitochondria are comprised of two membranes, each with a unique lipid and protein composition, subdividing this organelle into the outer mitochondrial membrane (OMM), the intermembrane space (IMS), the inner mitochondrial membrane (IMM) and the mitochondrial matrix. The building blocks of membranes are phospholipids which are mainly synthesized in the endoplasmic reticulum (ER). Besides the ER, mitochondria also harbour enzymes residing in the IMM converting ER-derived precursors into phosphatidyl-ethanolamine (PE) or the mitochondrial signature lipid cardiolipin (CL). In contrast to the endomembrane system, phospholipid trafficking in mitochondria is not connected by vesicular transport. Hence, other lipid transfer mechanisms are required to maintain the mitochondrial membrane structure and integrity. Recently, the lipid transfer protein (LTP) Ups1/Mdm35 was found in the mitochondrial IMS of yeast. This soluble heterodimeric protein complex shuttles phosphatidic acid (PA) from the OMM to the IMM for CL synthesis. Though, the structure and binding specificities of the Ups1/Mdm35 complex were extensively investigated, little is known about its complete molecular mechanism.

In this study, we used a combination of *in vitro* and *in silico* approaches to further investigate the molecular mechanism of the LTP Ups1/Mdm35. We discovered that the Ups1/Mdm35 complex displays curvature inducing abilities by deforming artificial membrane vesicles into tubulated structures *in vitro*. Besides that, we unravelled an unexpected role of the Ups1/Mdm35 complex to act as a membrane curvature sensor. Our findings demonstrate that the membrane curvature inducing and sensing ability of the Ups1/Mdm35 complex are key to the extraction of lipids from membranes under low energy costs. Moreover, we found that the Ups1/Mdm35 complex tethers membranes of artificial vesicles into clusters while being enriched at membrane contact sites *in vitro*. Lastly, we showed oligomerization of the Ups1/Mdm35 complex in this study.

1 Introduction

1.1 Membrane compartmentalization in eukaryotic cells

Eukaryotic cells are characterized by a high degree of compartmentalization leading to several membrane enveloped organelles. Each of these compartments comprises of a specific lipid and protein composition which is of great morphological and functional relevance. Membranes enclosing these organelles provide a barrier that is vital to create different reaction rooms so that several processes can take place simultaneously and independently from each other (Figure 1.1).

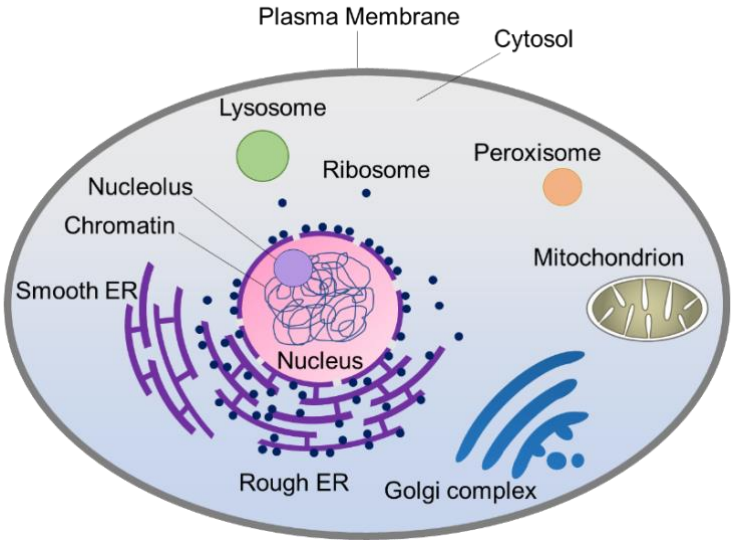

Figure 1.1 Membrane compartmentalization in the eukaryotic cell.

The eukaryotic cell is highly compartmentalized which creates several membrane enveloped organelles. Each organelle has its specific lipid and protein composition while the regulated supply of these lipids and proteins is crucial to maintain the structure and integrity of eukaryotic cells. Some of these complex structures are illustrated.

In cellular membranes, lipids represent the main component of a bilayer that serves as a permeability barrier for cells and organelles. Further, lipid membranes act as a matrix for proteins that are involved in a variety of cell processes like ATP synthesis or signal transduction (Dowhan, 1997). Glycerophospholipids like phosphatidylcholine (PC), phosphatidylethanolamine (PE), phosphatidic acid (PA) and phosphatidylserine (PS) are the major building blocks in eukaryotic cell membranes which are composed of a hydrophilic headgroup and a hydrophobic portion containing diacylglycerol (DAG). PC represent the most abundant

phospholipid in eukaryotic membranes making up more than 50% of total lipid content (Gerrit Van Meer et al., 2008).

The endoplasmic reticulum (ER) is considered as a major organelle responsible for the biosynthesis of lipids (Bishop & Bell, 1988). Besides the synthesis of phospholipids, the ER also produces the majority of cholesterol (in mammals) and ergosterol (in yeast). From the ER, lipids have to be supplied to other organelles which are devoid of enzymes for their synthesis (Gerrit Van Meer et al., 2008). The involvement of specific carrier proteins, membrane contact sites or vesicular trafficking pathways are crucial for the distribution of lipids (Flis & Daum, 2013). Hence, a regulated and well-organized lipid transfer is of upmost importance to maintain the membrane structure and integrity of each organelle in eukaryotic cells.

1.2 Mitochondrial architecture and membrane composition

Mitochondria, the powerhouse of the cell, are sub-compartmentalized by two membranes dividing this organelle into the outer membrane of mitochondria (OMM) and the inner membrane of mitochondria (IMM) as well as the two aqueous sub-compartments, the intermembrane space (IMS) and the mitochondrial matrix. The outer membrane is flat while the inner membrane is highly folded forming cristae structures (Figure 1.2).

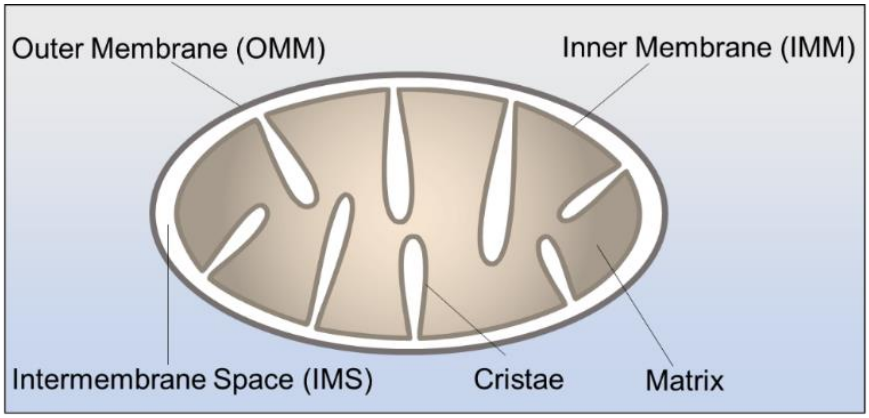

Figure 1.2: Schematic illustration of mitochondrial ultra-structure.

A mitochondrion consists of two membranes dividing the organelle into the following sub-compartments: the outer membrane of mitochondria (OMM), the inner membrane of mitochondria (IMM), the intermembrane space (IMS) and the matrix.

Each of the mitochondrial membranes comprises of a specific and characteristic lipid, protein and enzyme composition to maintain membrane integrity and proper cellular function (Horvath & Daum, 2013; Hovius et al., 1990; Zinser & Daum, 1995). Mitochondria do not carry all enzymes to synthesize their complete lipid repertoire, thus depending largely on lipid import from other organelles (Daum & Vance, 1997). The majority of mitochondrial lipids and its precursors are synthesized in the ER. From there, lipids are first supplied to the OMM and then further transferred through the IMS to the IMM by different transport mechanisms that require the involvement of close membrane contact sites or lipid transfer proteins rather than vesicular transport(Flis & Daum, 2013; Osman et al., 2011; Tatsuta et al., 2014). Especially, lipids like PS, PI and PC have to be imported into mitochondria. Nevertheless, mitochondria also harbour enzymes involved in the biogenesis of phospholipids like PG, PE, PA and the mitochondrial signature lipid cardiolipin (CL) (Daum, 1985; Flis & Daum, 2013; Horvath & Daum, 2013; Zinser et al., 1991).

PC and PE represent the bulk of phospholipids found in mitochondria. In addition, the concentration of CL is relatively high in mitochondria, while sterols and sphingolipids are only present at very low concentrations (Daum & Vance, 1997; Horvath & Daum, 2013; Zinser & Daum, 1995). Another specific characteristic of mitochondria is a high degree of lipid asymmetry between its two membranes. While the relatively flat OMM is composed of 44-59% PC, 20-35% PE, 5-20% PI and low amounts of PS and PA, the IMM contains 38-45% PC, 32-39% PE, 2-7% PI and 14-23% CL. The presence and the high content of the non-bilayer lipids PE and CL in the IMM is consistent with its highly curved morphology compared to the OMM (Tarasenko & Meinecke, 2021; Gerrit Van Meer et al., 2008).

1.3 Biosynthesis of PA, PG and CL in yeast

1.3.1 Synthesis of PA in yeast

PA plays a key role as a central precursor in the biosynthesis of glycerophospholipids and triacylglycerols (TGA) in eukaryotic cells. In yeast there are two different acylation pathways for the *de novo* synthesis of PA known, which are called the glycerol-3-phosphate (G3P) and dihydroxyacetone phosphate (DHAP) pathway. In the first pathway, the enzyme G3P acyltransferase (GPAT) catalyses the acylation of G3P to 1-acylglycerol-3-phosphate (lyso-phosphatidic acid or LPA) while the acylation in the second pathway is promoted by a DHAP acyltransferase (DHAPAT) resulting in the formation of 1-acyl-DHAP (Athenstaedt, 2021; Athenstaedt et al., 1999; Athenstaedt & Daum, 1999; Racenis et al., 1992). *Saccharomyces cerevisiae* has two enzymes with overlapping functions called Sct1 and Gpt2 that mediate the acylation in both pathways (Athenstaedt, 2021; Zheng & Zou, 2001). In an NADPH-dependent manner, 1-acyl-DHAP is reduced to LPA by a 1-acyl dihydroxyacetone phosphate reductase which is called Ayr1 in yeast (Athenstaedt & Daum, 2000). Finally, another enzyme 1-acyl-glycerol-3-phosphate acyltransferases (AGPAT) converts lyso-PA to PA. In yeast two AGPAT enzymes are known which are termed Slc1 (Nagiec et al., 1993) and Ale1 (Benghezal et al., 2007; Chen et al., 2007; Jain et al., 2007; Riekhof et al., 2007; Tamaki et al., 2007). Besides the *de novo* pathway other alternative pathways exist to obtain PA in yeast including a hydrolysis of glycerophospholipids (PL) by a phospholipase D (PLD) or by phosphorylation of diacylglycerol (DAG) mediated by a diacylglycerol kinase (Athenstaedt, 2021).

1.3.2 Synthesis of PG and the mitochondrial signature lipid CL in yeast

Cardiolipin (CL; diphosphatidylglycerol) is a unique phospholipid dimer which contains four acyl chains and two PA headgroups linked to glycerol. Further, CL carries two negative charges and due to its form and shape it is a non-bilayer forming lipid (Schlame, 2008; Schlame et al., 2000). CL was fist isolated and purified from beef heart by Pangborn in 1945 which explains its name (Pangborn, 1942). Further, CL is a signature lipid in the IMM of eukaryotes including yeast (Schlame et al., 1993, 2000). However, small fractions of CL were also found in

the OMM playing a role in the biogenesis of OMM proteins (Gebert et al., 2009). Besides the OMM, the peroxisomal membranes also contain small amounts of CL (Zinser et al., 1991). The synthesis of CL is restricted to mitochondria and takes place via an enzyme cascade on the matrix site of the IMM (Schlame & Haldar, 1993; Schlame & Ren, 2009). Initially, the biosynthesis of CL was thought to begin with the conversion of PA to CDP-DAG (cytidine diphosphate-diacylglycerol) mediated by the CDP-DAG synthase Cds1 in yeast (H. Shen et al., 1996) while the localization of CDP-DAG synthase was shown in the ER and mitochondria (Kuchler et al., 1986). However, later a new protein was found in yeast, termed Tam41, which turned out to be the actual CDP-DAG synthase in mitochondria that catalyses the first step in the formation of CDP-DAG from PA in a CTP-dependent manner. Tam41 resides in the IMM and is facing the matrix (Kutik et al., 2008; Tamura et al., 2006, 2013). The authors reported that yeast has two CDP-DAG synthases where Cds1 resides exclusively in the ER, while Tam41 is the one being involved in the first step of CL biosynthesis in mitochondria (Tamura et al., 2013). The second step in the synthesis of CL is the conversion of CDP-DAG and G3P to phosphatidylglycerol phosphate (PGP) mediated by a PGP synthase Pgs1 (Chang, et al., 1998a). In the next step, PGP is dephosphorylated to phosphatidylglycerol (PG) mediated by an enzyme named PGP phosphatase Gep4 (Osman et al., 2010). The final step in the CL biosynthesis cascade is catalysed by a cardiolipin synthase Crd1 that converts PG and CDP-DAG to CL (Chang, et al., 1998b; Jiang et al., 1997; Michael Schlame & Greenberg, 2017; Tuller et al., 1998).

Remodelling of the acyl chains is the next processing stage leading to a maturation of CL which is performed in two steps. First, CL undergoes a deacylation by the phospholipase Cld1 resulting in the formation of monolysocardiolipin (MLCL) (Beranek et al., 2009). Second, MLCL is reacylated by the acyltransferase Taz1 which completes the synthesis of CL in yeast (Gu et al., 2004; Z. Shen et al., 2015).

1.4 Phospholipid trafficking between ER and Mitochondria in yeast

The ER is considered as the major organelle harbouring enzymes for lipid biosynthesis (Bishop & Bell, 1988). Organelles such as the ER, the plasma membrane, lysosomes, endosomes and the Golgi apparatus are all part of the endomembrane system which is connected by vesicular transport. Via this trafficking, ER-derived phospholipids are delivered to the respective destination in these compartments (Palade, 1975; Stenmark, 2009; Tamura et al., 2014; Whyte & Munro, 2002). In contrast, mitochondria are not part of the endomembrane system. Thus, a different non-vesicular transport route for lipids between ER and mitochondria has to exist in the cell. Since spontaneous lipid exchange between two membranes through an aqueous compartment is a very slow process, close membrane contact sites between ER and mitochondria may provide one advantageous opportunity to facilitate lipid trafficking (Lev, 2010; Tamura et al., 2014).

Consequently, it has been shown that a subfraction of the ER, which is termed mitochondria associated membranes (MAM), also contributes to the supply of phospholipids to mitochondrial membranes. MAM are specifically associated with mitochondria through a juxtaposition supporting phospholipid exchange between these organelles (Daum & Vance, 1997; Vance, 1990). One characteristic of MAM in mammals (Vance, 1990) and yeast (Gaigg et al., 1995) is that they show a high enrichment of certain lipids and enzymes for lipid biosynthesis.

Through a synthetic biological screen, Kornmann et al., discovered a tethering complex bridging ER and mitochondria in yeast that was termed the ER-mitochondria encounter structure (ERMES) which is involved in calcium and phospholipid exchange (Kornmann et al., 2009). ERMES is composed of the following five core subunits Mmm1 (an integral membrane protein of the ER), Mdm34 (a protein of OMM), Mdm10(a β-barrel protein in OMM), Mdm12 (a soluble cytosolic protein) and Gem1 (a mitochondrial rho-like GTPase) (Kornmann et al., 2009, 2011; Stroud et al., 2011). Further, Kornmann et al., found that a yeast strain lacking the mitochondrial phosphatidylserine decarboxylase Psd1 showed phenotypical similarities to mutants of the ERMES complex. The enzyme Psd1 is involved in the *de* novo biosynthesis pathway of amino-glycerophospholipids by

the decarboxylation of ER-derived PS to PE. PE is then transported back to the ER, where it can be used to synthesize PC. Similarities in the phenotypes of ERMES mutants to that of *psd1*Δ which showed phospholipid abnormalities and an impaired conversion of PS to PC, gave hints to the involvement of ERMES in lipid biosynthesis (Kornmann et al., 2009). Further, three of the ERMES proteins Mdm12, Mdm34 and Mmm1 possess a synaptotagmin-like mitochondrial lipid-binding protein (SMP) domain which is part of the tubular lipid-binding protein (TULIP) superfamily involved in lipid transfer, suggesting that the ERMES complex might also function in lipid exchange (Kopec et al., 2010). However, later Nguyen et al., reported contradicting findings which show that the ERMES complex and Gem1 might not be involved in the phospholipid transport of PS from the ER to mitochondria. Further, they found that the conversion of PS to PE was not affected in the absence of Gem1 or the other ERMES components. Hence, the authors suggest that the role of the ERMES complex is only restricted to a structural function in maintaining mitochondrial morphology (Nguyen et al., 2012). Due to these contradicting results, the lipid transfer ability of the ERMES complex was under debate. Nevertheless, binding of the SMP domains of Mdm12 and Mmm1 to phospholipids was indeed confirmed in several structural analyses (AhYoung et al., 2015; Jeong et al., 2016). Later, Kawano et al., showed in an *in vitro* assay that the hetero-oligomeric complex of Mdm12 and Mmm1 facilitates lipid transfer. Mutations in Mdm12 or Mmm1 led to a decrease in the lipid transfer activity of the Mdm12-Mmm1 complex and impaired the ER-derived PS transport to mitochondria (Kawano et al., 2018). Conclusively, the authors suggested that the ERMES complex is not only a physical membrane tether between ER and mitochondria but that it acts as a lipid transfer complex (Kawano et al., 2018).

1.5 Intramitochondrial trafficking of phospholipids in yeast

The inner membrane of mitochondria can be further subdivided into the inner boundary membrane (IBM) and invaginations towards the matrix termed cristae membranes (CM), both of which are connected by the so-called cristae junctions (Figure 1.3).

The relatively flat OMM and the highly folded IMM can form membrane contact sites (MCS) in mitochondria. These contact sites were first found via electron microscopy in mammals (Hackenbrock, 1968; Ohlendieck et al., 1986) and yeast (Pon et al., 1989). Early studies in mammals (Ardail et al., 1991) and yeast (Simbeni et al., 1991) showed that the MCSs are not only involved in protein import but also play an important role in phospholipid translocation. In yeast, Simbeni et al., found a phospholipid pattern at these MCSs that was different from the lipid content of the OMM and IMM. Here, the yeast contact sites contained reduced amounts of PI and PC compared to the levels found in the OMM and IMM (Simbeni et al., 1991). In contrast to that, the content of PE and CL were increased at these contact sites, illustrating that non-bilayer forming lipids might stabilize the formation of a hexagonal phase which could, in turn stabilize the structure of MCS. Besides that, the authors confirmed the involvement of these contact sites in the PS lipid transfer pathway (Simbeni et al., 1991). For mammals, similar results were obtained by Ardail et al., indicating that the translocation of PS to the IMM is connected to MCSs (Ardail et al., 1991).

Later, a multi-subunit protein complex was found in yeast that is localized at cristae junctions termed as mitochondrial contact sites and cristae organizing system (MICOS) which plays an important role in the maintenance of the mitochondrial morphology and architecture. The MICOS complex is conserved from yeast to humans. In yeast, the MICOS complex is composed of the membrane proteins Mic60, Mic10, Mic12, Mic19, Mic26 and Mic27 (Harner et al., 2011; Hoppins et al., 2011; Pfanner et al., 2014; von der Malsburg et al., 2011). Loss of MICOS components result in an altered and disrupted architecture of the IMM, characterized by a loss in cristae junctions and internal membrane stacks (Harner et al., 2011; Hoppins et al., 2011; John et al., 2005; Pfanner et al., 2014; Tarasenko & Meinecke, 2021; von der Malsburg et al., 2011). Remarkably, the importance of the MICOS complex is not only restricted to its function in maintaining the IMM morphology but also in its involvement in providing contact sites between the OMM and IMM through various interactions with proteins of the OMM (Pfanner et al., 2014). Another finding by Hoppins et al., show the genetical interaction of the MICOS complex with genes of the ERMES complex. Further, the authors found a negative genetical interaction of MICOS with the CL synthesis pathway, implicating a role of MICOS in phospholipid trafficking (Hoppins et al., 2011).

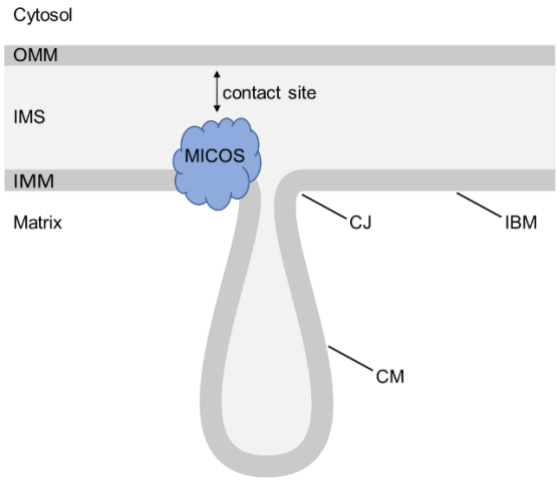

Figure 1.3: Contact sites between the outer and inner membrane of mitochondria.

Schematic illustration of mitochondrial subcompartments: the cytosol, OMM (outer mitochondrial membrane), IMS (inter membrane space), IMM (inner mitochondrial membrane) and the matrix. Further it shows the IBM (inner boundary membrane) the CJ (cristae junctions) with its CM (cristae membrane) and the MICOS complex. This architecture promotes the formation of contact sites (adapted from from Tarasenko and Meinecke, 2021 and Pfanner et al., 2014)

Since no intramitochondrial vesicular transport was detected so far, different transport mechanisms need to exist for lipid exchange. In general, the following three mechanisms are described for a non-vesicular transfer either within one or between two membranes: the monomeric lipid exchange, the lateral diffusion and the transbilayer flip-flop (Lev, 2010; Sleight, 1987; G. Van Meer, 1989). A monomeric lipid exchange represents the major mechanism in lipid transport through aqueous compartments. It can be either achieved by a spontaneous lipid transfer which is thought to be a very slow process or via lipid transfer proteins (LTP) which accelerate this process. Another mechanism of lipid transport is characterized via the lateral diffusion in the lateral plane of the membrane. Lastly, a flip-flop, which is a transversal movement of lipids between two membrane leaflets, represents the third mechanism that is involved in non-vesicular lipid trafficking. The lipid flip-flop can either be spontaneous or mediated by energy-depended and independent flippases and translocases which help in the maintenance of the lipid asymmetry between two membrane bilayer leaflets (Holthuis & Levine, 2005; Lev, 2010). All three mechanisms involved in non-vesicular transport are illustrated in the following (Figure 1.4).

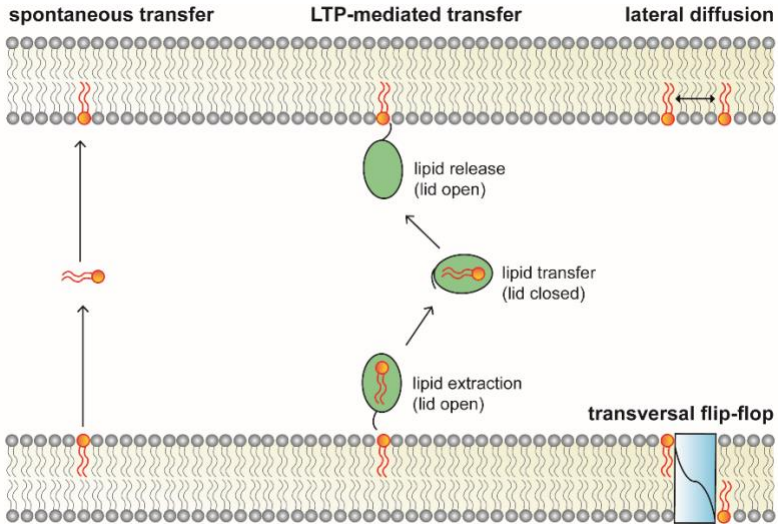

Figure 1.4: Mechanisms of non-vesicular lipid transport.

Non-vesicular transfer of lipids is basically characterized by the three following mechanisms: the monomeric lipid exchange, a lateral diffusion and the flip-flop. The monomeric transport of lipids can be subdivided into a spontaneous lipid transfer and transfer via lipid transfer proteins (LTPs). Lateral diffusion of lipids is restricted to a movement in the lateral plane of the membrane. Lipid transport via the flip-flop (transbilayer movement) mechanism takes place either spontaneously or with the help of flippases and translocase adapted from (Lev, 2010).

1.5 Mitochondrial lipid transfer proteins (LTP) in yeast

In eukaryotic cells, a variety of LTPs were found to transfer specific lipids such as sterols, phospholipids and sphingolipids (Lev, 2010). Initially, LTPs were found to shuttle lipids between membranes *in vitro* (Wirtz & Zilversmit, 1968). Later, the role of LTPs in intramitochondrial phospholipid trafficking gained more and more interest (Peretti et al., 2020). LTPs were considered to not only act as a carrier but also as a catalyst by accelerating the transfer of lipids through an increase of the desorption rate of lipids from a membrane (Lev, 2010). Recent *in vitro* studies revealed the Ups1/Mdm35 (Connerth et al., 2012) and Ups2/Mdm35 complex (Aaltonen et al., 2016) as a LTPs in the IMS of mitochondria in yeast. In the following chapter previous studies about the function and molecular mechanism of these mitochondrial LTPs will be presented.

1.5.1 The UPS-PRELI family

Previously, conserved proteins from the yeast *S.cerevisiae* Ups (unprocessed) and mammalian PRELI (protein of relevant evolutionary and lymphoid interest) family

were found in the IMS of mitochondria playing an important role in intramitochondrial phospholipid trafficking. Proteins of the conserved Ups1/PRELI family contain a PRELI/MSF1p domain at the N-terminus which is of unknown function while the yeast Msf1p domain was suggested to play a role in mitochondrial sorting (Dee & Moffat, 2005; Nakai et al., 1993; Osman et al., 2011). So far, three homologous proteins Ups1, Ups2 and Ups3 were identified in yeast (Osman et al., 2009; Sesaki et al., 2006; Tamura et al., 2009; Tatsuta et al., 2014). In humans, four orthologous proteins were found, namely PRELI1 and PRELI2 (protein of relevant evolutionary and lymphoid interest 1 and 2) as well as SLMO1 and SLMO2 (slowmo homologue 1 and 2) (Dee & Moffat, 2005; Tatsuta et al., 2014).

Sesaki et al., were the first to identify Ups1 (unprocessed 1) as a 20 kD protein in the mitochondrial IMS of yeast. Ups1 was initially found to be involved in the sorting of the dynamin-related GTPase Mgm1p (homolog of OPA1 in human) which is a protein involved in mitochondrial fusion and morphology. Further, the authors found the human PRELI protein to fully restore the shape and growth defects in mitochondria of *ups1*∆ cells illustrating their conserved function (Sesaki et al., 2006).

Besides the role in Mgm1 processing, later studies by (Osman et al., 2009) showed Ups1 and its homologue Ups2 (or Gep1, genetic interactor of prohibitin protein 1) to genetically interact with prohibitins that are thought to form ring-like complexes in the IMM, suggested to function as protein and lipid scaffolds and maintaining mitochondrial cristae morphology and integrity (Osman et al., 2009). Interestingly, Ups1 and Ups2 were then identified as novel regulators in the mitochondrial phospholipid accumulation of CL and PE, respectively. Previous results showed that, *ups1*∆ cells were characterized by a decrease in mitochondrial CL levels while *ups2*∆ mitochondria had reduced PE levels. Surprisingly, an additional deletion of *UPS2* in *ups1*∆ cells restored CL levels whereas an overexpression of *UPS2* led to a decrease in the CL amount, illustrating the antagonistic role of these proteins in CL metabolism (Osman et al., 2009; Tamura et al., 2009). Additionally, the PE-precursor lipid PS was accumulated in *ups1*∆ cells (Tamura et al., 2009). Hereafter, Ups proteins turned to be increasingly investigated in terms of their structure, function and regulation in phospholipid import and transport.

Miyata et al., showed that a deletion of not only *UPS2* but also of the two enzymes *PSD1* and *CHO1*, which encode proteins involved in PE synthesis, could restore CL levels in *ups1*Δ cells (Miyata et al., 2017). According to the authors, low levels of PE in the cell induce an Ups1-independent pathway for CL accumulation in which the three IMM proteins of the FMM-dependent pathway (Fmp30, Mdm31 and Mdm32) are involved. Here, Fmp30 physically interacts with Mdm31 and Mdm32 (Miyata et al., 2017; Miyata & Kuge, 2018). The IMM protein Fmp30 was found to be important for mitochondrial morphology and acts in maintaining normal CL levels in yeast, when cells are lacking PE synthesis (Kuroda et al., 2011). Fmp30 from yeast is homologous to the mammalian *N*-acylethanolamine (NAPE)-specific phospholipase D which mediates the formation of NAPE to N-acylethanolamine and PA (Merkel et al., 2005).

1.5.2 The yeast Mdm35 protein forms a complex with Ups1 and Ups2 in the IMS

Since majority of mitochondrial proteins are synthesized on cytosolic ribosomes, their translocation into the mitochondrial compartments depends on regulated import systems. The so-called translocases of the inner and outer mitochondrial membrane (TIM22, TIM23 and TOM) fulfil the task of importing and sorting mitochondrial proteins by recognizing specific targeting signals and assisting these proteins to reach their destination in mitochondria (Chacinska et al., 2009; Endo & Yamano, 2009). The TOM complex is considered as the main mitochondrial entry gate. Precursor proteins containing pre-sequences are imported through the TOM and TIM23 complexes into mitochondria (Genge & Mokranjac, 2022). Whereas, TIM22 mediates the translocation of polytopic proteins into the IMM (Jensen & Dunn, 2002).

Proteins of the IMS are nuclear encoded and exclusively synthesized in the cytosol from where they are imported into mitochondria by different mechanisms. Some IMS proteins possess cleavable N-terminal bipartite pre-sequences, while the majority of IMS proteins are devoid of such a pre-sequence but carry characteristic cysteine motifs instead (Backes & Herrmann, 2017). These cysteine-containing IMS proteins are substrates of Mia40, an oxidoreductase, which can form disulfide

bonds with precursor proteins in the IMS to help in their folding and maturation (Backes & Herrmann, 2017; Chacinska et al., 2009).

The three homologous IMS proteins Ups1, Ups2 and Ups3 in yeast neither carry a bipartite pre-sequence nor a cysteine motif. Hence, the question arises how these proteins are imported into the IMS. In 2010, two groups made the interesting observation that Ups proteins form a heterodimeric complex with another small IMS protein called Mdm35 (mitochondrial distribution and morphology protein 35) (Potting et al., 2010; Tamura et al., 2010). Mdm35 is an approximately ~ 10 kDa yeast protein that was initially found to be involved in maintaining mitochondrial tubular network (Dimmer et al., 2002). Further, it is a member of the twin CX_9C protein family characterized by a helix-loop-helix fold containing four cysteine residues that form two disulfide bonds similar to Mia40 which also contains such a CX_9C motif (Gabriel et al., 2007; Herrmann & Riemer, 2012; Longen et al., 2009). Tamura et al., suggested that precursor Ups proteins are translocated into mitochondria through the TOM channel, guided by the two TOM receptors Tom20 and Tom22. The incoming Ups proteins are then trapped by the IMS protein Mdm35 which forms a complex with them. Mdm35 acts as a chaperone that drives the import of Ups proteins into mitochondria upon complex formation and their stabilization in the IMS. Further, the authors showed that a deletion of Mdm35 disrupted an efficient Ups1 import due to an arrest of these proteins at the TOM complex (Tamura et al., 2010).

Accordingly, Potting et al., obtained similar results for the intrinsically unstable Ups1 and Ups2 proteins which are only imported into and stable in the IMS when in complex with Mdm35. Only then these proteins are protected against degradation by the i-AAA protease Yme1 and in the case of Ups1 also by the metallopeptidase Atp23 (Potting et al., 2010).

Furthermore, both studies found that deletion of *MDM35* can indeed restore normal mitochondrial CL levels in *ups1*Δ (Potting et al., 2010; Tamura et al., 2010) while similar results were observed in previous studies for the additional deletion of *UPS2* (Osman et al., 2009; Tamura et al., 2009).

Later, the human homologue of Mdm35 termed TRIAP1 (TP53-regulated inhibitor of apoptosis 1) was found to form a complex with PRELI in the IMS protecting this protein against YME1L-mediated proteolysis (Potting et al., 2013).

1.5.3 The Ups1/Mdm35 complex is a PA-specific LTP in the IMS

For many years, the mechanism of the non-vesicular intramitochondrial phospholipid trafficking in eukaryotic cells remained unclear. The fact that the enzymes for the synthesis of PE or the mitochondrial signature lipid CL reside in the IMM, arises the question how these ER-derived lipids and precursors are transferred in between the two mitochondrial membranes through the aqueous IMS.

In 2012, (Connerth et al., 2012) were the first to report that the Ups1/Mdm35 complex in yeast is a PA-specific LTP complex that is involved in phospholipid trafficking for CL synthesis. The authors were able to show that the co-expressed and purified Ups1/Mdm35 complex facilitates the transfer of PA between liposomes (artificial membrane vesicles) *in vitro*. Although Ups1 was binding preferably to negatively charged lipids, the transfer activity of Ups1 was only efficient and highly selective for PA. In contrast to that, Mdm35 did not bind to any of these lipids in the *in vitro* assay but its complex formation with Ups1 was required to transfer PA (Connerth et al., 2012). Thus, the authors suggested the following scenario: Ups1 binds to PA in the membrane and after lipid uptake Mdm35 associates with Ups1 to form a transferable complex. Then Ups1 binds to the negatively charged lipids in the acceptor membrane, followed by a dissociation of Mdm35 and PA release into the membrane (Connerth et al., 2012). The following figure illustrates the PA-specific transfer of the LTP Ups1/Mdm35 from the OMM to the IMM through the IMS in yeast (Figure 1.5).

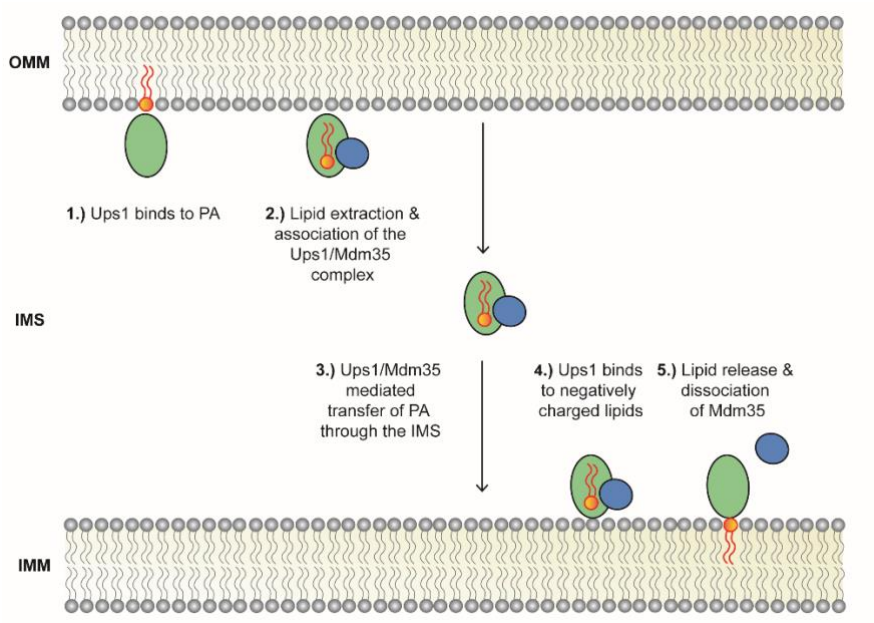

Figure 1.5: Ups1/Mdm35 mediated lipid transfer of PA in the IMS of yeast.

Schematic illustration of the Ups1/Mdm35 mediated transfer of PA through the IMS described by (Connerth et al., 2012). The Ups1 protein is shown in green. Mdm35 is shown in blue. The phospholipid PA is shown in orange.

Moreover, an accumulation of PA was observed at mitochondrial contact sites in Δ*ups1* mitochondria suggesting that PA transfer by Ups1/Mdm35 might also occur at these spots *in vivo*. Interestingly, high CL levels inhibited membrane dissociation of Ups1 from the IMM which led to a subsequent degradation of Ups1 followed by an inhibited PA transfer and disrupted CL synthesis. Hence, the Ups1/Mdm35 mediated phospholipid transfer of PA for CL synthesis was suggested to be feedback regulated (Connerth et al., 2012).

Later, (Potting et al., 2013) could obtain similar results for the human homologous complex PRELI/TRIAP1 which was found to facilitate the transfer of PA between liposomes *in vitro*. Accordingly, PRELI/TRIAP1 acts as an LTP shuttling PA through the IMS, thus, ensuring an accumulation of CL in the IMM. Interestingly, cells lacking TRIAP or PRELI1 were characterized by reduced CL levels resulting in a release of cytochrome c from mitochondria which caused an activation of apoptosis (Potting et al., 2013).

1.5.4 The Ups2/Mdm35 complex is a PS-specific LTP in the IMS

In 2016, two independent studies showed that the homologous Ups2/Mdm35 complex acts as an LTP in the IMS which transfers ER-derived PS from the OMM to the IMM for PE synthesis (Aaltonen et al., 2016; Miyata et al., 2016). Research by Aaltonen et al., suggested that mitochondrial PE synthesis which is mediated by the enzyme phosphatidylserine decarboxylase (Psd1), occurs via two pathways in yeast (Aaltonen et al., 2016). In the first pathway, the lipid transfer protein Ups2/Mmd35 is shuttling ER-derived PS through the IMS to reach the enzyme Psd1 located in the IMM, where it converts PS to PE. In a second pathway, a close juxtaposition of both mitochondrial membranes and the MICOS complex are required for the biosynthesis of PE by Psd1 which decarboxylases PS to PE in the OMM in trans. The second pathway is independent from the PS-specific Ups2/Mdm35 transfer (Aaltonen et al., 2016). Additionally, the authors found that defects in mitochondrial respiration and disturbed cristae morphology in MICOS deficient cells could be restored by a deletion of Ups2 which inhibits transfer of PS to the IMM and reduces PE accumulation. Apart from that, the expression of the human SLMO2 resulted in restored PE accumulation in mitochondria of Δ*ups2* cells *in vivo* while the SLMO2/TRIAP1 complex showed PS transfer activity *in vitro*. Hence, SLMO2 was suggested to be the human functional ortholog of Ups2 (Aaltonen et al., 2016).

Strikingly, it becomes evident that intramitochondrial phospholipid trafficking in yeast seems to be regulated by close MCSs and by the presence of LTPs in the IMS. In both cases, their involvement maintains phospholipid homeostasis, proper mitochondrial morphology and architecture. Nevertheless, how these two pathways are mechanistically linked to each other is still under debate.

1.5.5 Structural and mechanistical insight into the Ups1/Mdm35 LTP complex

To gain more insight into the mechanism of the mitochondrial yeast LTP complex, structural analysis was performed by two groups in 2015 revealing the X-ray crystal structure of Ups1/Mdm35 with and without PA in its binding pocket (Watanabe et al., 2015; Yu et al., 2015). In the same year, the crystal structure of the human homologue SLMO1/TRIAP1 was published and compared with Ups1 from yeast (Miliara et al., 2015). Without showing any significant sequence homology,

Ups1/Mdm35 was reported to share structural similarity to a fold that was found in the mammalian phosphatidylinositol transfer proteins (PITP) (K. W. A. Wirtz et al., 2006) and the steroidogenic acute regulatory protein (StAR)-related lipid transfer (START) domain (Miliara & Matthews, 2016; Soccio & Breslow, 2003; Watanabe et al., 2015).

The obtained X-ray structure of Ups1/Mdm35 revealed that Ups1 comprises of three α-helices (α1- α3) and a seven-stranded antiparallel β-sheet (β1-β7; forming a half-barrel structure) while Mdm35 comprises of three α-helices (α1- α3) (Watanabe et al., 2015; Yu et al., 2015). Mdm35 contains an α-hairpin motif connected by two disulfide bonds making it a member of the twin CX_9C protein family (Gabriel et al., 2007; Herrmann & Riemer, 2012; Longen et al., 2009; Watanabe et al., 2015; Yu et al., 2015). The structural analysis further showed that Ups1/Mdm35 is characterized by a deep lipid-binding pocket and a small α2 helix/loop (Ω-loop) (from Ups1) (Watanabe et al., 2015; Yu et al., 2015). The Ω-loop was reported to act as a flexible lid for the pocket similar to the loop that was found in PITP and the START domain. Deletion of this Ω-loop in Ups1 showed a drastic decrease in the lipid transfer activity for Ups1/Mdm35 *in vitro* supporting its important role in lipid transfer and acting as a gate for lipid uptake and release (Watanabe et al., 2015).

Studies by Miliara et al., 2005 support these finding by showing that a double mutation of hydrophobic amino acids to Alanine (L62A and W65A) in the Ω-loop of Ups1 led to a decrease in the lipid transfer activity of Ups1/Mdm35 *in vitro* (Miliara et al., 2015). The phospholipid PA was shown to bind into the pocket with its negatively charged phosphate head first which is stabilized by positively charged residues at the bottom while the acyl chains of the lipids are interacting with hydrophobic residues in the pocket (Watanabe et al., 2015). In previous studies a dissociation of Mdm35 from Ups1 was reported upon binding to liposomes *in vitro* (Connerth et al., 2012). Interestingly, it was confirmed that dissociation and association of Mdm35 from and with Ups1 are important for membrane binding and lipid transfer (Watanabe et al., 2015). The following figure (Figure 1.6) shows the structure of the PA-bound Ups1/Mdm35 complex by (Watanabe et al., 2015).

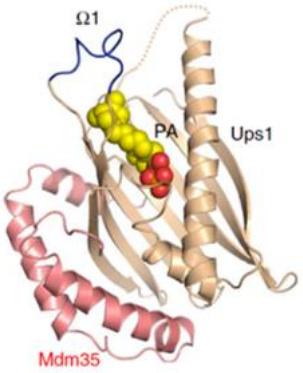

Figure 1.6: Schematic representation of the structure of a PA-loaded Ups1/Mdm35 LTP complex from yeast.

Schematic representation of the ribbon diagram for PA-bound Ups1/Mdm35. The figure is taken from (Watanabe et al., 2015).

Previous studies additionally showed that the asymmetric unit of the crystal was composed of two Ups1-Mdm35 molecules showing similar conformations while two Ups1 molecules were characterized by forming a domain-swapped dimer which was first believed to be a crystallization artefact (Watanabe et al., 2015).

Later, (Lu et al., 2020) expanded the structural and mechanistical insight into the Ups1/Mdm35 LTP complex via crystallographic analysis, molecular dynamics simulation and mutagenesis studies. Interestingly, it was reported that besides the α2-loop of Ups1, the L2-loop and the α3-helix are involved in membrane binding. In the α3-helix some positively charged residues interact with negatively charged lipids on the membrane. Hence, mutation of these positively charges residues to negatively charged Glu impairs the lipid transfer activity *in vitro*. Moreover, the authors suggest that the two hydrophobic residues W65 and F69 in the α2 loop (also referred to as α2 helix or Ω-loop) of Ups1 insert into the membrane undergoing conformational changes while their mutation impairs the lipid transfer activity *in vitro* (Lu et al., 2020).

1.6 Membrane curvature

In cells, membrane-bound organelles can form a variety of different shapes which are characterized by flat, positively (convex surface) or negatively curved (concave surface) regions (Antonny, 2011). Biological membranes constantly undergo regulated changes in their shape creating high curvature intermediates in form of vesicles or tubules which is of upmost importance for dynamic trafficking processes in the cell. Maintenance of the structure and morphology of these shapes requires specific mechanisms in which membrane curvature sensing and curvature inducing proteins are involved (McMahon & Gallop, 2005).

The lipid composition and their asymmetric distribution already defines the shape of a membrane, which can be explained by the packing parameter of an amphiphilic lipid. Basically, the packing parameter describes the molecular geometry of a lipid, taking the size of its headgroup as well as the volume and the length of the fatty acid chains into consideration (Israelachvili et al., 1977; Pomorski et al., 2014). Perturbation in the packing of lipids can cause lipid packing defects which are considered as regions in a bilayer showing low atomic density which occurs when a lipid doesn't fit with its shape into the curvature of a membrane (Antonny, 2011).

When the cross-sectional area of the hydrophilic lipid portion is larger than that of the hydrophobic portion, the lipid has an inverted conical shape and will preferably self-assemble into micelles with a positive curvature. Phospholipids like PC and PS are characterized by a cylindrical shape which shows a similar cross-section area of their head group and their acyl chains. These lipids are considered to self-assemble into a planar membrane bilayer (bilayer-forming lipids). In contrast to that, the cross-section areas of the hydrophilic head group of PE, CL and PA are smaller than that of the hydrophobic lipid portion, thus these lipids have a conical shape which will lead to negative curvature and the formation of a hexagonal phase (non-bilayer forming lipids) (Cullis et al., 1979; Flis & Daum, 2013; Van Den Brink-Van Der Laan et al., 2004). The insertion of conical shaped lipids into a planar bilayer will induce bilayer packing defects and curvature stress resulting in membrane bending (Van Den Brink-Van Der Laan et al., 2004). The geometry of a lipid also depends on the saturation of its acyl chains. Hence, the presence of unsaturated bonds can cause a kink in the hydrophobic portion of the lipid, inducing

packing defects and membrane curvature (McMahon & Boucrot, 2015; Pinot et al., 2014; Vanni et al., 2014).

Membrane deformation in the cell can be induced via different mechanisms that result in a positive or negative curvature of varying degrees (McMahon & Gallop, 2005). Some of these mechanisms are presented in the following.

One way to create membrane curvature is due to an asymmetry of the lipid composition in between both monolayers of a bilayer (Figure 1.7, A). As mentioned before, lipids already have an intrinsic shape given by their geometry which will shape the membrane of the monolayer accordingly. Consequently, the change in one monolayer can cause a change in the opposite monolayer and thus, the entire bilayer can be deformed because both membranes are still coupled (bilayer coupling hypothesis) (McMahon & Boucrot, 2015; McMahon & Gallop, 2005; Sheetz & Singer, 1974).

Another way of inducing membrane curvature can be obtained by the scaffolding ability of curved peripheral membrane proteins like those containing the so called, Bin/Amphiphysin/Rvs (BAR)-domain (Figure 1.7, B) (Jarsch et al., 2016; Peter et al., 2004; Tarasenko & Meinecke, 2021).

Membrane curvature can also be induced through the hydrophobic insertion of an amphipathic helix into one monolayer of the membrane resulting in a positive curvature. Further, a hydrophobic loop of a protein can be inserted into one leaflet of the bilayer acting like a wedge which will perturbate the packing of lipids inducing membrane curvature (Figure 1.7, C) (McMahon & Boucrot, 2015; McMahon & Gallop, 2005).

Further, partitioning of transmembrane proteins (Figure 1.7, D) that already have an intrinsic conical shape can induce asymmetry in the bilayer leading to curvature (Jarsch et al., 2016; McMahon & Boucrot, 2015). Furthermore, Clustering and oligomerization of transmembrane proteins can enhance membrane curvature induction. One example is the IMM protein Mic10 which is a core subunit of the MICOS complex. Homo-oligomerization of Mic10 promotes its membrane curvature inducing abilities (Barbot et al., 2015).

Lastly, the protein crowding mechanism (Figure 1.7, E) represents another way of inducing membrane curvature (Stachowiak et al., 2012), where membrane bending is mediated by highly concentrated proteins locally bound to a membrane. In this mechanism the protein collision leads to a lateral pressure which can result in

curvature induction (McMahon & Boucrot, 2015; Stachowiak et al., 2012; Tarasenko & Meinecke, 2021).

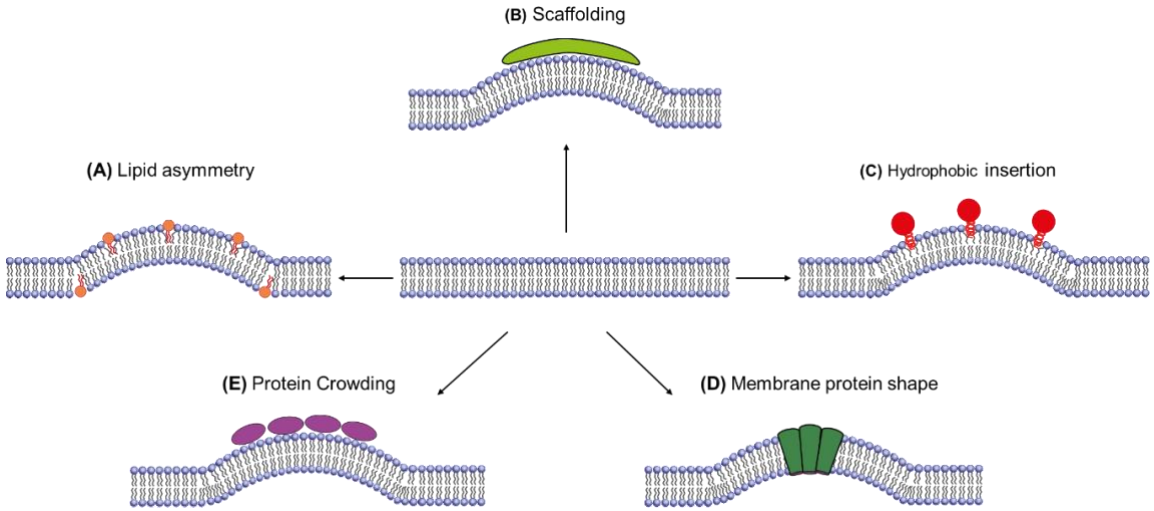

Figure 1.7: Schematic representation of different mechanisms of inducing membrane curvature.

Schematic representation of different mechanisms that can induce membrane bending induction resulting in a positive (convex) or negative (concave) curvature. Membrane curvature induction via (A) an asymmetry in the lipid composition of the bilayer, (B) scaffolding ability of curved peripheral membrane proteins, (C) the insertion of hydrophobic loops or amphipathic helices, (D) insertion of already shaped transmembrane proteins, (E) protein crowding. Adapted from (Chabanon et al., 2017; McMahon & Gallop, 2005; Tarasenko & Meinecke, 2021).

In recent years, the role of specific proteins involved in membrane curvature sensing besides membrane curvature induction has become increasingly important. Membrane curvature sensors are involved in a variety of cellular processes such as lipid transfer, membrane tethering and dynamics of protein coats (Antonny, 2011).

In principle, three classes of proteins are involved in membrane curvature sensing which were also found to induce membrane curvature. Hence, a clear-cut differentiation between curvature sensing and curvature induction is hard to define (Antonny, 2011; Baumgart et al., 2011). The first group is represented by the already mentioned BAR domain which is a crescent-shaped dimer that can induce and sense membrane curvature through its concave surface which has positively charged residues. These positively charged residues on its concave surface, promote curvature sensing and binding to positively curved convex membrane domains, containing negatively charged lipids (Peter et al., 2004). The second

group of proteins involved in membrane curvature induction through a scaffold mechanism is the dynamin protein family which also plays an important role in membrane curvature sensing (Roux et al., 2010). Lastly, proteins containing amphipathic helices do not only induce membrane curvature, as mentioned before, but also sense membrane domains with lipid packing defects. One example for these curvature sensors are proteins containing the so-called ALPS (Amphipathic Lipid Packing Sensor) motifs that can fold into an amphipathic helix (Antonny, 2011; Baumgart et al., 2011; Mesmin et al., 2007).

2 Aims of this study

Mitochondria are characterized by two functionally and morphologically distinct membranes that provide compartmentalization to these organelles. Recently, the Ups1/Mdm35 complex was found in the mitochondrial IMS of yeast acting as a PA-specific LTP, that maintains the synthesis and accumulation of the mitochondrial signature lipid CL in the IMM.

In previous studies, structure and function of Ups1/Mdm35 was revealed to show that the complex comprises of a lipid binding pocket as well as a hydrophobic Ω-loop that acts as a lid. This lid was further suggested to be of upmost importance for the membrane binding and lipid transfer activity of the Ups1/Mdm35 complex.

In this study, we aimed to further investigate the molecular mechanism of the Ups1/Mdm35 complex by addressing the question of how the Ups1/Mdm35 complex can decrease the energy barrier to accelerate the extraction of a lipid from a membrane for its transfer through the aqueous IMS compartment? We hypothesized that the hydrophobic Ω-loop in the Ups1/Mdm35 complex possesses curvature inducing and sensing abilities, that might help in the extraction of a lipid under low energy costs from a curved membrane region.

In order to unravel the molecular mechanism of the Ups1/Mdm35 complex, we aimed to perform a combined strategy of various *in vitro* assays using artificial model membranes and *in silico* approaches to investigate the membrane binding and membrane deformation properties of the Ups1/Mdm35 complex.

3 Material and Methods

3.1 Material

3.1.1 Chemicals and reagents

The standard chemicals and laboratory consumables used in this study were ordered from Sigma Aldrich (Taufkirchen, Germany), Sarstedt (Nürmbrecht, Germany), Carl Roth (Karlsruhe, Germany) while other specific chemicals and reagents as well as all commercial kits and lipids are listed in the tables below.

Table 3.1: List of chemical reagents and their supplier used in this study

Reagent	Supplier
Ampicillin	Carl Roth
Chloroform	Merk
Coomassie Briliant Blue R-250	Carl Roth
Dimethylformamide (DMF)	Sigma Aldrich
Desoxynucleotide triphosphate mix	5 PRIME
Enhanced chemiluminescence (ECL)	Thermo Scientific
Ethidiumbromide 0.07%	AppliChem
GeneRuler DNA Ladder 1kb	Thermo Scientific
Histodenz	Sigma Aldrich
Imidazole	Roth
Isopropyl-β-D-1-thiogalactopyranoside (IPTG)	Roth
Kanamycin sulfate	Roth
PageRuler Prestained Protein Ladder	Thermo Scientific
Phenylmethylsulfonyl fluoride (PMSF)	Sigma Aldrich
Phusion DNA Polymerase	Thermo Scientifc

Polyvinylidene difluoride (PVDF) transfer membrane	Maine Manufacturing LCC
Proteinase inhibitor pills (EDTA-free)	Roche
Spectra Multicolour Low Range Protein Ladder	Thermo Scientific
Trichloroacetic acid (TCA)	Carl Roth
Tween-20	Carl Roth
Uranyl acetate · 2 H_2O	SERVA Electrophoresis

Table 3.2: List of commercial kits used in this study

Commercial kit	Supplier
Wizard SV Gel and PCR Clean-Up	Promega
Wizard SV Mini-Prep	Promega

Table 3.3: List of lipids used in this study

Lipid	Supplier
Cardiolipin (CL)	Avanti Polar Lipids
L-α-Phosphatidylcholine (PC)	Avanti Polar Lipids
L-α-Phosphatidylethanolamine (PE)	Avanti Polar Lipids
L-α-Phosphatidylethanolamine-N-(lissamine rhodamine B sulphonyl) (Rhodamine PE)	Sigma Aldrich
L-α-Phosphatidylserine (PS)	Avanti Polar Lipids
L-α-Phosphatidic acid (PA)	Avanti Polar Lipids

3.1.2 Instruments and software

Table 3.4: List of instruments and specific devices used in this study

Instrument/device	Manufacturer
ÄKTA prime plus	GE Healthcare
Carbon-coated grids	Agar Scientific
CAWOMAT developing machine	CAWO Photochemisches Werk GmbH
Cell disruptor sonicator W-220F	Heatsystems Ultrasonics
(Centrifuge) 5415 R	Eppendorf
(Centrifuge) 5424	Eppendorf
(Centrifuge) 5810 R	Eppendorf
(Centrifuge) Optima MAX-XP	Beckman Coulter
(Centrifuge) Sorvall LYNX 4000	Thermo Scientific
(Centrifuge) Sorvall RC 6 Plus	Thermo Scientific
(Centrifuge) Optima L-90K Ultracentrifuge	Beckman Coulter
Desiccator	Vacuubrand
EmulsiFlex C5 homogeniser	Avestin
Filters PVDF	Roth
GUV generation chamber Nanion Vesicle Prep Pro	Nanion Technologies GmbH
Hamilton syringe	Avanti polar lipids
HisTrap FP 5ml	GE Healthcare
Horizontal electrophoresis system Sub-Cell GT cell	Bio-Rad
Incubator B-6120	Heraeus GmbH
Unitron incubator shaker	Infors HT

Intas gel documentation system	INTAS Science Imaging Instruments
LSM780 confocal microscope	Carl Zeiss Microscopy
Mini-extruder	Avanti Polar Lipids Inc.
Invitrogen Mini Gel Tank system	Thermo Scientific
Mini-PROTEAN Tetra Vertical Electrophoresis Cell	Bio-Rad
NanoDrop 2000	Thermo Fisher Scientific
PD MididTrap G-25	GE Healthcare
(Rotor) F12 6x500 LEX	Thermo Scientific
(Rotor) SS-34	Thermo Scientific
(Rotor) TLA 55	Beckman Coulter
(Rotor) TLA 100.3	Beckman Coulter
(Rotor) SW 60 Ti	Beckman Coulter
SpeedVac concentrator	Savant
Superdex 75 16/600 gel-filtration column	GE Healthcare
Thermomixer comfort	Eppendorf
TPersonal 48 thermocycler	Biometra
Talos L120C transmission electron microscope	Thermo Scientific

Table 3.5: List of software used in this study

Software	**Manufacturer**
Adobe Illustrator C26	Adobe Systems
Fiji (ImageJ)	Wayne Rasband
Microsoft office 2019	Microsoft Corporation
SnapGene Viewer Version 4.1.9	GLS Biotech

PyMOL Version 2.3.1	DeLano Scientific

3.1.3 Microorganisms

Table 3.6: List of E.coli strains used in this study

***E.coli* strain**	**Genotype**	**Supplier**
XL1 Blue	recA1 endA1 gyrA96 thi-1 hsdR17 supE44 relA1 lac [F´ proAB lacIqZM15 Tn10 (Tetr)]	Stratagene
Origami B(DE3)pLysS	F- ompT hsdSB(rB- mB-) gal dcm lacY1 ahpC (DE3) gor522:: Tn10 trxB pLysS (CamR, KanR, TetR)	Novagen

3.1.4 Plasmids

Table 3.7: List of plasmids used in this study

Name of the plasmid	**Vector backbone**	**Insert**	**Selection marker**	**Source**
MM208	pET-Duet1	empty	Amp	AG Rehling
MM354	pET-Duet1	Ups1 in MCS1	Amp	This study
MM355	pET-Duet1	Ups1 in MCS1 and Mdm35 in MCS2	Amp	This study
MM356	pET-Duet1	L62A in MCS1 and Mdm35 in MCS2	Amp	This study
MM357	pET-Duet1	L62AW65A in MCS1 and Mdm35 in MCS2	Amp	This study

MM358	pET-Duet1	A87C in MCS1 and Mdm35 in MCS2	Amp	This study

3.1.5 Oligomers

Table 3.8: List of oligomers used in this study

Oligomer/Primer	Sequence 5‘ – 3‘
MMP340F	ATGGGGAATATAATGTCAGCTAGTT
MMP340R	TCATTTGTCAACTTCTTTTAGTTTG
MMP358F	ATGGTCCTTTTACACAAAAGCACAC
MMP358R	TCAAAACTGAGGATTTCTCGCCTCT
MMP366F	GCGCGCGAATTCGATGGTCCTTTTACACAAAA
MMP366R	GCGCGCAAGCTTTCAAAACTGAGGATTTCTCG
MMP368F	GCGCGCCATATG GGGAATA TAATGTCAGC TAG
MMP368R	GCGCGCTTAATTAATCATTTGTCAACTTCTTT
MMP377F	GGGTTTGACAGCTGTGGGAGCCTTTCCGGA
MMP377R	AAAAAGTCCGGAAAGGCTCCCACAGCTGTCAAACCCTTTTTA
MMP378F	AAAAAGTCCGGAAAGGCTCCCACAGCTGTCAAACCCTTTTTA
MMP378R	TAAAAAGGGTTTGACAGCTGTGGGAGCCTTTCCGGACTTTTT
MMP383F	AAAAAGTCCGGAAAGGCTCCCACATGGGTCAAA
MMP383R	TTTGACCCATGTGGGAGCCTTTCCGGACTTTTT
MMP398F	TCCGTAGTGAACCCCTGTAACTCCACAATGAAA
MMP398R	TTTCATTGTGGAGTTACAGGGGTTCACTACGGA

3.1.6 Antibodies

Table 3.9: List of primary antibodies used in this study

Antigen	Antibody type	Recommended dilution	Manufacturer
Poly His tag	Mouse monoclonal	1:6000	Sigma-Aldrich

Table 3.10: List of secondary antibodies used in this study

Antigen	Antibody type	Recommended dilution	Manufacturer
Mouse	Goat	1:10000	Dianova

3.1.7 Enzymes

Table 3.11: List of enzymes used in this study

Enzymes	Supplier
DpnI	Thermo Scientific
EcoRI	Thermo Scientific
HindIII	Thermo Scientific
NdeI	Thermo Scientific
PacI	Thermo Scientific
Phusion High-Fidelity DNA Polymerase	Thermo Scientific
T4 DNA Ligase	Thermo Scientific
Q5 DNA Polymerase	NEB

3.1.8 Fluorophores

Table 3.12: List of fluorophores used in this study

Fluorophores	Company
Atto 488 maleimide	ATTO-TEC GmbH (Siegen, Germany)

3.2 Methods

3.2.1 Molecular cloning

3.2.1.1 Isolation of plasmid DNA from *E.coli* cells

A single colony of *E.coli* cells was transferred into 5 mL of LB medium and supplemented with the corresponding antibiotics (see section 3.2.2.1). The preculture was grown over night at 37°C and 220rpm. On the following day, the isolation of plasmid DNA from these *E.coli* cells was conducted with the Wizzard Plus SV Mini-prep DNA Purification System (Promega) following manufacturer's instructions.

3.2.1.2 Polymerase chain reaction (PCR)

Amplification of DNA fragments used in this study was obtained by polymerase chain reaction (PCR) from plasmid DNA or gDNA from yeast *Saccharomyces cerevisiae*. A 50 µL PCR reaction mix was prepared following the manufacturer's instructions

Table 3.13: PCR reaction mix

Component	50 µL reaction	final concentration
5X Q5 reaction buffer	10 µL	1X
10 mM dNTPs	1 µL	200 µM
10 µM forward primer	2.5 µL	0.5 µM
10 µM reverse primer	2.5 µL	0.5 µM
Template DNA	variable	< 1,000 ng
Q5 Hot Start High-Fidelity DNA Polymerase	0.5 µL	0.02 U/µL
Nuclease-free water	to 50 µL	

The following PCR program was used according to the manufacturer's instructions for the Q5 DNA Polymerase (NEB) depending on the template and primer properties.

Table 3.14: PCR Program

Step	Temperature	Time
Initial Denaturation	98°C	30 sec
25-35 cycles	98°C	5-10 sec
	NEB Tm Calculator	10-30 sec
	72°C	20-30 sec/kb
Final extension	72°C	20-30 sec/kb
Hold	4-10°C	∞

3.2.1.3 Agarose gel electrophoresis

The analysis of PCR products was performed by agarose gel electrophoresis. For preparation of agarose gels, 1% Agarose (Carl Roth) was dissolved in 1 × TAE buffer containing 40 mM Tris, 20 mM acetic acid and 1 mM EDTA. Additionally, 0.1% (V/V) ethidium bromide solution 250µg/ml (Carl Roth) was added for visualization of separated DNA. Next, 10X FastDigest Green Buffer (Thermo Fisher Scientific) was added to the DNA samples. After loading the samples into the gel, the electrophoresis was conducted at 105 V for ~ 30 min. Visualization of the gel was performed under UV light with an Intas gel documentation system (INTAS Science Imaging Instruments). When DNA samples were extracted from the agarose gel, a clean-up of these PCR products was performed with the Wizard SV Gel and PCR CleanUp System (Promega) following the manufacturer's protocols.

3.2.1.4 DNA Restriction Digestion

For cloning of a desired construct optimal restriction enzyme sites on a vector sequence were chosen. Then, the protein coding DNA fragment which was planned to be inserted into the vector carries the same restriction sites which were amplified via PCR. Then both, the vector and the protein coding DNA fragment, were digested using the desired restriction endonucleases (Thermo Fischer Scientific). The double digest was performed by following the manufacturer's instructions. Subsequently, the digested samples were separated via agarose gel electrophoresis (see section 3.2.1.3). After extraction of the DNA from the gel,

samples were purified using a Wizard SV Gel and PCR CleanUp System (Promega) according to the manufacturer's instructions.

3.2.1.5 DNA ligation

After restriction digestion and purification, ligation of the protein coding DNA fragments and the desired vector was performed using the T4 DNA Ligase enzyme (Thermo Fischer Scientific). For this purpose a 20 µL ligation reaction mix was prepared containing 1X T4 DNA Ligase buffer, 1.5 U of T4 DNA Ligase, 50 ng of the digested vector as well as the DNA inserts in a molar ratio of 1:3 (vector:insert). The ligation reaction was incubated at 4°C overnight or at 16°C for 18 h. On the following day, the ligation mix was transformed into XL1-blue cells (see section 3.2.2.2).

3.2.1.6 Site directed mutagenesis

In this study, the site directed mutagenesis was performed in order to introduce a single amino acid or a double point mutation into a desired DNA sequence. For this purpose, primer pairs were designed carrying a desired DNA base mutation in their centre by taking the desired plasmid as a template for PCR. For each site directed mutagenesis a 50 µL PCR reaction mix was prepared containing 1X Phusion HB buffer, 0.2 µM of each forward and reverse, 100 ng DNA template, primer, 0.2µM dNTP mix, 3% DMSO as well as 1 U Phusion DNA polymerase. The PCR program was set following the manufacturer's recommendations for the Phusion DNA polymerase (Thermofisher) and by taking the primers and the template condition and properties under consideration. After amplification, the PCR product was digested with 1 µL Dpn1 and then transformed into 50 µL *E.coli* XL1-blue cells (see section 3.2.2.2). Clones were picked for DNA isolation (see section 3.2.1.1) and verified (see section 3.2.1.7).

3.2.1.7 DNA sequencing

All of the DNA samples were sequenced by Microsynth Seqlab (Göttingen, Germany).

3.2.2 Cultivation and transformation of *E.coli* cells

3.2.2.1 Cultivation of bacterial *E.coli* cells

For a cultivation of bacterial cells, XL1-blue or Origami B(DE3)pLysS *E.coli* strains were grown in LB media (1% tryptone,1% NaCl, 0.5% yeast extract). Cells were supplemented with 100 mg/L of ampicillin while the Origami cells were additionally supplemented with the following antibiotic selection markers 34 mg/mL chloramphenicol, 50 mg/mL kanamycin, 10 mg/mL tetracycline. The cell cultures were grown in baffled glass flasks and incubated at 37°C, and 220 rpm.
For growing bacterial cells in petri dishes, solid media was supplemented with agar-agar (15 g/L) and the respective antibiotics.

3.2.2.2 Transformation of chemically competent *E.coli* cells

For a single transformation 50 µL chemically competent XL1-blue or Origami B(DE3)pLysS *E.coli* strains were used by addition of ~ 100 ng of the purified plasmid DNA. The cells were gently mixed and the suspension was incubated on ice for 10 min followed by a quick heat-shock at 42°C for 45 sec. To recover the cells after the heat-shock, the bacterial cells were incubated on ice (~2 min). Then 300 µL of pre-warmed LB media was added and the cells were incubated for 1 h at 37°C, and 220 rpm. Lastly, the bacterial culture was plated on LB-agar plates which contained the corresponding antibiotic selection markers. Lastly, the plates were incubated overnight at 37°C.

3.2.2.3 Preparation of bacterial *E.coli* whole cell lysate

In order to analyse the efficiency and success of recombinantly over-expressed protein levels in Origami B(DE3)pLysS *E.coli* cells, a test expression was performed for each construct under different time and temperature conditions. For this purpose, 80 mL of a culture of Origami B(DE3)pLysS cells containing the plasmid with a gene of interest and the corresponding antibiotics was grown to OD = 0.6. Then 20 mL of the cells were transferred into a new flask for the corresponding temperatures to be tested (here 20°C; 30°C and 37°). 1 mL of a non-induced sample was taken as a control. Then 1 mM IPTG was added into each

flask for induction of protein expression and the cells were incubated at their corresponding temperature condition at 220 rpm. After 3 h, 6 h and 20 h another 1 mL sample was taken of the induced cells at the corresponding temperature conditions and the OD of the cells was measured. All samples were adjusted to same OD as to the non-induced sample and collected by centrifugation at 13 000 rpm speed for 5 min. Next, the obtained pellet was resuspended in the SDS sample loading buffer. Then a sonication was performed for the sample (3 times for 10 sec each) for cell disruption. In order to monitor the success of the protein over-expression the disrupted bacterial lysate was used for SDS-PAGE analysis (see section 3.3.3.4) followed by a western blot analysis and immunodetection (see section 3.3.3.6).

3.3.3 Protein biochemistry

3.3.3.1 Recombinant protein expression and cell lysis

In this study the wild type Ups1/Mdm35 as well as the mutants Ups1^{A87C}/Mdm35 and Ups1^{L62AW65A}/Mdm35 were expressed and purified according to the previously published protocol by (Connerth et al., 2012). For a recombinant expression of His-tagged proteins, the desired constructs were first transformed into Origami B(DE3)pLysS *E.coli* cells (see section 3.2.2.2.). Then a test expression was performed and optimal expression conditions were defined (see section 3.2.2.3). After defining the optimal expression condition, a preculture of 5 mL was inoculated in the morning at 37 °C for 6 h with a single colony from the corresponding cells expressing the desired construct (see section 3.2.2.1). An overnight culture was then inoculated in 300 mL LB medium by addition of the corresponding antibiotics and the cells were grown overnight at 37°C. On the following day, the overnight culture was inoculated in 12 litre LB medium by addition of the required antibiotics. The culture was grown to OD = 0.6 at 37 °C. Next, the cells were induced with 1 mM IPTG at the corresponding optimal expression condition. Lastly, the culture was harvest at 4000 rpm for 20 min at 4°C and the pellet was stored at -20 °C until use.

For cell lysis, the pellet was thawed and resuspended in lysis buffer containing (50 mM Tris, 250 mM NaCL, 1 pill per 50mL of complete protease inhibitor cocktail

without EDTA, 1 mM PMSF, pH 8.0). Next, the cells were lysed using an EmulsiFlex-C5 (Avestin). The lysate was then centrifuged at 14000 rpm at 4 °C for 30 min. Lastly, the pellet was discarded and the supernatant was filtered through a 0.45 µm filter and used for a His-tag affinity chromatography (see section 3.3.3.2).

3.3.3.2 Recombinant protein purification via affinity His-tag chromatography

The His-tagged wild type Ups1/Mdm35 as well as the mutants Ups1^{A87C}/Mdm35 and Ups1^{L62AW65A}/Mdm35 were purified according to the previously published protocol by (Connerth et al., 2012). Purification was performed at 4°C in a cold room using a 5 mL HisTrapFF (GE Healthcare) and the ÄKTAprime plus system (GE Healthcare). After injection of the His-tagged sample to the column, the column was washed with a buffer containing 250 mM NaCL, 50 mM Tris/HCl, 20 mM Imidazole, pH 8.0. The elution of bound proteins was obtained by using the following elution buffer (250 mM NaCL, 50 mM Tris/HCl, 500 mM Imidazole, pH 8.0) and the peak fractions were collected and further purified via size-exclusion chromatography (see section 3.3.3.3)

3.3.3.3 Size-exclusion chromatography

In order to increase the purity, the proteins that were isolated (see fraction 3.3.3.2) were further purified through size-exclusion chromatography (SEC) with a HiLoad 16/600 75 pg (GE Healthcare) column and the ÄKTAprime plus system (GE Healthcare). The SEC was performed at 4 °C and the column was first equilibrated with the size-exclusion chromatography buffer containing 150 mM NaCL, 50 mM Tris/HCl, pH 7.4. Next, the HisTrap elution fractions (see section 3.3.3.2) were concentrated using an Amicon filter (Merck Milipore) and centrifuged at max. speed in a table-top centrifuge at 4°C. The volume of the sample was adjusted to 5 mL and subsequently injected with a flow rate of 1mL/min.

3.3.3.4 Sodium dodecyl sulfate polyacrylamide gel electrophoresis (SDS-PAGE)

Separation of protein was obtained by sodium dodecyl sulfate polyacrylamide gel electrophoresis (SDS-PAGE). For the SDS-PAGE, the protein samples were

mixed with 4X sample loading buffer containing 1% β-mercaptoethanol, 10% glycerol, 2% SDS, 60 mM Tris/HCl pH 6.8 as well as 0.01% bromophenol blue. Separation gels were casted containing 15% (30/0.8) acrylamide / bisacrylamide, 386 mM Tris/HCl pH 8.8, 0.1% SDS, 0.08% TEMED, 0.1% APS. The self casted stacking gel was composed of 5 % (30/0.8) acrylamide/ bisacrylamide, 126 mM Tris/HCl pH 6.8, 0.2% TEMED, 0.1% SDS, 0.1% APS. A running buffer (Laemmli) was prepared and used for SDS-PAGE containing 25 mM Tris, 0.1 % SDS and 191 mM glycine,. Then, a vertical SDS gel electrophoresis was performed in the Mini-PROTEAN Tetra Vertical Electrophoresis Cell (Bio-Rad) at constant 180 V. PageRuler prestained protein marker or Spectra^{TM} Multicolor Low Range Protein Ladder was used a protein standard marker. SDS-PAGE using precast Novex 10-20% Tricine gels was conducted using 1X Tricine SDS running buffer and the Invitrogen Mini Gel Tank system (Thermo Scientific) according to the manufacturer's instructions.

3.3.3.5 Protein visualization after SDS-PAGE

After SDS-PAGE, the proteins were visualized using Coomassie Brilliant Blue. The gel was stained in a solution containing 10% acetic acid, 25% ethanol, and 0.1% Coomassie Brilliant Blue R-250. Next, the gel was de-stained in a solution containing 25% ethanol and 10% acetic acid to remove the background stain. In order to receive a higher detection sensitivity, the gel was stained overnight in colloidal Coomassie stain instead, containing 0.12 % Coomassie Brilliant Blue G-250, 20 % methanol, 10 % phosphoric acid and 10 % ammonium sulfate. For de-staining, the gel was washed and incubated in ddH_2O.

3.3.3.6 Western Blot analysis and immunodetection

The Western blot analysis and immunodetection were conducted after SDS-PAGE for protein detection. After SDS-PAGE, the gel was equilibrated in blotting buffer containing 20 mM Tris, 0.02% SDS, 150 mM Glycine and 20% methanol. Then the gel was assembled into the following transfer sandwich composed of two blotting papers (soaked in transfer buffer) at the bottom, a PVDF membrane (activated in methanol), then the gel and two more blotting papers on top. The western blotting was performed in a semi-dry (Peqlab) system for 1 h at 125 mA and 13 V. After

blotting, the PVDF membrane was blocked in 5 % milk containing TBS-T buffer (20 mM Tris, 125 mM NaCl, 0.1 % Tween 20, pH 7.5) for 1 h at room temperature. Subsequently, the membrane was rinsed in TBS-T followed by an incubation with an anti-His primary antibody (dissolved in TBS-T buffer containing 5 % milk) for 1 h at RT. Next, the membrane was washed (3 times for 10 min) in TBS-T buffer, followed by another 1 h incubation at room temperature with an HRP coupled secondary antibody diluted (1:10000) in TBS-T buffer containing 5 % milk. Then, the membrane washing step was repeated (3 times for 10 min) in TBS-T buffer. After addition of the ECL (Thermo Scientific) solution to the membrane, the signals could be visualized and detected on the X-ray film through a developing in a CAWOMAT machine.

3.3.3.7 Blue native PAGE

In this study, a blue native PAGE (BN-PAGE) was performed using the NativePAGE Novex Bis-Tris Gel System (Invitrogen). Samples were loaded into a precast NativePAGE 4-16% Bis-Tris gel (Invitrogen) and BN-PAGE was conducted at a constant 150 V according to the manufacturer's instructions and guidelines. NativeMark Unstained Protein Standard was used as a marker. After BN-PAGE, the gel was stained in colloidal Coomassie stain for protein visualization (see section 3.3.3.5). For a western blot and immunodetection analysis after BN-PAGE, the gel was incubated for 20-30 min in SDS running buffer followed by a western blot which was conducted at 25 V, 250 mA for 2 h while the rest of the experiment was performed according to the previously mentioned protocol (see section 3.3.3.6)

3.3.3.8 Protein precipitation by TCA

For the protein precipitation by TCA the protein sample was mixed with 10 % ice-cold trichloroacetic acid (TCA) and incubated for 30 min on ice, followed by a centrifugation at maximal speed for 30 min at 4°C. After centrifugation, the supernatant was carefully discarded. In the following step, the pellet was washed using 1 mL ice-cold acetone which was followed by another round of centrifugation at same condition. The supernatant was discarded again and the samples were

dried in a SpeedVac concentrator for 1 h and subsequently resuspended in 4x SDS sample loading buffer and analysed via SDS-PAGE (see section 3.3.3.4).

3.3.3.9 Protein labelling

In order to perform GUV assays, the cysteine containing mutant Ups1^{A87C}/Mdm35 was fluorescently labelled with Atto 488 maleimide (Atto-TEC) according to the manufacturer's instructions and guidelines. To remove the dye excess, the labelled protein was separated by size-exclusion chromatography with a G-25 gravity column (GE Healthcare) following the manufacturer's instructions.

3.3.4 Working with artificial lipid membranes

3.3.4.1 Preparation of artificial membrane vesicles (liposomes)

Lyophilised powders of L-α-Phosphatidylethanolamine (PE), L-α-Phosphatidic acid (PA), L-α-Phosphatidylcholine (PC), L-α-Phosphatidylethanolamine-N-(lissamine rhodamine B sulfonyl) (Rhod PE), L-α-Phosphatidylserine (PS) and cardiolipin (CL) were prepared as stock solutions in chloroform (Avanti Polar Lipids). For generation of liposomes, lipids were mixed in the desired molar ratios (mol-%) in glass tubes. The following liposomes were prepared in different molar ratios: PC/PE/PA (50:20:30), PC/PE/PA (65:20:15), PC/PE/CL/PA (55:20:10:15), PC/PE/CL (65:20:15); PC/PE/PS (65:20:15); PC/PE/PS (50:20:30). The lipid mixtures in chloroform were dried shortly under a stream of nitrogen gas, followed by an incubation in a desiccator for 2 h. The dried lipids were re-hydrated by addition of the liposome buffer (150 Mm NaCl, 10 mM MES/NaOH, pH 5.5) to a final concentration of 12 mM. In order to generate unilamellar vesicles, the lipid mixture was then subjected to 10 freeze (in liquid nitrogen) and thaw (at room temperature) cycles and the sample was vortexed in between the step for 2 min. In order to achieve liposomes of a specific size like large unilamellar (LUVs) or small unilamellar vesicles (SUVs), the mixture was extruded 31 times through polycarbonate membranes (Whatman) using a mini-extruder (Avanti Polar Lipids). Here, a membrane pore size of 30 nm or 50 nm was used for SUVs and 200nm,

400nm or 800nm for LUVs. In order to receive SUVs, the lipid suspension was subjected to sonification.

For a pH-dependent flotation assay 200 nm LUVs composed of PC/PE/CL/PA (55:20:10:15) were generated according to the previously described protocol using the following buffers with different pH values. Here, 10 mM MES and 150 mM NaCL was used for pH 5.5, pH 6.0 and pH 6.5 while a buffer containing 50 mM Tris and 150 mM NaCl was used for pH 7.0 and pH 7.4.

For RIfS measurements SUVs were generated by mixing lipids in chloroform in small glass tubes to yield 0.25 mg in molar ratios shown in the following table.

Table 3.15: Lipid mixtures used for SUVs

lipid mixture	molar ratio
PC, PE, CL, PA	55:20:10:15
PC, PE	75:25

The solvent was removed under a stream of nitrogen gas at 35 °C for 30 min and the lipid films were then dried under reduced pressure for about 3 h at 35 °C. The test tubes were sealed and stored at 4 °C until use. Next, the generation of SUVs was initiated by swelling the lipid films in 250 µl MES 5.5 for 30 min at 45 °C and vortexed and reheated three times afterwards. The emerging dispersion was sonicated for 30 min to yield SUVs.

3.3.4.2 Preparation of Giant Unilamellar Vesicles (GUVs)

The generation of Giant unilamellar vesicles (GUVs) was performed following the electroformation protocol in an external alternating (AC) electrical field (Angelova and Dimitrov, 1986, Angelova et al., 1992). A lipid mixture of PC/PE/PA/Rhod-PE (60.5:24:15:0.5) were prepared to a final lipid concentration of 5 mM in chloroform. Then 15 µL of that mixture was spread as small droplets onto two indium tin oxide (ITO)-coated glass slides (ITOs, Nantion Technologies), incubated for 30 sec at 50 °C and subsequently put in a desiccator with applied vacuum for another 30 min for drying. Next, the ITO slides were placed with a rubber spacer ring in between, filled with 625µL of a GUV sucrose buffer (10 mM MES/NaOH, 150 mM NaCl, 300 mM sucrose, pH 5.5), into a GUV generation chamber Nanion Vesicle Prep Pro

(Nanion Technologies). Then, an electric field was applied for 3 h by starting at 30 mV which was continuously increased to 1.1 V at 12 Hz leading to the electroformation of the GUVs. In order to detach the GUVs from the ITO slides the field frequency was decreaded to 4 Hz at 2 V for 30 min. Microscopic visualization of GUVs under the absence and presence of protein was performed as described (see section 3.3.5.2).

3.3.4.3 Co-migration assay

For the co-migration (flotation) assay 5 mM of the desired LUVs or SUVs were incubated with 10 µM of the protein in the corresponding liposome buffer in a total reaction volume of 100 µL using the corresponding buffer that was used for the generation of liposomes. The sample was incubated at room temperature for 30 min. Then, after incubation, 100 µL of the sample was mixed with 700 µL of 40% Histodenz and transferred carefully into the bottom of an ultracentrifuge tube. Then a layer of 20 %, 10 %, 5 % (each 900 µL) and the corresponding liposome buffer was added creating a discontinuous Histodenz gradient from high density to low density (40%/20%/10%5%/0%). The sample was subjected to ultracentrifugation at 55000 rpm at 4 °C for 1 h. After ultracentrifugation, a photo of the ultracentrifuge tube was taken, showing the flotation pattern. Lastly, 9 fractions of 500 µL were taken and precipitated with TCA (see section 3.3.3.8) and subsequently prepared for an SDS-PAGE (see section 3.3.3.4) by addition of 40 µL 4X sample loading buffer (Figure 3.1). Through the co-migration assay a separation of unbound protein, unbound liposomes and protein-bound liposomes can be achieved by ultracentrifugation in a discontinuous Histodenz gradient (Figure 3.1). The unbound protein will stay at high density area (bottom of the tube) after centrifugation. The unbound liposomes as well as the protein-bound liposomes will migrate or co-migrate to lower density areas, respectively.

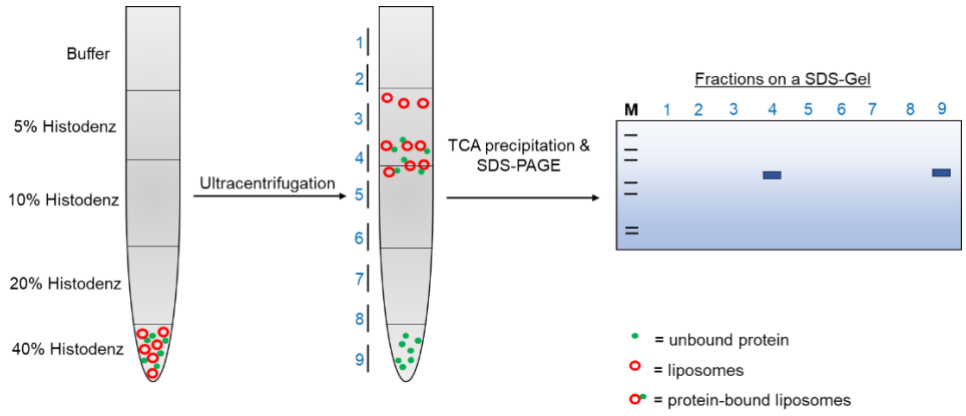

Figure 3.1: Schematic illustration of the co-migration (flotation) assay.

Protein and liposomes are incubated, then loaded into ultracentrifugation tubes in a discontinuous Histodenz gradient. Unbound protein, liposomes and protein-bound liposomes (co)-migrate to their corresponding density. After ultracentrifugation, 9 fractions are taken and subjected to TCA precipitation. Samples are prepared for an SDS-PAGE for protein visualization.

3.3.4.3 Lipid Transfer Assay

The transfer assay for Ups1/Mdm35 was performed according to a previously published protocol (Connerth et al., 2012) with some modifications and changes in this study. Heavy donor liposomes (100 nm) were performed composed of PC/PE/CL/PA (55:20:10:15) in a 15 % Histodenz containing buffer (150 mM NaCl, 5 mM Tris/HCl, pH 7.4, 15 % Histodenz) (see section 3.3.4.1) and light acceptor liposomes (100 nm) composed of PC/PE/PA (65:20:15) were generated in the same buffer (150 mM NaCl, 5 mM Tris/HCl, pH 7.4) devoid of Histodenz. Then in a 100 µL total reaction mix, 5 mM of each donor and acceptor liposomes were incubated with 0.5 µM of the Ups1/Mdm35 complex in the corresponding buffer. The samples were then incubated at RT for 1 h. After incubation, 100 µL of the sample was carefully transferred into the bottom of an ultracentrifuge tube and overlaid with 15 %, 5 %, 0 % Histodenz in the following buffer (150 mM NaCl, 20 mM Tris/HCl, pH 7.4) in order to create a discontinuous gradient from high density to low density. The sample was then subjected to an ultracentrifugation performed at 55000 rpm for 1 h at 4°C.Then 2.5 mL of the acceptor (top fraction) and 2 mL of the donor (bottom fraction) was taken. Extraction of a lipid fraction was performed using chloroform/methanol (2:1, v/v) according to (Connerth et al., 2012). The nonpolar phase was then dried under a stream of nitrogen and subsequently dissolved in 20 µl chloroform. For the thin layer chromatography (TLC), the sample was spotted onto a TLC 60 plate (Merck KGaA) together with a corresponding

standard next to it. Then the lipids were separated in a solvent mixture composed of chloroform/methanol/acetic acid (65:35:8, v/v/v). Next, all of the lipid spots on the TLC plate were detected using 0.5 mg ml^{-1} primuline in a mixture of acetone/water (8:2, v.v) (White et al., 1998). Visualization was performed under 528 nm UV light and the spots corresponding to the lipids PC, PE, PA and CL were scraped off separately. Next, the preparation of methyl esters of fatty acids (FAMEs) for the analysis via gas chromatography/flame ionization detection (GC/FID) was conducted as previously published and described (Miquel & Browse, 1992). In order to perform an acidic hydrolysis, 2 % (v/v) dimethoxypropan and 1 ml methanol/toluene (2:1, v/v) containing 2.75 % (v/v) H_2SO_4 (95-97 %) was added to a silica gel. In order to quantify the fatty acids later on, 100 nmol pentadecanoic acid (PA: 10 nmol) was added to the sample followed by an incubation at 80 °C for 1 h. For the extraction of the resulting FAMEs, 1.5 ml of a saturated aqueous NaCl solution as well as 1.2 ml of hexane were used and added to the sample. Drying of the hexane phase under a stream of nitrogen gas was the next step, followed by addition of 20 µl acetonitrile (PA: 10 µl) for re-dissolving of the sample. Then the GC/FID analysis was conducted using an Agilent 6890 gas chromatograph (Waldbronn, Germany) and a capillary DB-23 column (J&W Scientific, Agilent). As a carrier gas Helium was used. Lastly, the ChemStation software (Agilent, Waldbronn, Germany) was used for peak integration. In this study, the TLC and the GC/FID analysis was performed using the equipment and devices from the group of Prof. Dr. Ivo Feussner (Department of Plant Biochemistry, University of Göttingen). The following figure (Figure 3.2) shows a schematic illustration of the lipid transfer assay in this study.

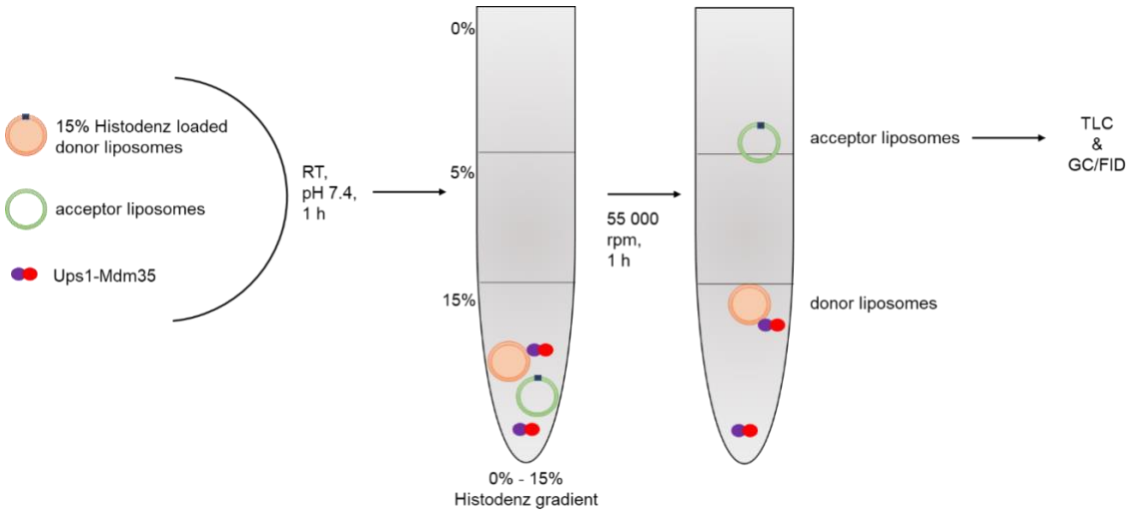

Figure 3.2: Schematic illustration of the lipid transfer assay.

The heavy donor liposomes which contain PA and are filled with 15% Histodenz, were incubated with light acceptor liposomes (devoid of PA and Histodenz) in the presence of the Ups1/Mdm35 complex. The sample was overlaid with Histodenz creating a discontinuous gradient from 15% to 0%. After ultracentrifugation, the acceptor and donor fractions were taken and the lipids were extracted and prepared for a thin layer chromatography (TLC) and quantified by gas chromatography/flame ionization detection (GC/FID).

3.3.4.4 RIfS measurements

Reflectometric interference spectroscopy (RIfS) experiments were performed with a home-built setup, consisting of a tungsten halogen light source (LS-1, Ocean Optics, Dunedin, Florida, USA), a flow chamber transparent for visible light which firmly covers a silicon wafer with 5 µm silicon oxide layer (Active Business Company, Brunnthal, Germany) and a spectrometer (Nanocalc-2000-UV/VIS, Ocean Optics). Through RIfS measurements one can analyse changes in the optical thickness *OT* on a thin film (transparent layers). Here, *OT* is given by the product of the refractive index (*n*) and the physical thickness (*d*) of the film. The detailed setup and data analysis to obtain values of the optical thickness were previously described (Stephan et al., 2014). The silicon wafers were cleaned in a mixture of ultrapure water, hydrogen peroxide and ammonia solution (5:1:1 by volume) at 75 °C for at least 20 min and stored in ultrapure water until use for not longer than two days. A solution of 0.8 mg/ml Ups1/Mdm35 in Tris 7.4 was aliquoted in different volumes, frozen by liquid nitrogen and subsequently stored at −20 °C until use. After purging the chamber with MES 5.5, the inlet and outlet of the flow chamber were put into the vesicle dispersion, which was dissolved in 500 µl MES 5.5, to obtain a close loop system. The SUV dispersion was flushed through the measurement chamber until a stable plateau of the optical thickness

was obtained. Afterwards, the formed supported membrane was rinsed with at least 15 ml of the appropriate buffer. For qualitative binding experiments, the inlet and outlet were put into a solution of Ups1/Mdm35 (100 µl of Ups1/Mdm35 solution dissolved in the appropriate buffer to obtain a volume of 500 µl). For quantitative experiments to obtain a Langmuir isotherm the same procedure was performed with increasing volume of Ups1/Mdm35 solution from 1 µl to 100 µl. Finally, in both cases the membrane was again rinsed with the appropriate buffer to record an unbinding curve. Buffers with different pH values were prepared and used. The following buffer containing 10 mM MES and 150 mM NaCL was used for pH 5.5, pH 6.0 and pH 6.5 while a buffer containing 50 mM Tris and 150 mM NaCl was used for pH 7.0 and pH 7.4. The mean of the plateau values of the optical thicknesses after each addition of protein were extracted and subtracted by the mean of the plateau value immediately before the first addition of proteins. The obtained optical thicknesses were plotted against the concentration with respect to the total volume of the measurement chamber, the connection tubes and the protein solution. A Langmuir isotherm was fitted to the data according to eq. 1.

$$OT = OT_{\max} \cdot K_{\mathrm{ass}} \cdot \frac{c}{1+K_{\mathrm{ass}} \cdot c} \quad (1)$$

Here, *OT* is the optical thickness, OT_{max} the equilibrium optical thickness at the maximum concentration of protein, *c* the concentration of the protein and K_{ass} the thermodynamic association constant. The thermodynamic dissociation constant (K_d) is the inverse of the association constant. All RIfS measurements in this study were performed by Dr. Marian Vache from the group of Prof. Dr. Andreas Janshoff at the Institute of Physical Chemistry, University of Göttingen.

3.3.5 Visualization techniques

3.3.5.1 Visualization of liposomes via transmission electron microscopy

For transmission electron microscopy (TEM) of LUVs, 5 mM of liposomes containing PC/PE/PA (50:20:30) were incubated in the absence and presence of 20 µM Ups1/Mdm35 in liposome buffer (150 Mm NaCl, 10 mM MES/NaOH, pH 5.5) for 30 min. The sample was diluted 1:40 in the corresponding liposome buffer and a drop of the sample was transferred onto a glow discharged carbon foil

covered grid. Then the sample was stained with 1% uranyl acetate and subsequently analysed with a Talos L120C transmission electron microscope (ThermoFischer Scientific, Eindhoven, and the Netherlands) at room temperature.

3.3.5.2 Visualization of GUVs via confocal light microscopy

After generation, 50 µL of GUVs were carefully diluted in 300 µL GUV salt buffer (10 mM MES/NaOH, 150 mM NaCL, pH 5.5) and transferred into chambered coverslips (ibidi) which were pre-coated for 1 h with lipid-free bovine serum albumin (Sigma-Aldrich) and washed 3 times with GUV salt buffer. Here, 7 mM of the Atto 488 labelled mutant Ups1^{A87C}/Mdm35 was added into the GUV suspension by gentle stirring. Images of the GUVs were taken in the absence and presence of the Atto 488 labelled mutant Ups1^{A87C}/Mdm35 and visualized with a Zeiss LSM780 confocal microscope.

3.3.6 Molecular Dynamics (MD) simulation studies

The curvature dependent binding free energy of Ups1-Mdm35 was determined according to a previously published protocol (Stroh & Risselada, 2021). This protocol employs molecular dynamics (MD) simulations in conjunction with umbrella sampling to quantify membrane curvature sensing of peripheral proteins on a simulated buckled membrane. Here, 674 lipids per leaflet (371 POPC, 202 POPE, 101 POPA) were put in the x-y plane of a 40 nm 10 nm 20 nm simulation box. The system was compressed in x-direction by applying a pressure in x-direction leading to an expansion in z-direction, while the y-dimension was kept fixed. For the simulation the protein structure with the PDB 4XHR by (Yu et al., 2015) was used. The simulated buckled membrane provides regions of zero, positive and negative curvature and the protein complex was pulled along this membrane. For further description and protocol see (Stroh & Risselada, 2021).
In order to determine the lipid desorption free energies on a buckled membrane in the absence of the protein complex, MD simulations and the Bennett Acceptance Ratio (BAR) method was used (Bennett, 1976). All MD simulations in this study were performed by Kai Stroh from the group of Prof. Dr. Herre Jelger Risselada (Institute for Theoretical Physics, University of Göttingen and Department of Physics, Technical University of Dortmund).

4 Results

4.1 Expression and purification of the yeast lipid transfer protein Ups1/Mdm35 and its mutants

4.1.1 Expression and purification of Ups1/Mdm35

Previously, the Ups1/Mdm35 complex was found as an LTP in the IMS of yeast mitochondria shuttling ER-derived PA from the OMM to the IMM for CL synthesis and accumulation in the IMM (Connerth et al., 2012). Recombinant Ups1 is known to be protected against aggregation and only stable when co-expressed with Mdm35. Thus, we co-expressed and purified Ups1/Mdm35 using previously published protocols (Connerth et al., 2012). Ups1/Mdm35 was cloned into the pET-Duet-1 expression vector carrying two multiple cloning sites 1 and 2 (MCS1 and MCS2). Here, Ups1 was cloned into the first cloning site carrying an N-terminal His-tag. The MCS2 usually carries a S-tag which we removed in this construct and the coding sequence of Mdm35 was inserted. Since Mdm35 contains a twin CX_9C motif forming two disulfide bonds (Gabriel et al., 2007; Herrmann & Riemer, 2012; Longen et al., 2009) we co-expressed the His-tagged Ups1/Mdm35 construct in Origami B(DE3)pLysS competent cells from Novagen that enhance disulfide bond formation. To find the optimal expression condition with the highest protein yield we performed a test expression in these cells under different time and temperature conditions in the presence of 1mM IPTG. After expression we took samples and the cells were lysed and prepared for SDS-PAGE. Since there were a lot of unspecific bands on the SDS gel and the overexpression of the Ups1 (21.9 kDa) and Mdm35 (9.7 kDa) proteins was hard to detect (Figure 4.1, A), we decided to do a western blot with an anti-His antibody to find the optimal condition (Figure 4.1, B). The signal for His-tagged Ups1 could be visualized in all samples after induction with IPTG. We further saw an unspecific band around 28 kDa in almost all of the samples with the highest signal at 6h time point and 37°C. Thus, we decided to use 30°C and 3 h as optimal expression conditions with a strong specific and a very weak unspecific band for Ups1.

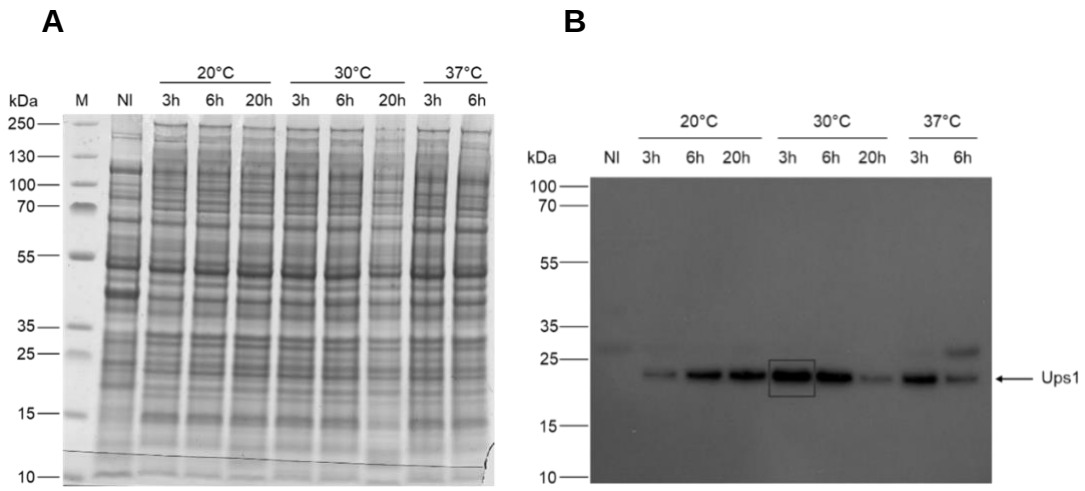

Figure 4.1: Test expression of Ups1/Mdm35 in *E.coli*.

Ups1 was cloned into the multiple cloning site 1 (MCS1) of the pET-Duet-1 co-expression vector carrying a N-terminal His-tag. Mdm35 was cloned into the second multiple cloning site and the S-tag of the MCS2 was removed. The complex was then recombinantly co-expressed in Origami B(DE3)pLysS competent cells by 1 mM IPTG induction. A non-induced "NI" sample and samples after induction at different time and temperature conditions were loaded on a SDS gel and analysed by SDS-PAGE and Coomassie brilliant blue staining **(A)**. The expression level of the His-tagged Ups1 protein was detected via western blot with an anti-His antibody. The black box indicates the optimal expression condition that was picked and defined for the Ups1/Mdm35 protein complex **(B)**. PageRuler^{TM} Plus Prestained Protein Ladder was used as a protein standard Marker (M).

In the next step we aimed to express Ups1/Mdm35 from a bigger culture at previously identified optimal expression conditions. We first started with a 2 litre culture but after several rounds of test-expression and optimization, we decided to scale up the culture volume to 12 liters to receive the highest yield. After expression, the cells were harvested, lysed and centrifuged to separate the cell debris (pellet) from the soluble protein (supernatant). In the following step, we took the supernatant for purification of the His-tagged protein via immobilised metal affinity chromatography (IMAC) using a Ni^{2+}-NTA column. After the HisTrap, the protein was further purified via size-exclusion chromatography (SEC) to increase the purity of the recombinant protein and to put the protein into more physiological buffer condition (pH 7.4 and 150 mM NaCl). Samples of each step after expression, lysis and purification for recombinant Ups1/Mdm35 were prepared and loaded on a gel for SDS-PAGE. Ups1 (21.9 kDa) and Mdm35 (9.7 kDa) could be successfully detected in the fraction of HisTrap elution (E) and size-exclusion chromatography (SEC) (Figure 4.2).

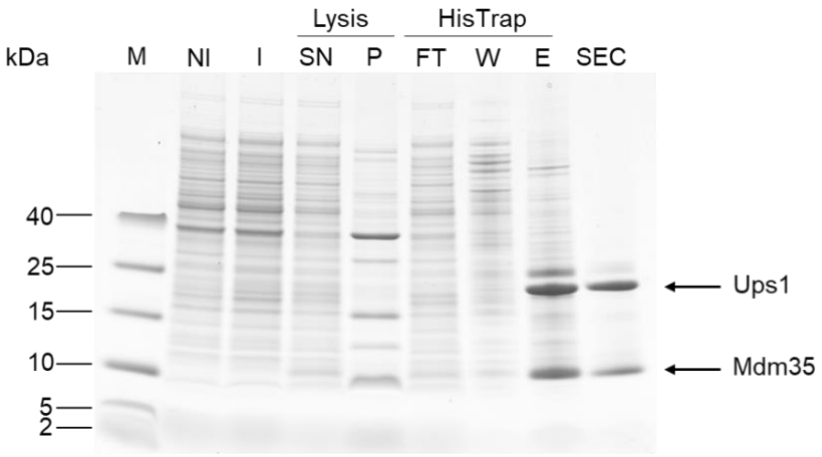

Figure 4.2: Purification of the recombinant protein complex Ups1/Mdm35.

The Ups1/Mdm35 complex was co-expressed in a 12 litre culture of Origami B(DE3)pLysS competent cells in the presence of 1 mM IPTG for 3 h at 30°C while a non-induced (NI) sample and a sample after induction were taken for analysis. After expression, the cells were lysed to separate the soluble protein in the supernatant (SN) from the cell debris in the pellet (P) by centrifugation. The recombinant protein was isolated via HisTrap purification. Samples were taken after each step of flow through (FT), wash (W) and elution (E). In a final step a size-exclusion chromatography (SEC) was performed to increase the purity of the recombinant proteins. All samples were loaded on a gel and analysed by SDS-PAGE and colloidal coomassie staining. Spectra™ Multicolor Low Range Protein Ladder was used as a protein standard marker (M).

4.1.2 Expression and purification of the mutant Ups1^{A87C}/Mdm35

In contrast to Mdm35 which contains two disulfide bonds, Ups1 is devoid of any cysteines. Thus, we created a cysteine mutation in the Ups1 coding sequence of the wild type construct via site-directed mutagenesis. This cysteine was later used for a conjugation with a fluorescent dye (here Atto488 maleimide) for fluorescence microscopy investigations. The coding sequence of Mdm35 in MCS2 of the pET-Duet-1 vector remained unchanged, because we still aimed a co-expression of both proteins. Next, we checked several amino acid positions for Ups1 with the PyMOL Molecular Graphics System to find the optimal mutation and to avoid steric hindrance. We found that a mutation of alanine at position 87 to cysteine in Ups1 might be the most favourable one. Expression and purification of this mutant was performed similar to the wild type protein Ups1/Mdm35. Here again, we started with a test expression in the Origami B(DE3)pLysS cells at different time and temperature condition in the presence of 1 mM IPTG. To unambiguously detect Ups1, western blot analysis with an anti-His antibody against the His-tagged

Ups1^{A87C} (21.9 kDa) was used (Figure 4.3). The strongest signal could be obtained at 30 °C and 6 h, which we defined as the optimal expression condition.

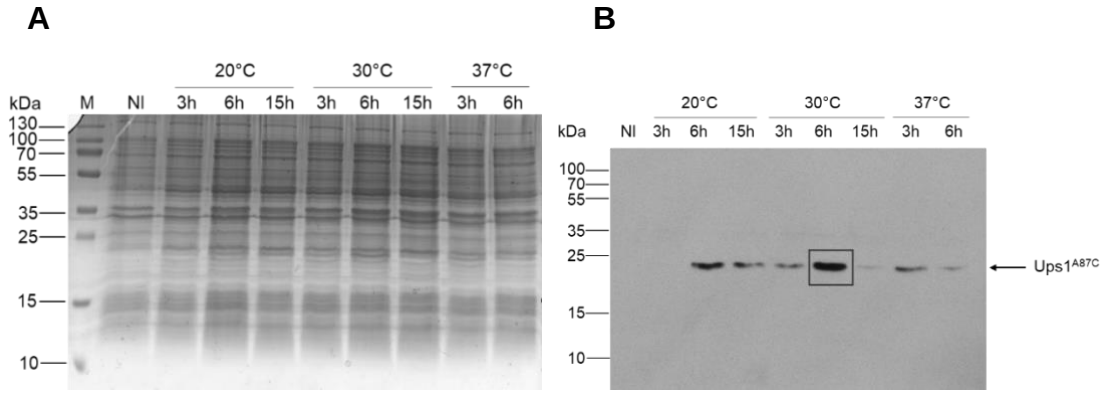

Figure 4.3: Test expression of the mutant Ups1^{A87C}/Mdm35 mutant in *E.coli*.

A mutation of alanine (A) to cysteine (C) at position 87 was introduced into the Ups1 sequence of the wild type Ups1/Mdm35 co-expression vector. The complex was then recombinantly co-expressed in Origami B(DE3)pLysS competent cells by 1 mM IPTG induction. A non-induced "NI" sample and samples after induction at different time and temperature conditions were loaded on a SDS gel and analysed by SDS-PAGE and colloidal coomassie staining (A). The expression level of His-tagged Ups1^{A87C} was detected via western blot with an anti-His antibody. The black box indicates the optimal expression condition that was picked and defined for the Ups1^{A87C}/Mdm35 protein complex (B). Spectra^{TM} Multicolor Low Range Protein Ladder was used as a protein standard marker (M).

In the next step we co-expressed and purified the Ups1^{A87C}/Mdm35 mutant from a 12 liter culture. After cell lysis and separation of the supernatant from the pellet, we performed a HisTrap and SEC. Samples after expression, lysis and purification were prepared and loaded on a gel for SDS-PAGE (Figure 4.4) while Ups1^{A87C} (21.9 kDa) and Mdm35 (9.7 kDa) could be successfully detected in the fraction of HisTrap elution (E) and SEC. Nevertheless, some unspecific bands after SEC were still visualizable similar to the previously obtained results for the wild type protein complex.

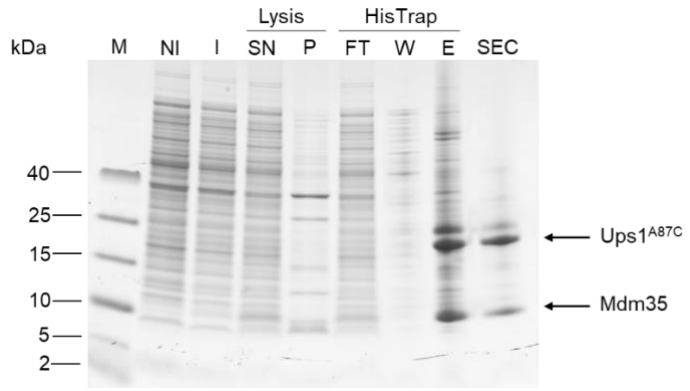

Figure 4.4: Purification of the recombinant protein complex Ups1^{A87C}/Mdm35.

The Ups1^{A87C}/Mdm35 complex was co-expressed in a 12 litre culture of Origami B(DE3)pLysS competent cells in the presence of 1 mM IPTG for 6 h at 30°C while a non-induced (NI) sample and a sample after induction were taken for analysis. After expression, the cells were lysed to separate the soluble protein in the supernatant (SN) from the cell debris in the pellet (P) by centrifugation. The recombinant protein was isolated via HisTrap purification. Samples were taken after each step of flow through (FT), wash (W) and elution (E). In a final step a size-exclusion chromatography (SEC) was performed to increase the purity of the recombinant proteins. All samples were loaded on a gel and analysed by SDS-PAGE and colloidal coomassie staining. Spectra^{TM} Multicolor Low Range Protein Ladder was used as a protein standard marker (M).

4.1.3 Expression and purification of the mutant Ups1^{L62AW65A}/Mdm35

In several previous structural analysis studies, it was shown that Ups1 carries a small and flexible α2-loop which is suggested to be functionally similar to the lipid exchange loop and the Ω-loop that was found in PITPs and the START domain, respectively. This loop is suggested to act as a lid that can cover the lipid binding pocket of the Ups1/Mdm35 complex (Lu et al., 2020; Miliara et al., 2015; Watanabe et al., 2015; Yu et al., 2015). In an *in vitro* study, a deletion of this loop caused a drastic decrease in the lipid transfer activity of Ups1/Mdm35 (Watanabe et al., 2015). Accordingly, studies by Miliara et al., confirmed these findings by showing that a double mutation of two hydrophobic amino acids in this loop to alanine (L62A and W65A) impairs the Ups1/Mdm35 mediated lipid transfer of PA (Miliara et al., 2015).

Since we also wanted to test this mutant in our studies, we created the L62AW65A mutation in the His-tagged Ups1 coding sequence in MCS1 of the wild type pET-

Duet-1 vector via site directed mutagenesis while the Mdm35 coding sequence in MCS2 remained unchanged. Expression and purification of this mutant was similar to that of the wild type protein complex Ups1/Mdm35. Here again, the overexpression of the proteins Ups1^{L62AW65A} and Mdm35 was hard to detect in the whole cell lysates on Coomassie stained SDS gel (Figure 4.5). Therefore, a western blot was performed which shows signals of the overexpressed and His-tagged Ups1^{L62AW65A} (21.8 kDa) protein in all samples after induction with 1 mM IPTG. We picked 37 °C and 3 h as the optimal condition for the expression of recombinant Ups1^{L62W65A}/Mdm35.

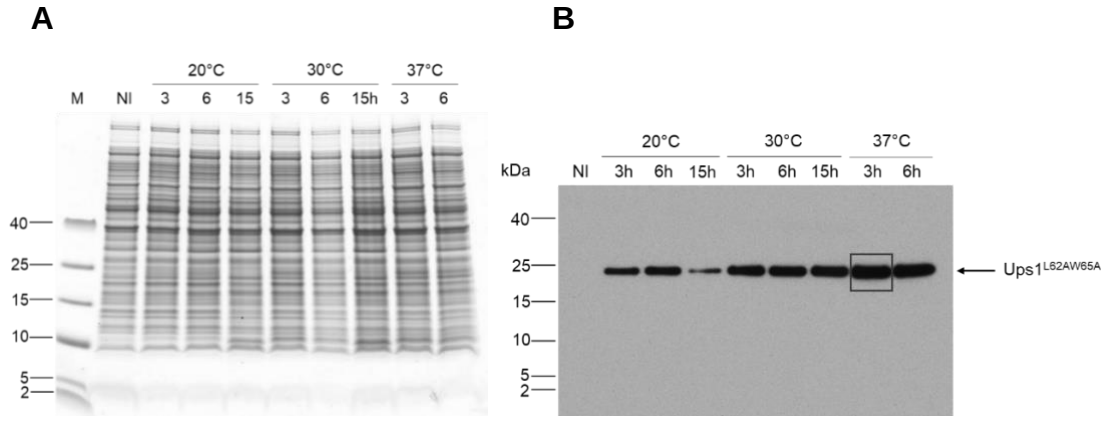

Figure 4.5: Test expression of the mutant Ups1^{L62AW65A}/Mdm35 in *E.coli*.

A double mutation of leucine (L) to alanine (A) at position 62 and tryptophan (W) to alanine at position 65 was introduced into the Ups1 sequence of the wild type Ups1/Mdm35 co-expression vector. The complex was then recombinantly co-expressed in Origami B(DE3)pLysS competent cells by 1 mM IPTG induction. A non-induced "NI" sample and samples after induction at different time and temperature conditions were loaded on a gel and analysed by SDS-PAGE and colloidal coomassie staining (A). The expression level of His-tagged Ups1^{L62AW65A} was detected via western blot with an anti-His antibody. The black box indicates the optimal expression condition that was picked and defined for Ups1^{L62AW65A}/Mdm35 protein complex (B). Spectra^{TM} Multicolor Low Range Protein Ladder was used a protein standard marker (M).

Next, we co-expressed and purified Ups1^{L62AW65A}/Mdm35 from a 12 litre culture according to the protocol for the wild type protein complex Ups1/Mdm35. Samples of all steps after expression, lysis and purification were loaded on a gel for SDS-PAGE analysis, showing that the experiment was successful. The proteins Ups1^{L62AW65A} (21.8 kDa) and Mdm35 (9.7 kDa) could be detected in the fraction of HisTrap elution (E) SEC (Figure 4.6).

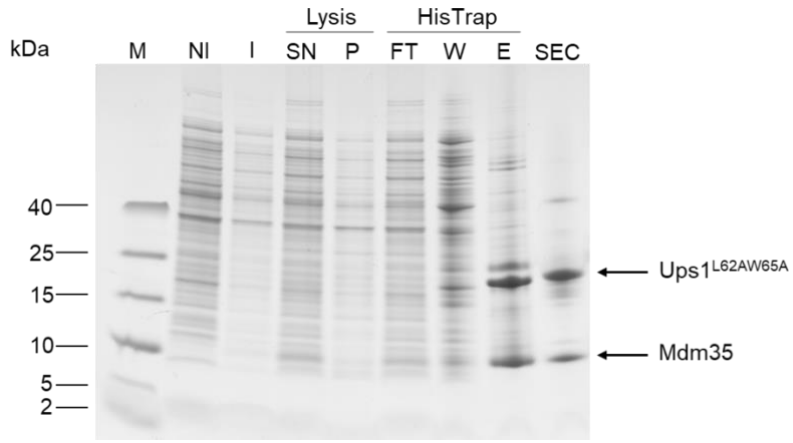

Figure 4.6: Purification of the recombinant protein complex Ups1^{L62AW65A}/Mdm35.

The Ups1^{L62AW65A}/Mdm35 complex was co-expressed in a 12 litre culture of Origami B(DE3)pLysS competent cells in the presence of 1 mM IPTG for 3 h and 37°C while a non-induced (NI) sample and a sample after induction were taken for analysis. After expression, the cells were lysed to separate the soluble protein in the supernatant (SN) from the cell debris in the pellet (P) by centrifugation. The recombinant protein was isolated via HisTrap purification. Samples were taken after each step of flow through (FT), wash (W) and elution (E). In a final step a size-exclusion chromatography (SEC) was performed to increase the purity of the recombinant proteins. All samples were loaded on a gel and analysed by SDS-PAGE and colloidal coomassie staining. Spectra^{TM} Multicolor Low Range Protein Ladder was used as a protein standard marker (M).

4.2 Lipid Transfer Assay of Ups1/Mdm35

Previously, the yeast protein Ups1 was found to be involved in the accumulation of CL in mitochondria (Osman et al., 2009; Tamura et al., 2009). Later, it was reported that Ups1 forms a stable heterodimeric complex with Mdm35 in the IMS (Potting et al., 2010; Tamura et al., 2010). In an *in vitro* co-migration (flotation) assay with liposomes, the Ups1/Mdm35 complex was shown to acts as a soluble LTP facilitating a specific transfer of PA between donor and acceptor liposomes (Connerth et al., 2012). We wanted to analyse the Ups1/Mdm35 mediated PA-specific transfer using a similar assay as previously published (Connerth et al., 2012). Here, we performed a gas chromatography/flame ionization detection (GC/FID) to quantify the lipids after Ups1/Mdm35 mediated transfer and changed some of the experimental conditions.

For the lipid transfer assay in this thesis, we prepared heavy donor liposomes composed of PC/PE/CL/PA (55:20:10:15) filled with 15% Histodenz and light acceptor liposomes composed of PC/PE/CL (65:20:15) devoid of Histodenz and PA. After incubation of Ups1/Mdm35 with these liposomes the samples were

separated via ultracentrifugation in a Histodenz gradient. Additionally, a control sample experiment was performed in the absence of protein. Pictures of the flotation tubes were taken after centrifugation (Figure 4.7, A and B). Since the acceptor LUVs were lighter they were found in the lower density portion of the gradient, while the heavier donor LUVs stayed in the higher density portion of the gradient. The flotation pattern of the LUVs indicated that our separation of donor and acceptor liposomes in the gradient was successful. Next, the acceptor and donor fractions were taken and loaded to a thin layer chromatography (TLC) plate to separate the lipids which were further quantified via GC/FID. We observed that the amount of PA in the acceptor fraction (1.75 mol-%) was indeed increased after Ups1/Mdm35-mediated lipid transfer by the factor 2.7 (Figure 4.7, C and E) compared to PA amount in the control sample (0.63 mol-%) (Figure 4.7; C and D).

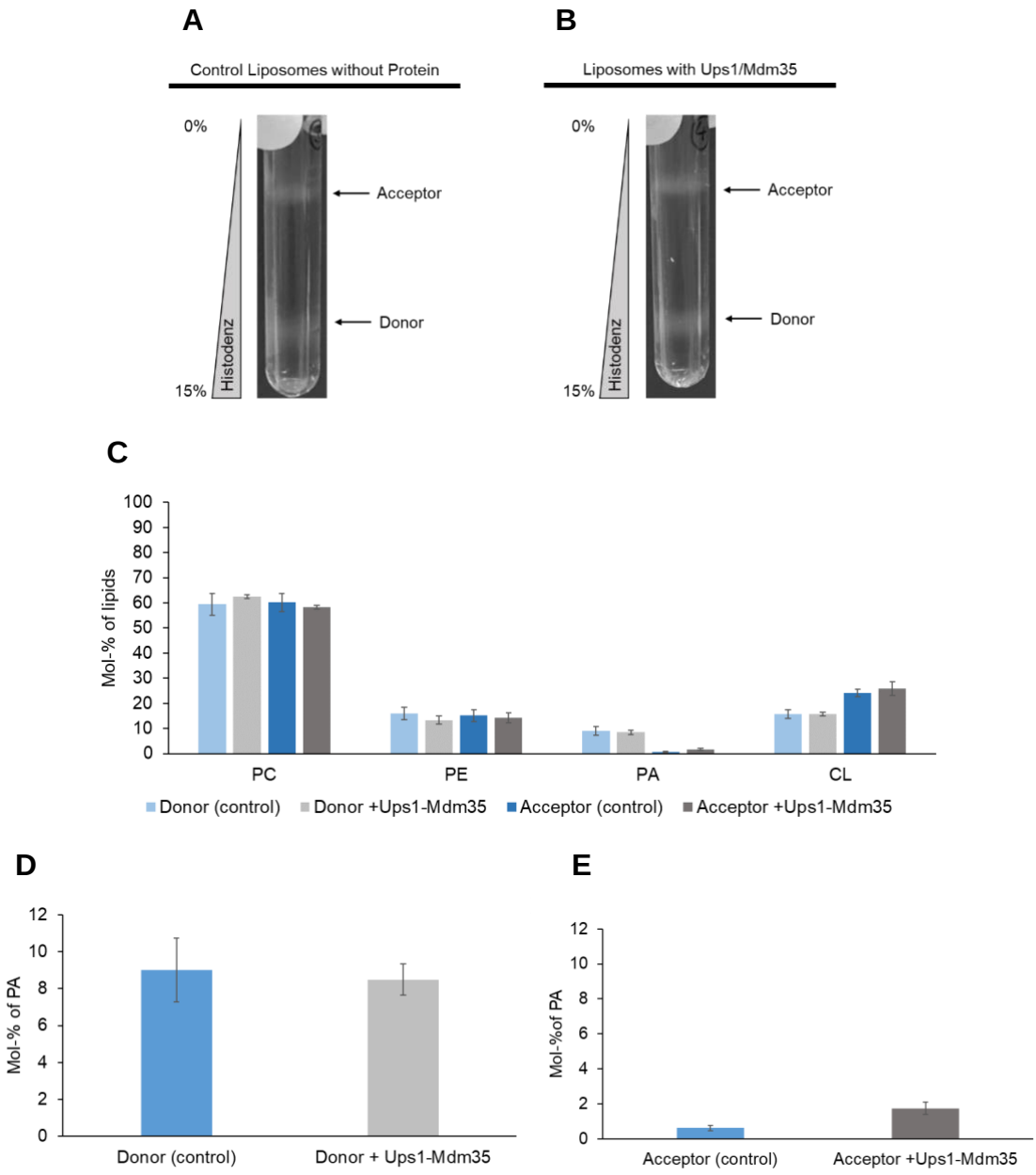

Figure 4.7: PA specific Lipid Transfer Assay for Ups1/Mdm35.

For the lipid transfer assay heavy donor liposomes PC/PE/CL/PA (55:20:10:15) were prepared and filled with 15% Histodenz. The acceptor liposomes PC/PE/CL (65:20:15) were devoid of Histodenz and PA. The protein complex Ups1/Mdm35 was incubated for 1 h with donor and acceptor liposomes and then separated in a Histodenz gradient by ultracentrifugation. Pictures of the tubes were taken after ultracentrifugation for liposomes in the absence (A) and presence (B) of the protein. Two fractions (donor and acceptor) were taken of each tube. The lipids were separated via TLC and quantified via GC/FID. Quantification of three independent experiments (n=3, mean±SD) (C). For a better illustration of PA transfer by Ups1/Mdm35 the values of mol-% for PA from (C) are plotted and shown again in (D) for both donor and in (E) both acceptor fractions.

4.3 Characterization of the membrane binding properties of Ups1/Mdm35

In an *in vitro* flotation assay the Ups1 protein was found preferably bound to negatively charged lipids in the liposomes such as PA, CL, PS, PI, PG or CDP-DAG. On the contrary, Mdm35 did not bind to liposomes at all (Connerth et al., 2012). Further, it was shown that flotation was enhanced when the pH was decreased in the flotation assay leading to a stronger binding of Ups1 to liposomes at pH 5.5 compared to pH 7.4 (Connerth et al., 2012). In order to gain a greater insight into the membrane binding properties of Ups1/Mmd35, we performed more refined flotation by taking specific different conditions like pH and lipid charges under consideration.

4.3.1 pH-dependent binding of Ups1/Mdm35 to LUVs

Before starting with any co-migration assay to test the binding behaviour of Ups1/Mdm35, we first performed a control flotation of Ups1/Mdm35 in the absence of LUVs in a Histodenz gradient to see where the protein is found after ultracentrifugation. We took nine fractions (1-9) after flotation and prepared them for SDS-PAGE analysis (Figure 4.8). We could clearly observe that both proteins Ups1 and Mdm35 are exclusively found in the last three fractions of the SDS gel (Figure 4.8). Since, this assay was devoid of liposomes to which the proteins could bind to and co-migrate with, the last three fractions (7-9) are defined as the unbound fraction and the first seven fractions (1-7) are defined as the bound fraction. Hereafter, this definition about bound and unbound fractions will be applied to all co-migration assays in this study.

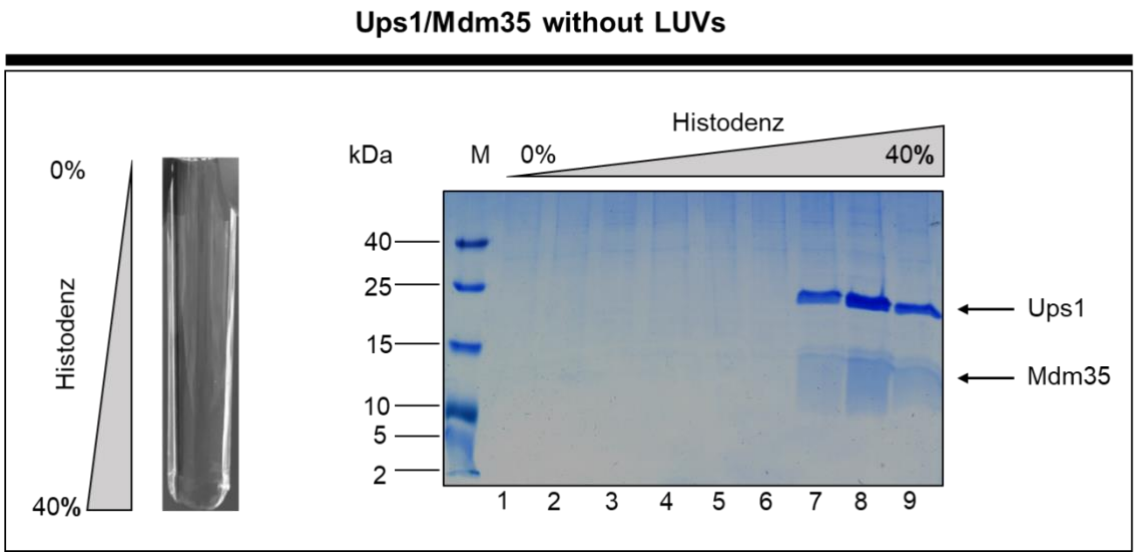

Figure 4.8: Control Flotation of Ups1/Mdm35 without LUVs.

A control flotation of Ups1/Mdm35 was performed in a Histodenz gradient at pH 5.5 in the absence of LUVs to see where the proteins are found after ultracentrifugation. A picture of the tube is shown after ultracentrifugation. Nine fractions were taken (1-9) and analysed by SDS-PAGE and Colloidal Coomassie stain. The first seven fractions (1-6) are defined as the "bound fraction". Ups1 and Mdm35 can be detected in the last three fractions (7-9) which are defined as the "unbound fraction". Samples were loaded on a 15% SDS gel. Spectra^{TM} Multicolor Low Range Protein Ladder was used as a protein standard marker "M".

In the next step we performed a pH-dependent co-migration assay for Ups1/Mdm35 with LUVs to characterize the binding affinity of the protein at different pH values. Here, the goal was to titrate the pH range in which the protein changed between bound and non-bound state to liposomes. We decided to use LUVs containing PC/PE/CL/PA (55:20:10:15) for our experiment, since these lipids are part of the inner mitochondrial membrane composition. We incubated the Ups1/Mdm35 complex with these liposomes at different pH ranging from pH 5.5. to pH 7.4. After incubation, the samples were separated in a Histodenz gradient via ultracentrifugation. Next, pictures of the tubes were taken showing the flotation pattern for each reaction (Figure 4.9). We took nine fractions of each tube and prepared them for SDS-PAGE analysis and quantified the corresponding band intensities of bound fraction (% total) that were seen on the SDS gels (Figure 4.9). We could clearly visualise a decrease in the bound fraction of Ups1 with increasing pH, confirming previously published data (Lu et al., 2020). In our assays, the strongest binding for Ups1 was detected at pH 5.5 where about 99 % of the protein was found in the bound fraction. On the contrary, the weakest binding for Ups1 was observed at pH 7.4 with 31 %. The turning point from the bound to the non-

bound state for Ups1 was between pH 6.5 and 7.0. Here, almost 70% of Ups1 was bound at pH 6.5 which was reduced to 46% at pH 7.0. For Mdm35 the situation was quite different. Mdm35, is actually known to dissociate from the Ups1 upon binding of the complex to the membrane *in vitro* (Connerth et al., 2012). In our flotation assays Mdm35 also co-migrated with the liposomes and fractions of bound Mdm35 could be detected at pH 5.5 (16%), pH 6.0 (20%) and 6.5 (10%).

At pH 7.0 and pH 7.4 no co-migration of Mdm35 could be observed. Moreover, we detected membrane bound fractions of an unspecific protein at pH. 5.5 to 6.5 with a size of more than 40 kDa on the SDS gels. Lastly, we further observed a change in the flotation pattern with an increase of pH (Figure 4.9). At pH 5.5 to pH 6.5 the liposomes migrated between the 0% and 5 % layer showing only one band. At pH 7.0 a second band appeared, which was clearly detectable at pH 7.4.

A

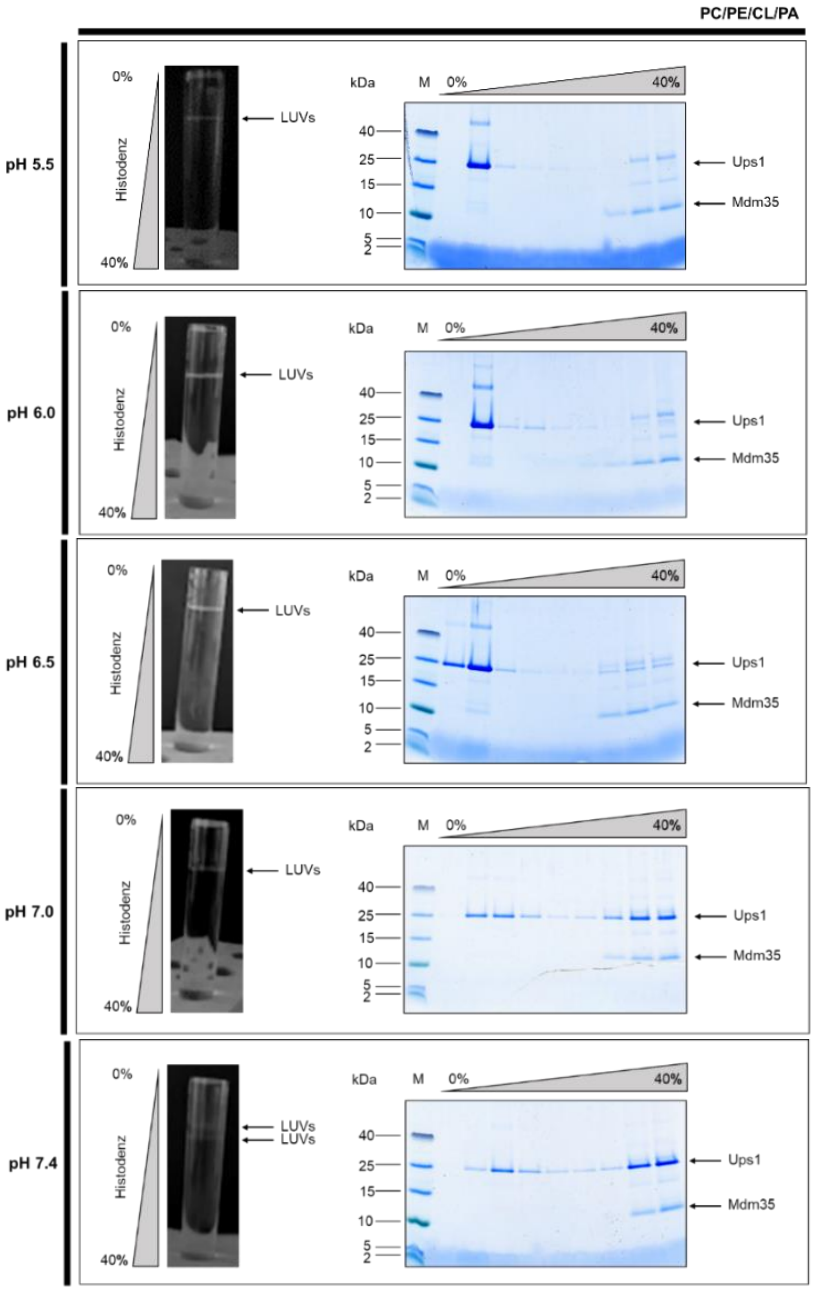

See figure B and the corresponding legend for A and B on the following page.

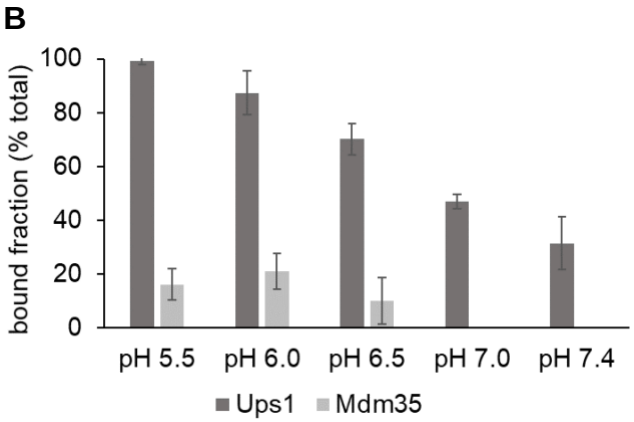

Figure 4.9: pH-dependent co-migration assay of Ups1/Mdm35 and LUVs.

pH-dependent co-migration assay of Ups1/Mdm35 with 200 nm LUVs composed of PC/PE/CL/PA (55:20:10:15). For the assay the protein was incubated with LUVs for 30 min at RT. After incubation samples were separated in a Histodenz gradient by ultracentrifugation. Images of each tube after ultracentrifugation are shown in the figure. Nine fractions were taken and analysed via SDS-PAGE and Colloidal Coomassie Stain. Spectra^{TM} Multicolor Low Range Protein Ladder was used as a protein standard marker "M" (A). Quantification of the bound fraction (% total) seen on the SDS gels. For each of the proteins Ups1 and Mdm35, the sum of band intensities in all nine fractions was set to 100%. Here, the quantification was done for three independent experiments and values for bound fraction (% total) are shown as the mean. The error bar represents the SD (B).

4.3.2 Determination of the K_D at different pH for Ups1/Mdm35 to membranes containing PC/PE/CL/PA

Despite the availability of several studies about the structure and transfer ability of Ups1/Mdm35, the biophysical parameters such as a binding constant have not been systematically characterized. Thus, we aimed to study the membrane binding affinities of Ups1/Mdm35 at different pH values. Our goal was to determine the dissociation constant K_D which is a quantitative measure for the binding affinity of a protein to a ligand, in this case the membrane. To determine the K_D of Ups1/Mdm35 for lipids, we used reflectrometric interference spectroscopy (RIfS). All experiments were done in a collaboration with the group of Prof. Dr. Andreas Janshoff and all RIfS measurements were performed by Dr. Marian Vache at the Institute of Physical Chemistry, University of Göttingen. RIfS measurements were conducted for Ups1/Mdm35 at pH 5.5; pH 6.0; pH 6.5; pH 7.0. and pH 7.4. We decided to test the same lipid mixture PC/PE/CL/PA (55:20:10:15) that we were using just previously for our co-sedimentation assays (see chapter 4.3.1). The K_D for the respective pH values was obtained by a Langmuir fit (Figure 4.10; Table 4.1).

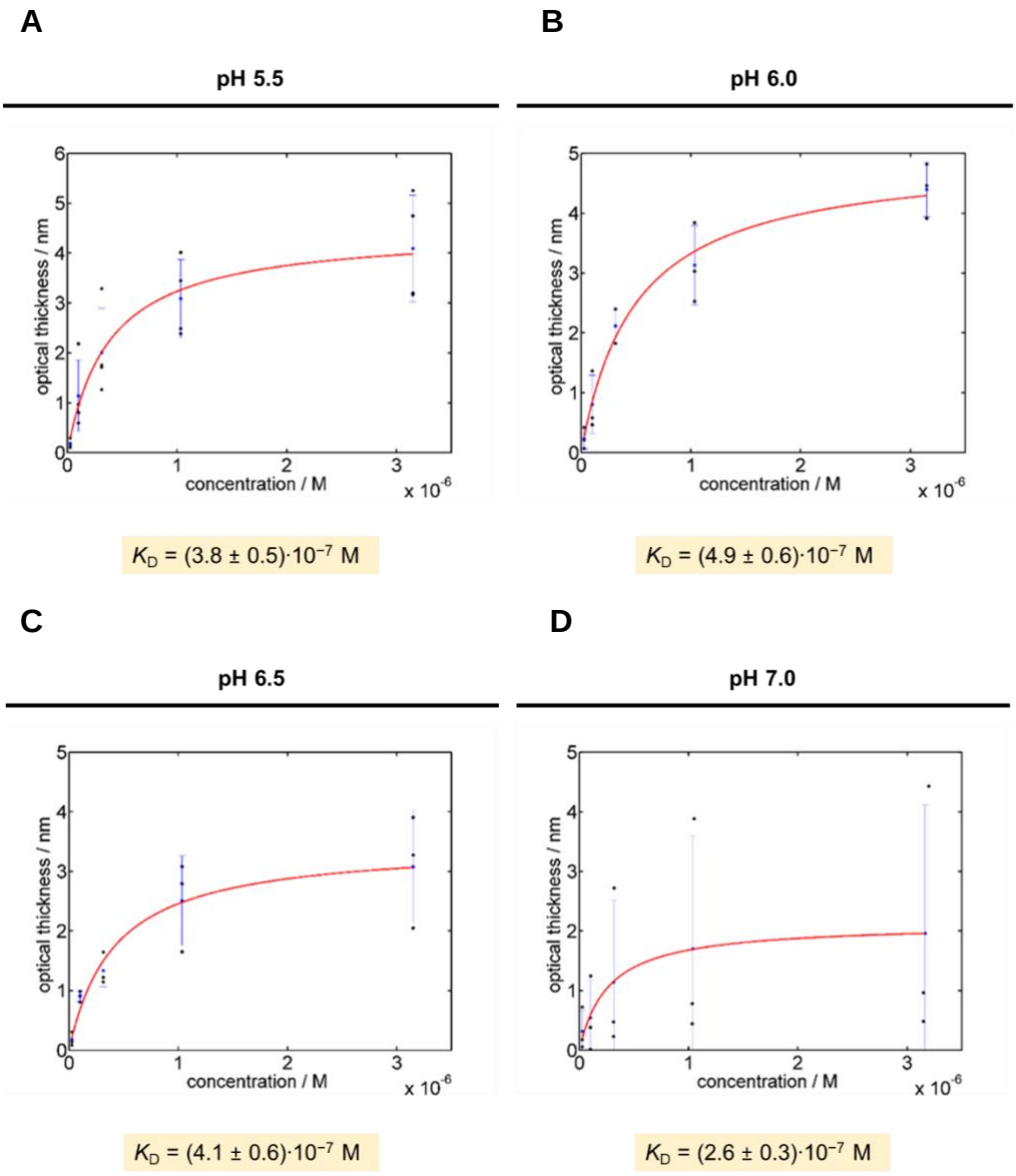

Figure 4.10: Langmuir fit of the optical thicknesses of PC/PE/CL/PA (55:20:10:15) at different pH values upon binding of Ups1/Mdm35.

The values of individual measurements are shown by black circles. The blue circles indicate the mean at the corresponding concentration. The standard deviation of the blue circles is indicated by the error bar. The red curve represents the Langmuir fit of the mean values. The Langmuir fit of the means results in a dissociation constant of $K_D = (3.8 \pm 0.5)\cdot10^{-7}$ M (N = 4) for pH 5.5; $K_D = (4.9 \pm 0.6)\cdot10^{-7}$ M (N = 3) for pH 6.0; $K_D = (4.1 \pm 0.6)\cdot10^{-7}$ M (N = 3) for pH 6.5; $K_D = (2.6 \pm 0.3)\cdot10^{-7}$ M (N = 3) for pH 7.0. Measurements were performed by Dr. Marian Vache.

Table 4.1: Determination of the dissociation constant K_D for Ups1/Mdm35 binding to PC/PE/CL/PA (55:20:10:15) containing membranes at different pH values. The K_D was obtained by calculating mean values and standard deviations of individual fit and by fitting the mean values at each concentration and condition.

experiment	K_D from mean of individual fits / µM	K_D results from fit of means / µM
Ups1/Mdm35 pH 5.5	0.45 ± 0.25	0.38 ± 0.05
Ups1/Mdm35 pH 6.0	0.48 ± 0.14	0.49 ± 0.06
Ups1/Mdm35 pH 6.5	0.41 ± 0.28	0.41 ± 0.06
Ups1/Mdm35 pH 7.0	0.35 ± 0.19	0.26 ± 0.03

All RIfS measurements were performed by Dr. Marian Vache

We plotted the values of the fits of individual measurements with the corresponding standard deviation from Table 4.1 (Figure 4.11). Through our RIfS measurements we obtained the smallest K_D at pH 7.0 for Ups1/Mdm35 binding to membranes composed of PC/PE/CL/PA (55:20:10:15). Thus, Ups1/Mdm35 showed highest affinity to membranes at this pH 7.0.

At pH 7.4 no binding of Ups1/Mdm35 to lipids could be observed in all of our RIfS studies.

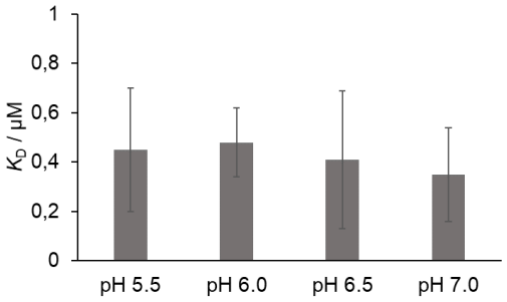

Figure 4.11: Plot of the K_D for Ups1/Mdm35 binding to PC/PE/CL/PA (55:20:10:15) containing membranes.

The K_D values from mean of individual fits are plotted with their corresponding standard deviation for the wild type Ups1/Mdm35 at different pH values. Measurements were performed by Dr. Marian Vache.

4.3.3 Determination of the K_D for the mutant Ups1^{L62AW65A}/Mdm35 to membranes containing PC/PE/CL/PA

In a next step, we wanted to test the mutant Ups1^{L62AW65A}/Mdm35 for its binding affinities and compared it to the wild type. This mutant has a double mutation in the hydrophobic Ω-loop of Ups1 (Miliara et al., 2015). The Ω-loop of Ups1 was found to act as a lid for the lipid binding pocket of the LTP (Watanabe et al., 2015; Yu et al., 2015) and mutations in this loop region impaired the lipid transfer activity of the Ups1/Mdm35 complex (Lu et al., 2020; Miliara et al., 2015; Watanabe et al., 2015).

Before starting with RIfS measurements for Ups1^{L62AW65A}/Mdm35, we first wanted to test if it is actually binding to the lipid composition in our LUVs. Thus, we did a co-migration assay with the Ups1$^{L62AW65A/}$Mdm35 complex at pH 5.5 using liposomes composed of PC/PE/CL/PA (55:20:10:15). Sample were separated in a Histodenz gradient via ultracentrifugation (Figure 4.12, A). The quantification of the SDS gel (Figure 4.12; B) showed that almost 93 % of Ups1^{L62AW65A} was found in the membrane bound fraction. Further, 21 % of Mdm35 could be detected in the bound fraction on the gel while most of it was found in the unbound fraction. All in all, the mutant Ups1^{L62AW65A} showed a similar binding behaviour like the previously investigated wild type Ups1/Mdm35 under same reaction conditions.

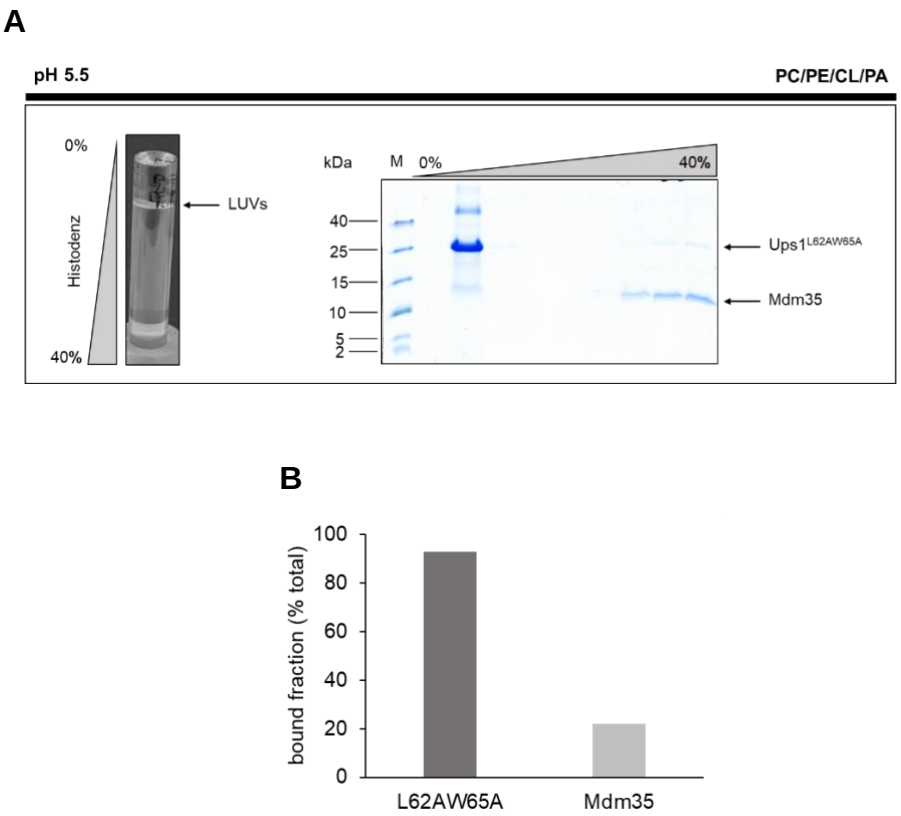

Figure 4.12: Co-migration assay for the mutant Ups1^{L62AW65A}/Mdm35 with LUVs.

Co-migration assay of the mutant Ups1^{L62AW65A}/Mdm35 with 200 nm LUVs composed of PC/PE/CL/PA (55:20:10:15). For the assay the protein was incubated with LUVs for 30 min at RT. After incubation samples were separated in a Histodenz gradient by ultracentrifugation. Image of the tube after ultracentrifugation is shown in the figure. Nine fractions were taken and analysed via SDS-PAGE and Colloidal Coomassie Stain. Spectra^{TM} Multicolor Low Range Protein Ladder was used as a protein standard marker "M" (A). Quantification of the bound fraction (% total) for each of the proteins seen on the SDS-Gels (B).

After confirming the binding properties of the mutant, we performed RIfS measurements at pH 5.5. and compare them to the wild type Ups1/Mdm35 protein complex. We could successfully obtain a K_D by a Langmuir fit of the optical thickness of Ups1^{L62AW65A}/Mdm35 binding to membranes containing PC/PE/CL/PA (55:20:10:15) at pH 5.5 (Figure 4.13, Table 4.2). Strikingly, the dissociation constant for Ups1^{L62AW65A}/Mdm35 $K_D = (3.6 \pm 0.4)\cdot10^{-7}$ M was similar to that of the wild type $K_D = (3.8 \pm 0.4)\cdot10^{-7}$ M at pH 5.5. The mutant was further tested at pH 7.4. Here again, similar as for the wild type, the mutant did not bind to our lipid mixture PC/PE/CL/PA (55:20:10:15) at pH 7.4.

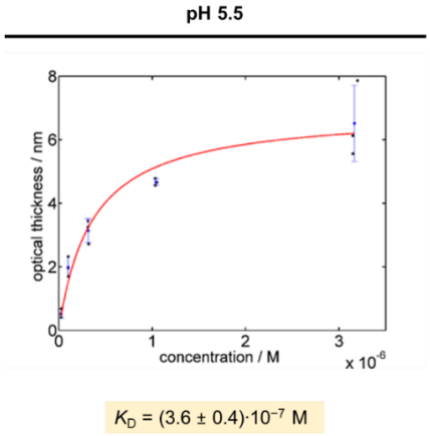

Figure 4.13: Langmuir fit of the optical thickness of Ups1^{L62AW65A}/Mdm35 binding to a membrane composed of PC/PE/CL/PA (55:20:10:15) at pH 5.5.

The values of individual measurements are shown by black circles. The blue circles indicate the mean at the corresponding concentration. The standard deviation of the blue circles is indicated by the error bar. The red curve represents the Langmuir fit of the mean values. The Langmuir fit of the means results in a dissociation constant of $K_D = (3.6 \pm 0.4) \cdot 10^{-7}$ M (N = 3). Measurements were performed by Dr. Marian Vache.

Table 4.2: Determination of the dissociation constant K_D for Ups1^{L62AW65A}/Mdm35 binding to PC/PE/CL/PA (55:20:10:15) containing membranes at pH 5.5. The K_D was obtained by calculating mean values and standard deviations of individual fit and by fitting the mean values at each concentration and condition.

experiment	K_D from mean of individual fits / µM	K_D results from fit of means / µM
Ups1/Mdm35 pH 5.5*	0.45 ± 0.25	0.38 ± 0.05
Ups1^{L62AW65A}/Mdm35 pH 5.5	0.45 ± 0.39	0.36 ± 0.04

* already measured and shown in Table 4.1. All RIfS measurements were performed by Dr. Marian Vache.

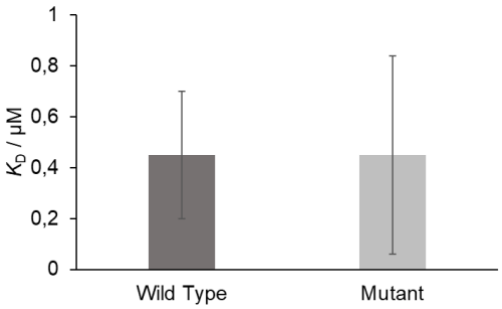

Figure 4.14: Plot of the K_D for the wild type Ups1/Mdm35 and the mutant Ups1^{L62AW65A}/Mdm35 binding to membranes composed of PC/PE/CL/PA (55:20:10:15) at pH 5.5.

The K_D from mean of individual fits are plotted with their corresponding standard deviation for the wild type Ups1/Mdm35 at different pH values. At pH 5.5 the values for the mutant Ups1^{L62AW65A} are also plotted. Measurements were performed by Dr. Marian Vache.

Despite similar K_D values for Ups1/Mdm35 and Ups1^{L62AW65A}/Mdm35 (Figure 4.14), both complexes showed a strong difference in their optical thickness at pH 5.5 where the values for the mutant were bigger compared to that of the wild type. From RIfS measurements, the optical thickness at the highest protein concentration was extracted and plotted and is shown in the following (Figure 4.15).

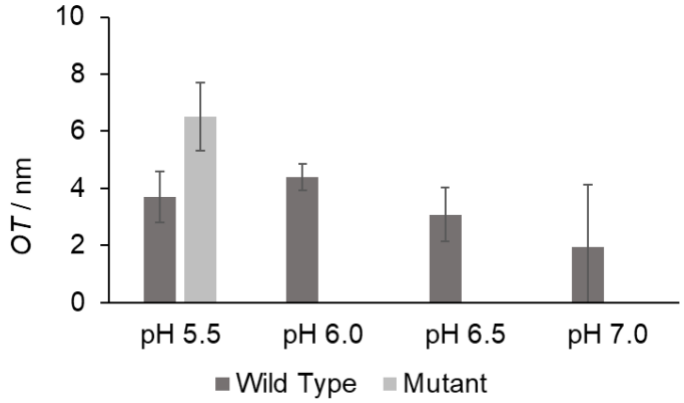

Figure 4.15: The optical thickness at the maximum protein concentration plotted for the wild type Ups1/Mdm35 and the mutant Ups1^{L62AW65A}/Mdm35.

The mean of the optical thickness at the maximum protein concentration is plotted in this figure for the wild type Ups1/Mdm35 and the mutant Ups1^{L62AW65A}/Mdm35. The error bar corresponds to the standard deviation. Measurements were performed by Dr. Marian Vache.

4.3.4 Charge-dependent binding of Ups1/Mdm35 to LUVs

In previous studies it was shown that Ups1 prefers binding to negatively charged lipids in *in vitro* flotation assays (Connerth et al., 2012). One observation that we made when starting to perform co-migration assays was that binding of Ups1 was the strongest when our LUV composition contained CL, similar to what was previously shown (Connerth et al., 2012). CL is a cone shaped lipid carrying two negative charges. In contrast to CL, the lipids PA and PS have only one negative charge (Holthuis & Menon, 2014; Kay & Grinstein, 2011). In previous studies, it was shown that binding of Ups1 to PA or PS containing liposomes was weaker compared to CL, when same mol-% of these lipids were used in the assays (Connerth et al., 2012).

In this study, we performed a charge dependent co-migration assay for Ups1/Mdm35 at pH 5.5 with LUVs containing varying concentrations of negatively charged lipids. Samples of each flotation were prepared for SDS-PAGE and the band intensities on each gel were quantified and bound fraction (% total) of Ups1 and Mdm35 are shown (Figure 4.16). We could observe that binding of Ups1 and Mdm35 was the strongest when LUVs contained 15% CL, since almost 91 % of Ups1 and 15 % of Mdm35 were found in the bound fraction (Figure 4.16, A and B). When we did the same flotation for LUVs in the absence of CL and with 15 % PA instead, only ~ 24 % of Ups1 and ~ 8 % of Mdm35 were found in the bound fraction on the SDS gel (Figure 4.16; C and D). Moreover, we increased binding of Ups1 (~ 81 %) to LUVs containing 30 % PA by adjusting the net charge to that of CL whereas no Mdm35 was found in the bound fraction of the gel anymore (Figure 4.16; E and F). The flotation of Ups1/Mdm35 with LUVs containing 15% PS showed that only 11 % of Ups1 and no Mdm35 were found in the bound fraction (Figure 4.16, G and H). Here again, we could increase binding of Ups1 to 67 % when we took LUVs with 30% PS to mimic the net charge of 15 % CL (Figure 4.16, I and J).

A

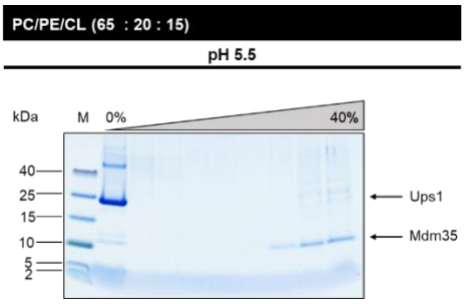

B

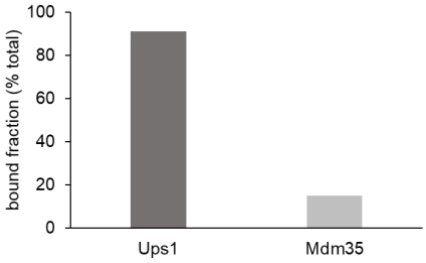

C

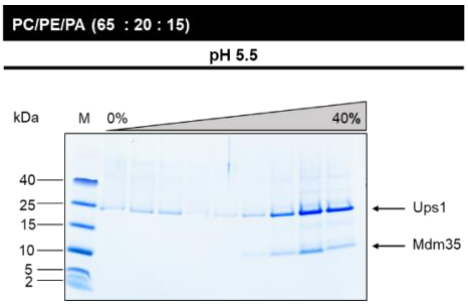

D

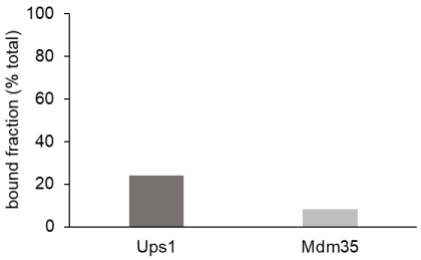

E

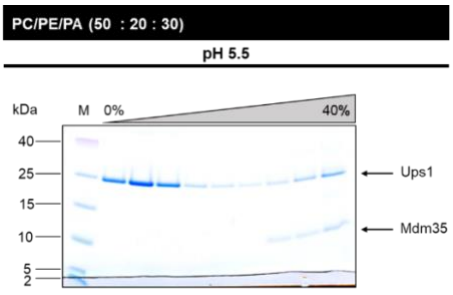

F

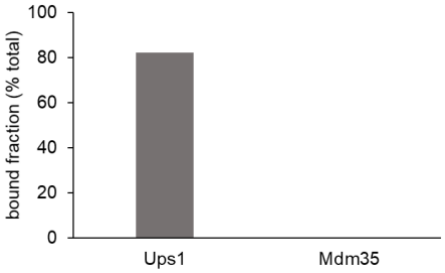

See figure G-J and legend on the following page.

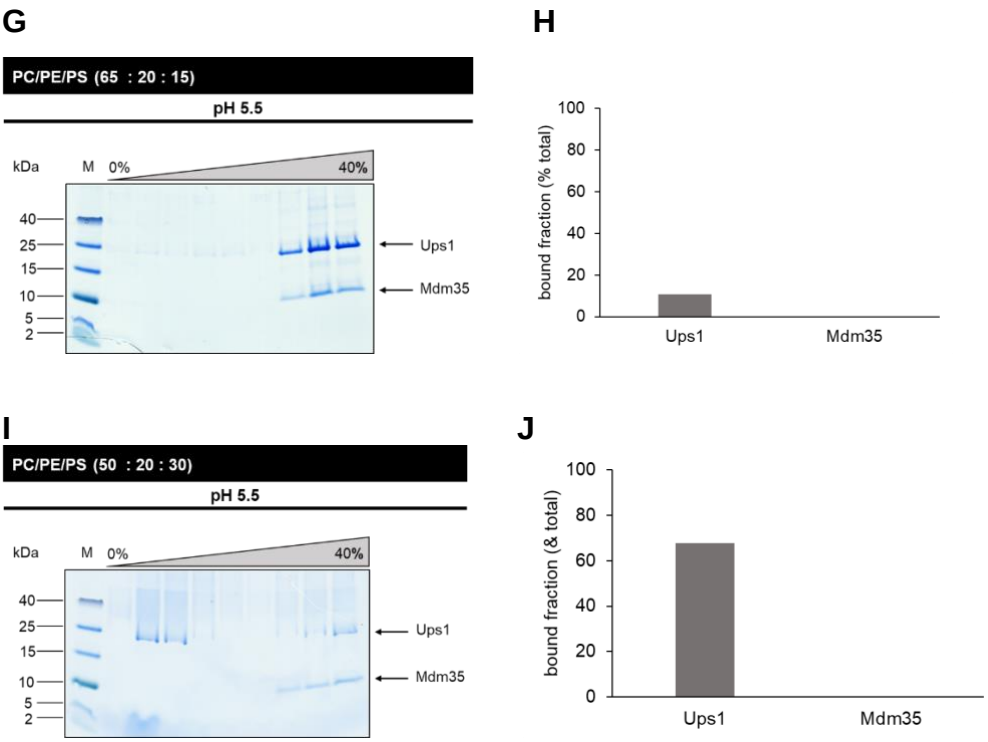

Figure 4.16: Co-migration assay for Ups1/Mdm35 with LUVs containing different negatively charged lipids.

Co-migration assay of Ups1/Mdm35 with 400 nm LUVs containing different negatively charged lipids PC/PE/CL (65:20:15) (A); PC/PE/PA (65:20:15) (C); PC/PE/PA (50:20:30) (E); PC/PE/PS (65:20:15) (G); PC/PE/PS (50:20:30) (I). Samples were separated in a Histodenz gradient by ultracentrifugation. Nine fractions were taken and analysed via SDS-PAGE and Colloidal Coomassie Stain. Spectra^{TM} Multicolor Low Range Protein Ladder was used a protein standard marker “M”. Quantification of the bound fraction (% total) for Ups1 and Mdm35 are shown next to the corresponding SDS gels (B, D, F, H, J).

4.4 Ups1/Mdm35 changes the morphology of LUVs

Although the structure and function of the Ups1/Mdm35 complex has been extensively investigated, the detailed mechanism of the LTP mediated transfer of PA remains elusive. Recently, work by Lu et al., gave some insight into the molecular mechanism of the intramitochondrial PA transport by Ups1/Mdm35 (Lu et al., 2020). However, little is known about the energy costs for extracting a lipid from a membrane by Ups1/Mdm35 and even more interestingly, how this LTPs is able to decrease the energy barrier by accelerating this seemingly energetically unfavourable reaction.

The Ups1/Mdm35 complex has a hydrophobic Ω-loop that interacts with the membrane (Watanabe et al., 2015; Yu et al., 2015). We investigated if membrane interaction of this loop causes membrane packing defects that could result in membrane curvature induction. Positive results would support our hypothesis that curvature induction of Ups1/Mdm35 might play an important role for its mechanism and help in the extraction of a lipid from a membrane.

In order to analyse if Ups1/Mdm35 induces membrane curvature and deformation on liposomes, we visualized the morphology of LUVs in the absence and presence of the protein complex through transmission electron microscopy (TEM). We decided to test LUVs containing PC/PE/PA (50:20:30) for which we could already show strong binding to Ups1 (see chapter 4.3.4). Indeed, we made the interesting finding that 33 % of LUVs were deformed in the presence of Ups1/Mdm35 (20µM) (Figure 4.17).

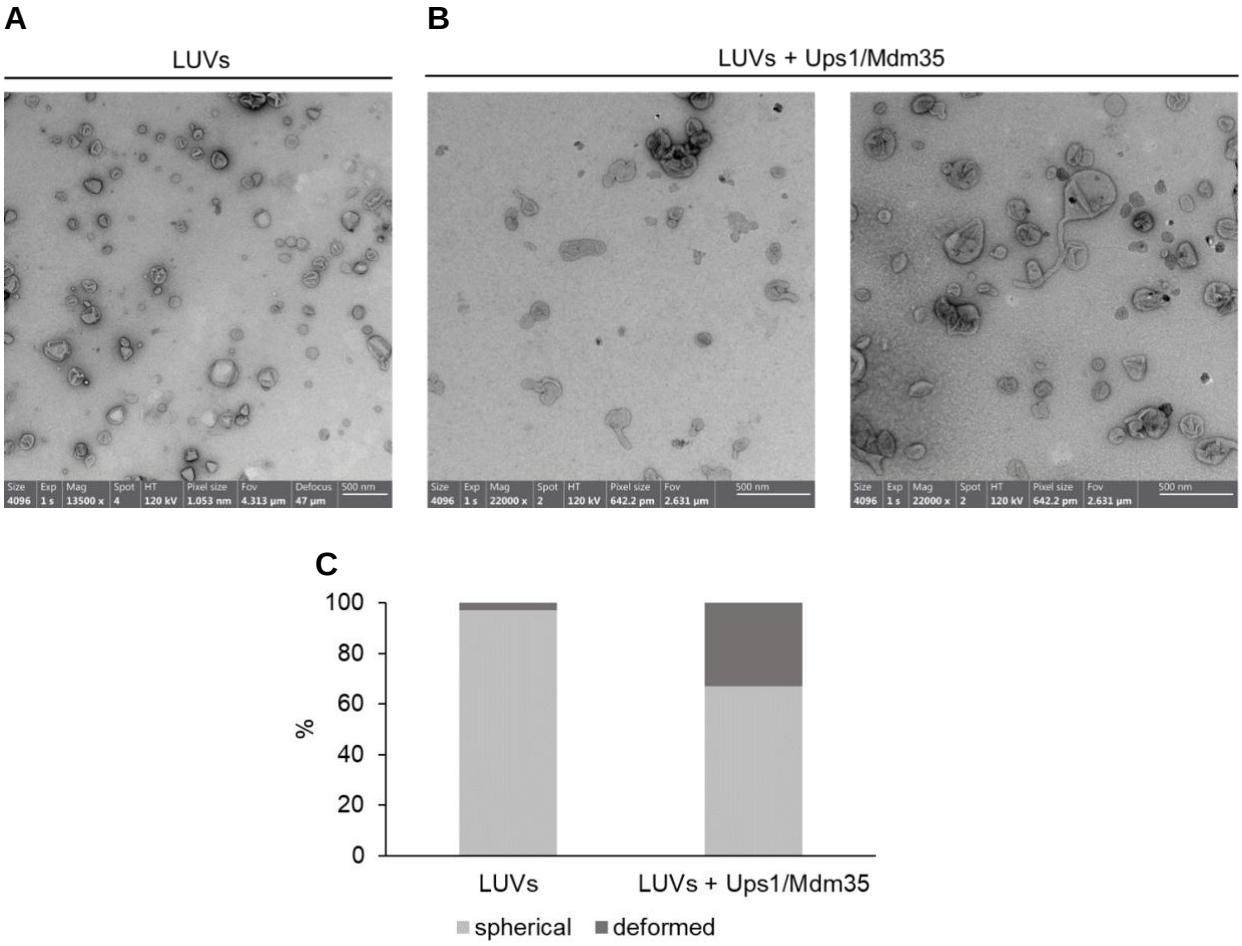

Figure 4.17: The Ups1/Mdm35 complex induces membrane deformation of LUVs.

Electron micrographs of liposomes (LUVs) in the absence (A) and presence (B) of the protein complex Ups1/Mdm35 (20 µM) are shown in this figure. LUVs are composed of PC/PE/PA (50:20:30). (C) Quantification of spherical and deformed shapes in control LUVs and in LUVs after incubation with Ups1/Mdm35. A minimum of 200 membranous structures were counted per condition. Scale bar correspond to 500 nm as indicated on the images. Images were taken by Gudrun Heim, Department of Structural Dynamics (Electron Microscopy), Max Planck Institute for Multidisciplinary Sciences, Göttingen.

4.5 *in silico* and *in vitro* curvature-dependent binding of Ups1/Mdm35

4.5.1 Molecular Dynamics simulation studies show that Ups1/Mdm35 is a membrane curvature sensing protein complex

A challenge when studying membrane curvature induction and membrane curvature sensing is that there might be no clear-cut differentiation between these two mechanisms. A protein that acts initially as a membrane curvature sensor might cause membrane curvature at high protein concentration on liposomes by a mass action effect which would mask its ability to rather sense curvature in the first place (Antonny, 2011).

So far, our results highly suggested that Ups1/Mdm35 complex showed curvature inducing abilities. In order to investigate if the Ups1/Mdm35 complex also acts as a membrane curvature sensor, we used molecular dynamics (MD) simulation. The MD simulation were done in collaboration with the group of Prof. Dr. Herre Jelger Risselada and all simulations were performed by Kai Stroh (Institute for Theoretical Physics, University of Göttingen and Department of Physics, Technical University of Dortmund).

For the simulation, a membrane composed of POPC, POPE and POPA was compressed in x-direction resulting in a buckled shape providing regions of zero curvature as well as negative and positive curvature. Along this buckled membrane the Ups1/Mdm35 complex was pulled *in silico*. Through a combination of the buckled membrane with an umbrella sampling the relative binding (partitioning) free energy was determined as a function of membrane curvature for Ups1/Mdm35 (Figure 4.18) according to a previously published method (Stroh & Risselada, 2021). For a membrane curvature ranging from -0.188 nm^{-1} (K_{min}) to +0.188 nm^{-1} (K_{max}) we obtained a change in the binding (partitioning) free energy of $\Delta F = 9.2\ k_bT \pm 1.5\ k_bT$ (95 % confidence interval). Here, Ups1/Mdm35 showed a preferred partitioning to membrane regions of positive curvature compared to zero curvature while binding to negative curvature was even more unfavourable. Strikingly, we confirmed our hypothesis that the Ups1/Mdm35 complex is a sensor for positively curved membranes.

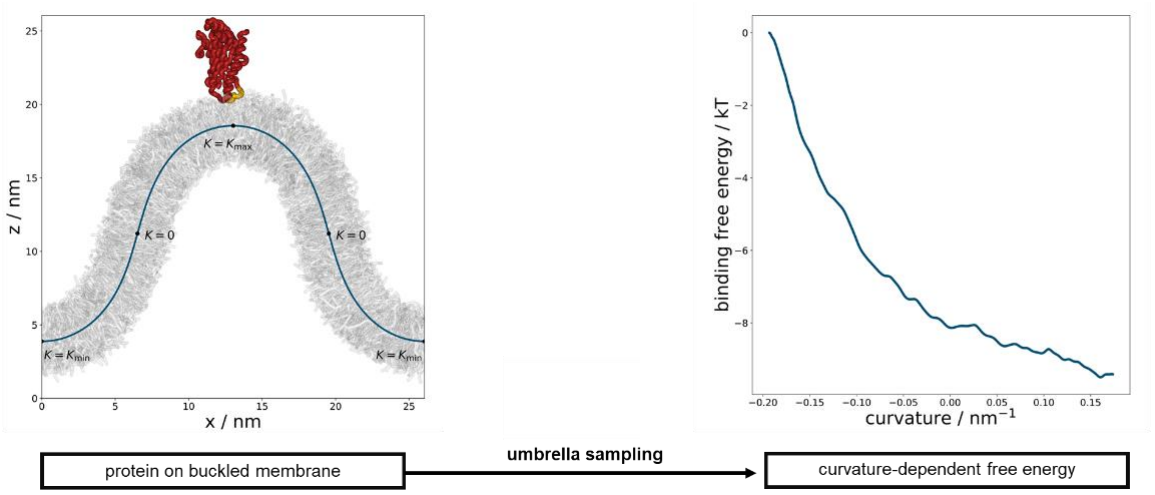

Figure 4.18: Ups1/Mdm35 is a membrane curvature sensing protein complex.

MD simulation of Ups1/Mdm35 (shown in red, with its hydrophobic loop shown in yellow) on a buckled membrane. The analytical membrane shape is described in the figure providing regions of positive curvature (convex), no curvature (flat) and negative curvature (concave) with K standing for curvature where K = K_{max} defines the maximum curvature, K = 0 describes no/zero curvature and K = K_{min} is the minimum curvature (left panel). The relative binding (partitioning) free energy as a function of membrane curvature that is obtained after umbrella sampling (right panel). This entire experiment was performed by Kai Stroh.

After successfully demonstrating that the LTP Ups1/Mdm35 is a curvature sensor, the next step was to show that a desorption of POPA is energetically favourable at regions of positive curvature which would further support our hypothesis that Ups1 binds to membrane regions that facilitate lipid extraction. Hence, we used the same buckled membrane in the absence of the protein and determined the desorption free energy for POPA via MD simulation and the so called Bennett Acceptance Ratio (BAR) method (Bennett, 1976). The aim was to obtain the POPA desorption free energy from regions of zero as well as negative and positive curvature. As expected, we found that the desorption of POPA from a positively curved membrane region was energetically favourable showing the lowest energy costs with 99.65 ± 0.82 kJ/mol (Table 4. ***3***). In comparison to that the POPA desorption free energy from a flat membrane (zero curvature) region with 100.08 ± 0.42 kJ/mol was higher. Again, the desorption from POPA from a negatively curved membrane region (103.18 ± 1.05 kJ/mol) was energetically even more unfavourable.

Table 4. 3: POPA desorption free energy at different regions of curvature on a buckled membrane in the absence of protein.

POPA desorption free energy (kJ/mol)	ΔF_{des}	$\Delta\Delta F_{des}$
zero curvature (flat membrane region)	100.08 ± 0.42	0
negative curvature	103.18 ± 1.05	3.10
positive curvature	99.65 ± 0.82	-0.43

This entire experiment was performed by Kai Stroh.

4.5.2 Curvature dependent binding of Ups1/Mdm35 shows that the protein prefers binding to SUVs over LUVs

Overall, our *in silico* MD data revealed that Ups1/Mdm35 is a curvature sensing protein complex. As a next step, we wanted to perform an *in vitro* assay in order to confirm our findings. We decided to perform a flotation assay for Ups1/Mdm35 using liposomes with various sizes providing different intrinsic curvature.

When using the Helfrich theory, one can determine the shape of a local deformation on a membrane by the two principal curvatures, $C_1 = 1/R_1$ and $C_2 = 1/R_2$ where R_1 and R_2 are the principal radii of curvature whereas the total curvature J is defined by $J = C_1 + C_2$ (Bassereau et al., 2014; Helfrich, 1973; Shibata et al., 2009; Zimmerberg & Kozlov, 2006).

We started to generate 50 nm SUVs composed of PC/PE/PA (65:20:15) and performed a co-migration assay with Ups1/Mdm35 to compare the results with those that we were previously showing for 400 nm LUVs in chapter 4.3.4 (Figure 4.16, A and B) with the same lipid composition. After flotation the samples were prepared for SDS-PAGE. Both co-migration assays are shown and quantified for 50 nm and 400 nm liposomes, respectively (Figure 4.19, A and B). When the flotation assay was performed with 400 nm LUVs, 81 % of Ups1 was found in the bound fraction of the gel. At increased curvature of the liposomes, when using 50 nm SUVs instead, binding of Ups1 could be maximized to 100 % indicating and verifying the curvature sensing ability for Ups1. Additionally, an unspecific band above ~ 40 kDa appeared in the membrane bound protein fraction on the gel.

Besides that, we see no binding of Mdm35 under this condition in both of our flotation assay with 50 nm and 400 nm liposomes, respectively.

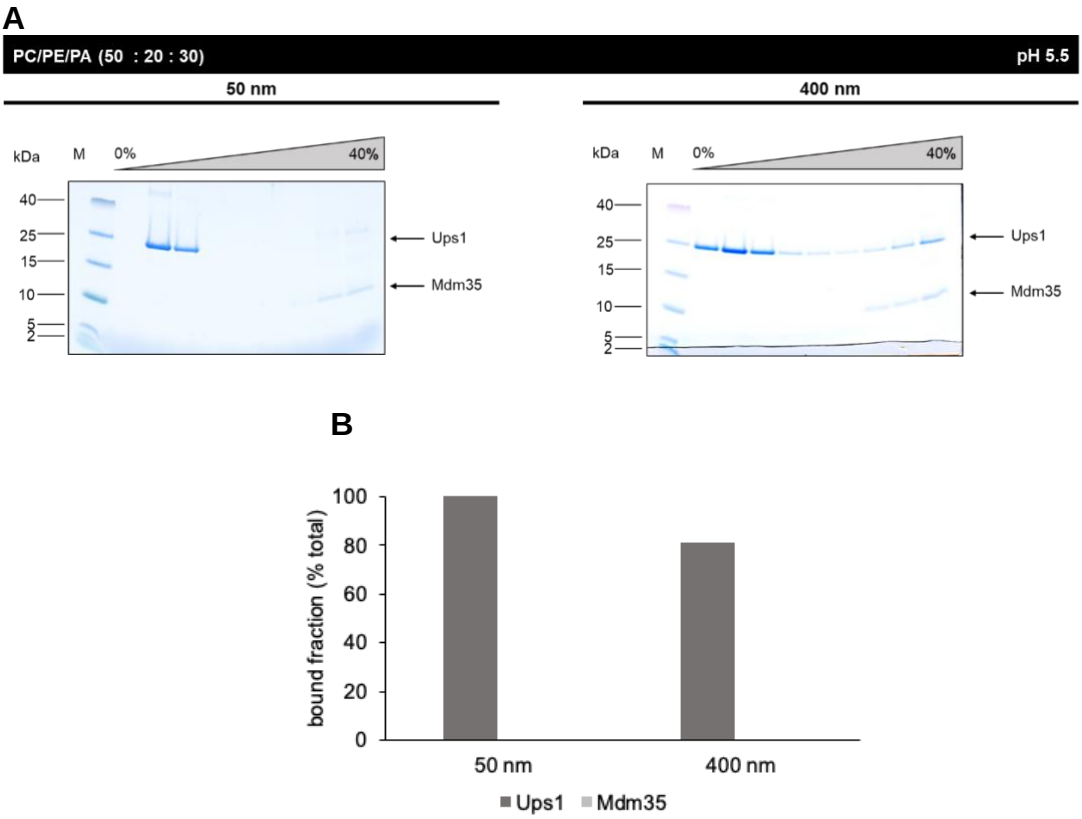

Figure 4.19: Co-migration of Ups1/Mdm35 with SUVs and LUVs of different intrinsic curvature.

Co-migration assay of Ups1/Mdm35 with different intrinsically curved SUVs (50 nm; high curvature) and LUVs (400 nm; small curvature) composed of PC/PE/PA (50:20:30). For each flotation assay the protein was incubated with liposomes for 30 min at RT and pH 5.5. After incubation samples were separated in a Histodenz gradient by ultracentrifugation. Nine fractions were taken and analysed via SDS-PAGE and Colloidal Coomassie Stain. Spectra^{TM} Multicolor Low Range Protein Ladder was used a protein standard marker “M” The flotation gel for 400 nm (here right panel in A) and its quantification (here in B) are taken from (Figure 4.16, A and B) and shown here again for a better comparison (A). Quantification of the bound fraction (% total) for Ups1 and Mdm35 (B).

Next, we wanted to see if we are able to enhance curvature sensing ability for Ups1/Mdm35 under different lipid compositions. Moreover, we increased the curvature difference of small and large liposomes by using highly curved 30 nm SUVs and 800 nm LUVs with small intrinsic curvature. We performed a flotation assay for Ups1/Mdm35 with 30 nm or 800 nm liposomes containing only 15 % PA (Figure 4.20, A and B). Here, again we observed a curvature sensing ability of Ups1 and an increased membrane binding of 60 % to the highly curved 30 nm SUVs compared to 800 nm LUVs where only 39 % of the protein has bound to.

Strikingly, Mdm35 was found with same amounts (~ 24%) in the bound fractions of both gels, hence, showing no curvature sensing ability.

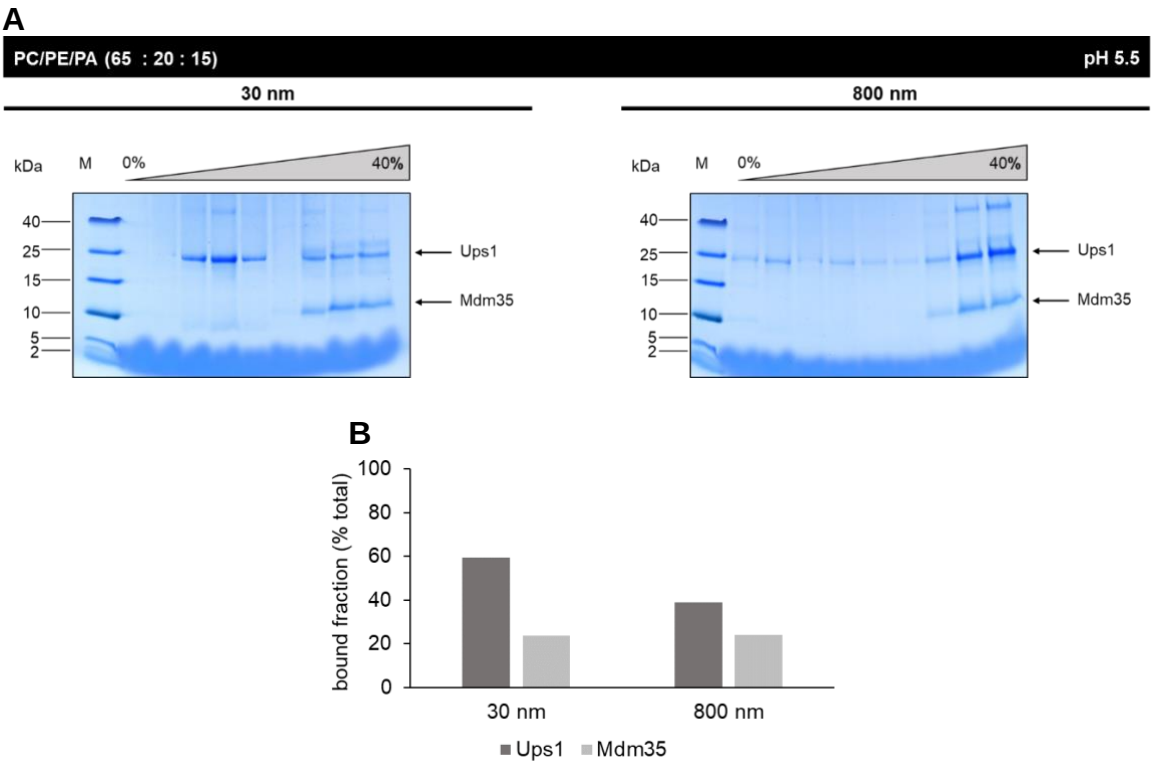

Figure 4.20: Co-migration of Ups1/Mdm35 with SUVs and LUVs of different intrinsic curvature.

Co-migration assay of Ups1/Mdm35 with different intrinsically curved SUVs (30 nm; high curvature) and LUVs (800 nm; small curvature) composed of PC/PE/PA (65:20:15). For each flotation assay the protein was incubated with liposomes for 30 min at RT and pH 5.5. After incubation samples were separated in a Histodenz gradient by ultracentrifugation. Nine fractions were taken and analysed via SDS-PAGE and Colloidal Coomassie Stain. Spectra^{TM} Multicolor Low Range Protein Ladder was used a protein standard marker “M” (A). Quantification of the bound fraction (% total) for Ups1 and Mdm35 (B).

We further tested 30 nm or 800 nm liposomes containing 10% PA and 15% CL for a co-migration with Ups1/Mdm35 (Figure 4.21, A and B). Here, the addition of CL to our lipid composition already resulted in a 100% binding of Ups1 independent from the size and curvature of the liposomes. Interestingly, 22 % of Ups1/Mdm35 was found in the bound fraction on the gel when the flotation was performed with 800 nm LUVs. Here again, an unspecific protein of more than 40 kDa in size, co-migrated with the SUVs and LUVs, respectively.

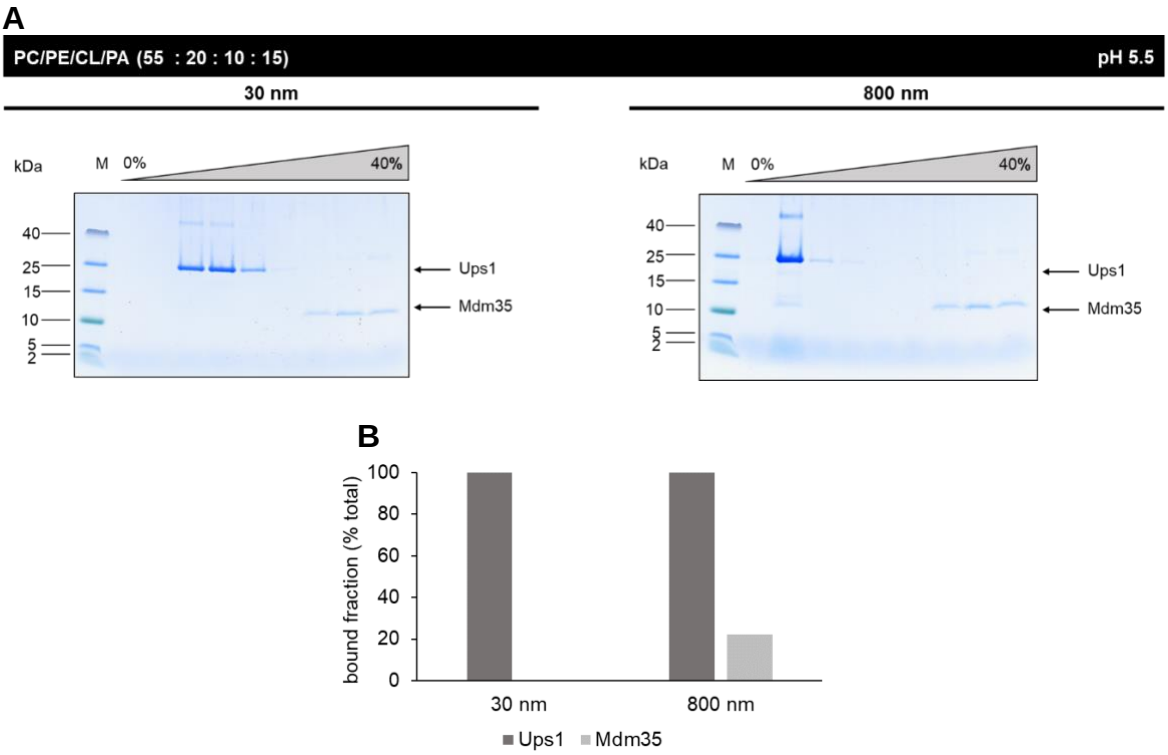

Figure 4.21: Co-migration of Ups1/Mdm35 with SUVs and LUVs of different intrinsic curvature.

Co-migration assay of Ups1/Mdm35 with different intrinsically curved SUVs (30 nm; high curvature) and LUVs (800 nm; small curvature) composed of PC/PE/CLPA (55:20:10:15). For each flotation assay the protein was incubated with liposomes for 30 min at RT and pH 5.5. After incubation samples were separated in a Histodenz gradient by ultracentrifugation. Nine fractions were taken and analysed via SDS-PAGE and Colloidal Coomassie Stain. Spectra^{TM} Multicolor Low Range Protein Ladder was used a protein standard marker "M" (A). Quantification of the bound fraction (% total) for Ups1 and Mdm35 (B).

In conclusion, our data showed a curvature sensing ability of Ups1/Mdm35 that depended on a specific interplay between lipid composition and curvature of liposomes. Also, lipid binding and curvature sensing was shown to be attributed to Ups1 only. In order to find out, if the hydrophobic Ω-loop of the Ups1 protein might be the actual part of the protein sensing curvature, we decided to test the Ups1^{L62AW65A}/Mdm35 mutant for its curvature sensing ability. We performed a flotation assay for the mutant with 30 nm or 800 nm liposomes composed of PC/PE/PA (65:20:15) (Figure 4.22, A and B). Indeed, quantification of the gel confirmed that the double mutation in the Ω-loop disturbed the curvature sensing ability where only 35 % of the mutant was found in the bound fraction to highly

curved liposomes whereas more protein was found in the bound fraction with 800 nm liposomes.

A

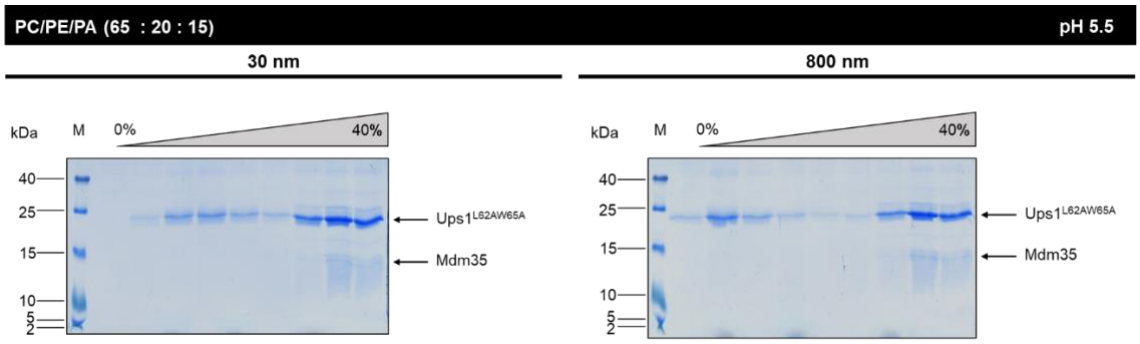

B

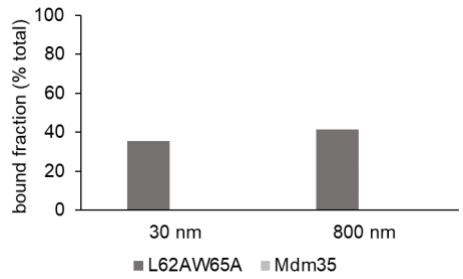

Figure 4.22: Co-migration of Ups1^{L62AW65A}/Mdm35 with SUVs and LUVs of different intrinsic curvature.

Co-migration assay of Ups1^{L62AW65A}/Mdm35 with different intrinsically curved SUVs (30 nm; high curvature) and LUVs (800 nm; small curvature) composed of PC/PE/PA (65:20:15). For each flotation assay the protein was incubated with liposomes for 30 min at RT and pH 5.5. After incubation samples were separated in a Histodenz gradient by ultracentrifugation. Nine fractions were taken and analysed via SDS-PAGE and Colloidal Coomassie Stain. Spectra^{TM} Multicolor Low Range Protein Ladder was used a protein standard marker "M" **(A)**. Quantification of the bound fraction (% total) for Ups1 and Mdm35 **(B)**.

4.6 The Ups1/Mdm35 complex tethers artificial membrane vesicles *in vitro*

An interesting observation that we made at a very early stage of our electron microscopy studies, was that the Ups1/Mdm35 complex did not only change the morphology of LUVs (see chapter 4.4) but also caused a strong clustering of liposomes (Figure 4.23).

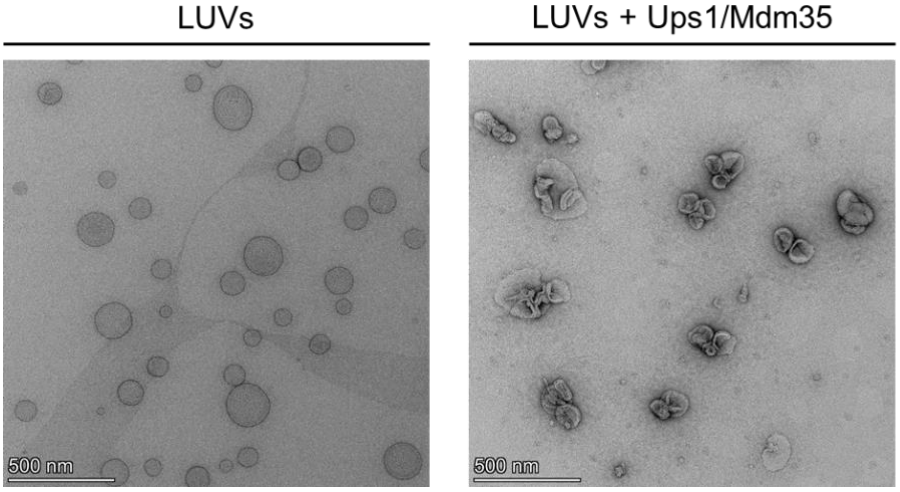

Figure 4.23: The Ups1/Mdm35 complex causes strong clustering of LUVs.

Electron micrographs of lisosomes (LUVs) in the absence (left panel) and presence (right panel) of the protein complex Ups1/Mdm35. LUVs are composed of PC/PE/PA (50:20:/30). Scale bars correspond to 500 nm. Images were taken by Gudrun Heim, Department of Structural Dynamics (Electron Microscopy), Max Planck Institute for Multidisciplinary Sciences, Göttingen.

To exclude that the observations that we made via TEM were an artefact or caused by negatively staining the liposomes, we decided use a different model membrane system to support our findings. Hence, we worked with giant unilamellar vesicles (GUVs) which are vesicles in the µm range that can be visualized by fluorescence microscopy. For the GUV assay we used fluorescently labelled lipids (rhodamine PE) and labelled the cysteine containing mutant Ups1^{A87C}/Mdm35 with Atto488 maleimide. To rule out that the mutant shows an impaired binding to liposomes due to its conjugation to a fluorescent dye, we first performed a control flotation with the Atto488 labelled mutant and liposomes containing PC/PE/PA/Rhod-PE (60.5:24:15:0.5) (Figure 4.24). Here, we could confirm that 70 % of Atto488 labelled Ups1^{A87C} was found preferably in the bound fraction of the SDS gel, indicating that its binding properties were not negatively affected by the modification.

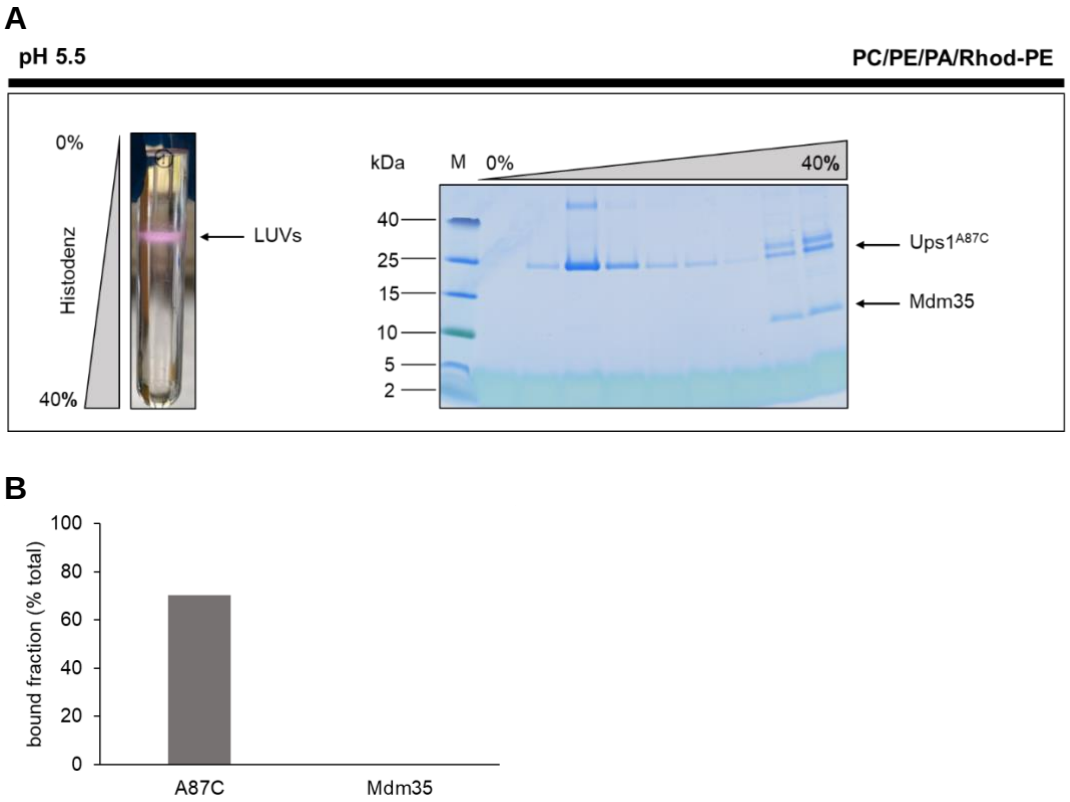

Figure 4.24: Co-migration assay for the Atto488 labelled mutant Ups1^{A87C}/Mdm35 with LUVs.

Co-migration assay of the Atto488 labelled mutant Ups1^{A87C}/Mdm35 with 200 nm LUVs composed of PC/PE/PA/Rhod-PE (60.5:24:15:0.5). For the assay the protein was incubated with LUVs for 30 min at RT and pH 5.5. After incubation samples were separated in a Histodenz gradient by ultracentrifugation. Image of the tube after ultracentrifugation is shown in the figure. Nine fractions were taken and analysed via SDS-PAGE and Colloidal Coomassie Stain. Spectra^{TM} Multicolor Low Range Protein Ladder was used a protein standard marker "M" (A). Quantification of the bound fraction (% total) for each of the proteins seen on the SDS-Gels (B).

Now that a successful binding of the mutant Ups1^{A87C}/Mdm35 to LUVs was verified in the flotation, we performed a GUV assay under same conditions. For this purpose, we incubated PC/PE/PA/Rhod-PE containing GUVs with the labelled mutant Ups1^{A87C}/Mdm35 and used confocal microscopy for visualisation (Figure 4.25). Interestingly, we could observe that the GUVs showed strong clustering and membrane tethering in the presence of the protein. Further, we found that the protein was almost exclusively binding at membrane contact sites.

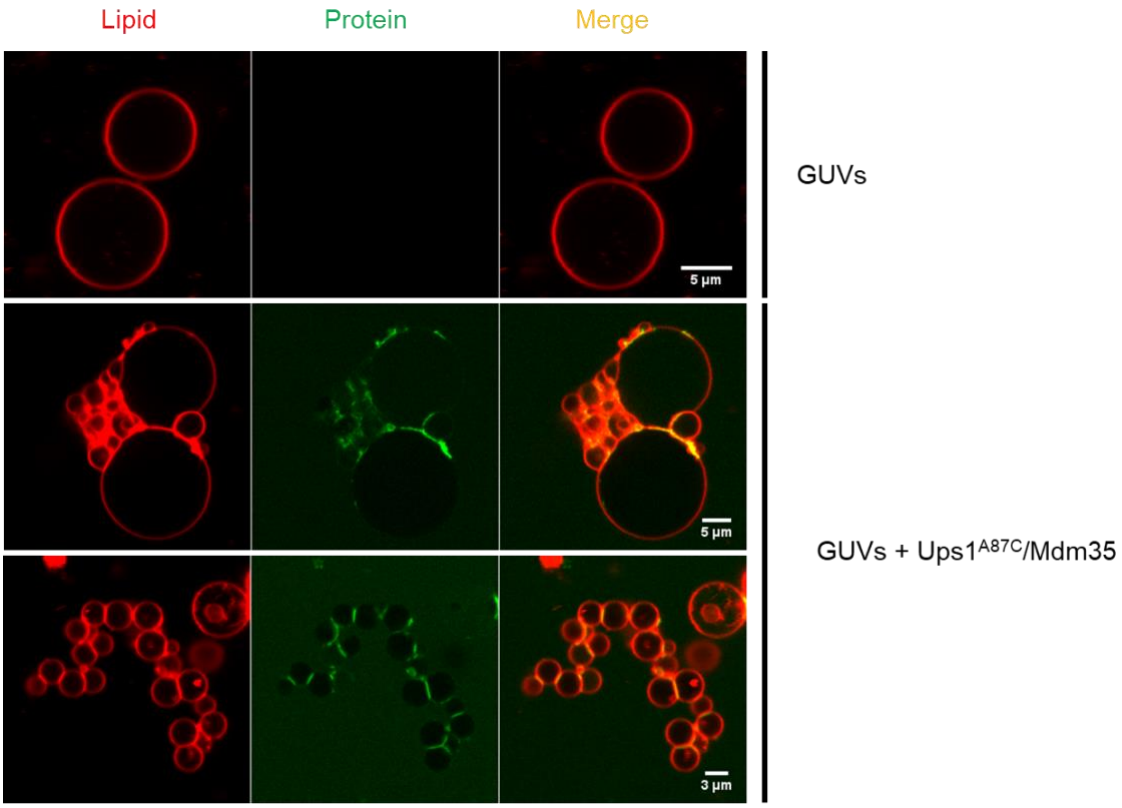

Figure 4.25: Ups1^{A87C}/Mdm35 causes strong clustering of GUVs and is found predominantly at membrane contact sites.

The Atto488 labelled mutant Ups1^{A87C}/Mdm35 was incubated with rhodamine-PE containing GUVs composed of PC/PE/PA/Rhod-PE (60.5:24:15:0.5). Confocal microscopy images of GUV in the absence and presence of the protein show strong clustering of GUVs after incubation with the protein. Furthermore, binding of the protein can be predominantly observed at membrane contact sites. Scale bars correspond to 5µm and 3µm, respectively.

4.7 The Ups1/Mdm35 forms oligomeric complexes

Our previous TEM and GUV studies successfully confirmed that membranes of artificial vesicles were strongly tethered and showed high degree of clustering in the presence of the Ups1/Mdm35 complex. Further, we observed that protein was enriched at these membrane contact sites. This gave rise to the question as to how a single protein complex can tether and bridge membranes when it only has one membrane binding site. We hypothesized, that oligomerization of the protein might be one possible explanation for this observation, since oligomerization of the LTP would provide several binding sites, which in turn could lead to crosslinking of the membrane vesicles. Besides that, in crystallographic studies two Ups1/Mdm35 complexes were found in the asymmetric unit whereas the two Ups1 proteins formed a so-called domain-swapped dimer (Watanabe et al., 2015).

In the next step, we performed a blue native PAGE (BN-PAGE) to see if recombinant Ups1/Mdm35 forms higher molecular complexes in its native state. Our results of the BN-PAGE indeed suggested the presence of several higher molecular bands on the gel (indicated in green arrows) (Figure 4.26, A) which were successfully confirmed through western blot analysis with an anti-His antibody (Figure 4.26, B).

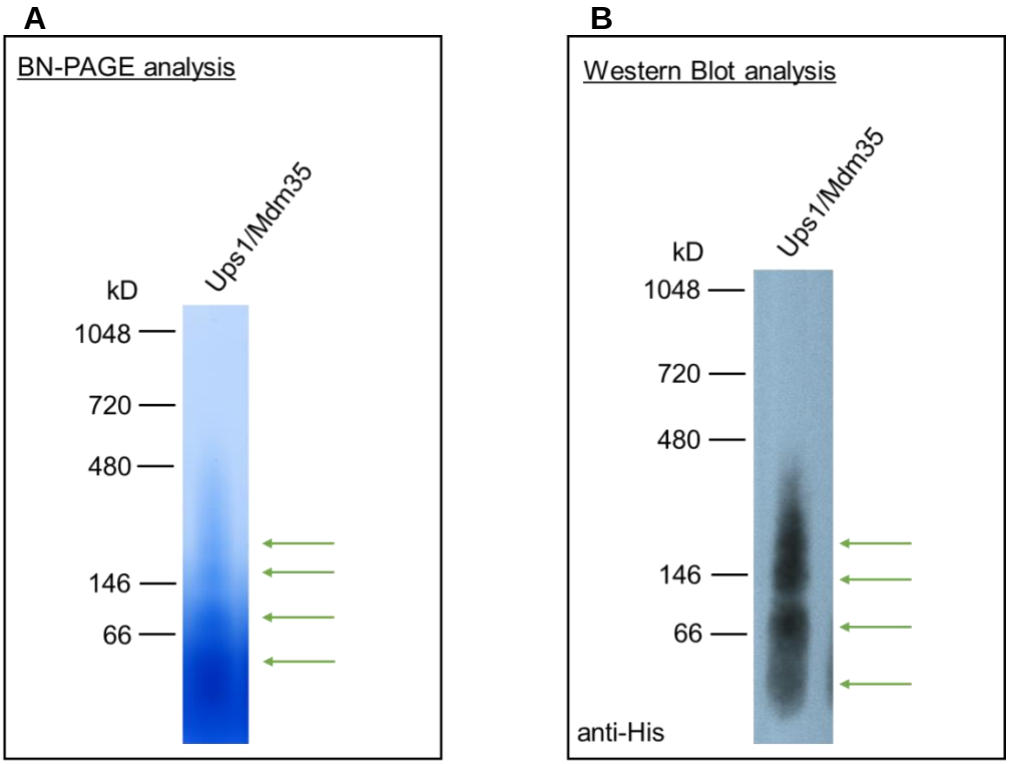

Figure 4.26: Oligomerization of Ups1/Mdm35.

Recombinantly expressed and purified Ups1/Mdm35 complex was loaded on a blue native gel and analysed through BN-PAGE and Colloidal Coomassie Stain (A). Protein signals were further confirmed and detected via western blot analysis with an anti-His antibody (B). Green arrows in both panels indicate higher molecular protein complexes. NativeMark Unstained Protein Standard was used as a protein standard Marker.

5 Discussion

Mitochondria comprise of two membranes, each, with a characteristic structure and lipid composition. In order to maintain membrane structure and integrity, lipids need to be exchanged between the two membranes through the aqueous IMS. Recently, a mitochondrial LTP complex named Ups1/Mdm35 was found in the IMS shuttling PA from the OMM to the IMM in yeast (Connerth et al., 2012). Transfer of PA to the IMM is crucial for the synthesis of CL which is restricted to mitochondria and takes place via an enzyme cascade on the matrix site of the IMM (M. Schlame & Haldar, 1993; Schlame & Ren, 2009). Though, the structure and function of the Ups1/Mdm35 has been extensively discussed and investigated, little is known about its complete molecular mechanism of action (Lu et al., 2020; Watanabe et al., 2015; Yu et al., 2015). What are the biophysical parameters for its affinity to membrane lipids? How does the Ups1/Mdm35 complex decrease the energy barrier to extract a lipid from a membrane and how does it accelerate this energetically unfavourable process? These are some of the unanswered questions in this field. In this study, we addressed these questions by conducting several *in vitro* assays based on biochemical and biophysical characterization in a combination with *in silico* approaches. Our study unravelled an unexpected role of the Ups1/Mdm35 complex as a membrane curvature inducer and sensor. Besides its curvature inducing and sensing ability, Ups1/mdm35 was found to tether membranes *in vitro*. Moreover, we could successfully show oligomerization of Ups1/Mdm35 in this study.

5.1 Characterization of Ups1/Mdm35 mediated lipid transfer and membrane binding

In yeast *S.cerevisiae*, the intrinsically unstable protein Ups1 forms a complex with Mdm35 in the IMS (Potting et al., 2010; Tamura et al., 2010). Complex formation protects Ups1 against degradation by the i-AAA protease Yme1 as well as the metallopeptidase Atp23 (Potting et al., 2010). Consequently, recombinantly expressed Ups1 in *E.coli* was found to aggregate while only a co-expression with Mdm35 resulted in a successful purification (Connerth et al., 2012). Hence, we co-expressed and purified Ups1/Mdm35 to homogeneity according to previously

published protocols (Connerth et al., 2012). In an *in vitro* Ups1/Mdm35 mediated lipid transfer assay with the recombinant protein complex, we could successfully confirm that Ups1/Mdm35 is a PA-specific LTP. However, in our *in vitro* system, the transfer activity of Ups1/Mdm35 for PA was much lower compared to previously obtained data (Connerth et al., 2012). One possible explanation for a lower transfer activity of Ups1/Mdm35 in our system might be that CL was shown to inhibit the transfer of PA when present in acceptor membranes at concentrations (10-20%) mimicking the IMM. Further, the Ups1/Mdm35 mediated lipid transfer was reported to be regulated by a negative feedback mechanism (Connerth et al., 2012). In yeast, high CL concentrations in the IMM were even suggested to cause an accumulation of the unstable Ups1 at the membrane making it prone to degradation by Yme1 (Connerth et al., 2012; Potting et al., 2010).

In this study, we performed the lipid transfer assay for Ups1/Mdm35 at pH 7.4 under unphysiological conditions. In human mitochondrial IMS, the presence of proton pumping respiratory chain complexes (I, III, IV) residing in the IMM account for a physiological pH of 6.88 which is lower than in the cytosol (Porcelli et al., 2005; Santo-Domingo & Demaurex, 2012). In yeast, the Ups1/Mdm35 complex is localized in the IMS. In order to investigate the binding properties of the Ups1/Mdm35 complex in a pH-dependent manner *in vitro*, we performed a pH-dependent co-migration assay with liposomes containing PC/PE/CL/PA (55:20:10:15). We titrated the pH range to find the transition state in which the protein changes between its bound and non-bound state to liposomes. We observed strongest binding for Ups1 at pH 5.5 and lowest at pH 7.4, confirming previously shown data (Connerth et al., 2012). Besides that, we found the transition from binding to unbinding between pH 6.5 and pH 7.0 which is in the range of the physiological pH of the IMS. In previous studies by Watanabe et al., binding of Ups1 was shown at pH 6.5 to liposomes containing PC/CL (80:20) only, while even no binding to LUVs composed of PC/PA (80:20) was reported. Thus, the authors suggested, that membrane binding of Ups1 at physiological pH depended on CL rather than on PA (Watanabe et al., 2015). Here in our studies, we found somewhat contradicting results, since we decided to use liposomes containing both lipids, PA and CL, in order to mimic the physiological inner mitochondrial membrane composition.

In our study, we detected binding of Mdm35 at pH 5.6, pH 6.0 and pH 6.5 but not at higher pH values. Since Mdm35 was previously reported to not bind to lipids at all but to dissociate from Ups1 upon binding to membranes, the amounts of Mdm35 in the bound fractions in our assay might represent Mdm35 which was still bound to Ups1 in a complex (Connerth et al., 2012). Recently, a similar pH-dependent assay was provided by Lu et al., who performed a co-sedimentation instead of a co-migration assay (Lu et al., 2020). Nevertheless, it has to be noted that the authors conducted their assay in the absence of CL. Thus, the lipid composition is distinct from our work which makes it hard to compare the results.

As limited biophysical parameters of the Ups1/Mdm35 membrane interactions are available, we performed RIfS measurements in a collaboration with the group of Prof. Andreas Janshoff. We aimed to determine, the dissociation (affinity) constant K_D of Ups1/Mdm35 for membranes composed of PC/PE/CL/PA (55:20:10:15) at various pH values. In general, our results showed similarly strong binding affinities at all pH values ranging from pH 5.5 to pH 7.0, while no binding was observed at pH 7.4. We obtained smallest K_D at pH 7.0 which might represent a pH at which non-complexed Ups1 shows highest affinity for membranes. This pH is also closest to the physiological state found in the IMS of human mitochondria (pH 6.88) (Porcelli et al., 2005; Santo-Domingo & Demaurex, 2012). Therefore, we can suggest that pH 7.0 might play and important role in the membrane binding affinity of the Ups1/Mdm35 complex. However, when comparing our RIfS measurements with our pH-dependent flotation assay data, we see that our results are somewhat contradictory, since in the flotation assay we observed strongest binding of the Ups1/Mdm35 complex to membranes at pH 5.5, whereas binding at pH 7.0 was even much weaker. This could be explained by the fact that we were working with two different membrane systems, on one hand with flat supported membranes and on the other hand with artificial membrane vesicles, that might have had an influence on the membrane binding properties of the Ups1/Mdm35 complex.

We also measured and compared values of the optical thickness (*OT*) at corresponding pH values. Strikingly, when we compared the values for the *OT* with our data from the pH-dependent flotation assays, we remarked and confirmed a clear relation of the *OT* to the amount of proteins bound to the membrane. When more protein (Ups1 or Mdm35) were found bound to the membrane, it resulted in higher values of the *OT* in the RIfS measurements.

In this study, we also analysed the previously described mutant Ups1^{L62AW65A} which was characterized by a decreased transfer activity due to its double mutation in the Ω-loop (Miliara et al., 2015). We successfully purified recombinantly co-expressed Ups1^{L62AW65A}/Mdm35 according to previously mentioned protocols (Connerth et al., 2012; Miliara et al., 2015) In our co-migration assay with LUVs containing PC/PE/CL/PA (55:20:10:15), the mutant Ups1^{L62AW65A} showed a similar binding profile to membranes like wild type Ups1. Here again, we found less amounts of Mdm35 binding to membranes in our experiments. In our RIfS measurements we further confirmed that both protein complexes Ups1/Mdm35 and Ups1^{L62AW65A}/Mdm35 had same binding affinity to membranes, since both shared almost the same K_D values. However, our results are somewhat distinct from previously obtained data where Ups1^{L62AW65A} was found almost exclusively binding to LUVs in a flotation assay whereas Mdm35 did not bind to membranes at all (Miliara et al., 2015). It has to be mentioned as well, that the authors (Miliara et al., 2015) performed their assay in the absence of CL, which reduces the binding properties of the protein. The higher amounts of bound Mdm35 in our flotation assay, here especially for the mutant, might also explain the differences in the *OT* that we observed for both protein complexes, where we found a higher *OT* for the mutant compared to the wild type. We explain this by the assumption that in the case of the mutant more of the protein complex might have bound to the membrane.

Previously, Ups1 was shown to bind preferably to negatively charged lipids such as CL, PA or PS. whereas no binding to neutral lipids like PE and PC was detected (Connerth et al., 2012). One observation that we made at an early stage of our study was that the addition of CL, which carries two negative charges, drastically increased membrane binding of Ups1 up to almost 100 % in our flotation assays. In comparison to CL, the lipids PA and PS have only one negative charge. Additionally, binding of Ups1/Mdm35 to PA or PS containing membranes was previously shown to be lower compared to CL containing LUVs in a flotation assay when same mol-% of these lipids were used (Connerth et al., 2012). Work by Watanabe et al., further confirmed that Ups1/Mdm35 preferably binds to CL-containing membranes (Watanabe et al., 2015). To test if the stronger binding of Ups1/Mdm35 to CL containing membranes is caused by a lipid specific or charge-dependent effect, we performed charge-dependent flotation assays with LUVs

composed of different negatively charged lipids. Strongest binding of Ups1 was obtained when LUVs contained 15% CL. When we performed a same flotation assay in the absence of CL and replaced LUVs with 15 % PA and 15 % PS, respectively, we observed a drastic decrease in binding of Ups1. We further found small amounts of Mdm35 bound to membranes which might indicate the complexed, not yet dissociated, form of the LTP. Interestingly, when we adjusted the net charge of LUVs to that of 15 % CL containing LUVs by using 30% PA or 30% PS instead, we obtained a strong increase in the binding of Ups1. Further, we were able to completely abolish binding of Mdm35 under these conditions. Hence, we can propose these conditions to be a state where Ups1 is binding exclusively in a non-complexed form to membranes. Overall, our data suggests that Ups1/Mdm35 indeed binds in a charge-dependent manner to negatively charged membranes. However, it has to be mentioned as well that despite increasing binding to membranes that mimic the net charge of CL containing LUVs, we were not able to maximize their binding up to almost 90 % to 100 % to reach same levels like for CL-containing LUVs. This might cause the impression that binding of Ups1/Mdm35 might not only be charge but also lipid (CL) specific. Nevertheless, previous data showed, that the conical shaped CL senses negative (concave) curvature in a buckled membrane (Elías-Wolff et al., 2019) or in the negatively curved inner leaflet of a nanotube (Beltrán-Heredia et al., 2019). When working with liposomes, we would expect a decrease in the net surface charge on these vesicles since CL might be preferably enriched in the inner leaflet (negatively curved, concave region) of the LUVs which then arises the question of how the addition of CL in LUVs can increase membrane binding for Ups1/Mdm35? Therefore, further, investigations need to be done to find out why the Ups1/Mdm35 complex preferably binds to CL containing membranes. Besides that, RIfS measurements with 30 % PA or 30 % PS containing membranes are also planned for the future to mimic the net charge of 15 % CL containing membranes and to compare the binding constants.

5.2 The Ups1/Mdm35 complex has membrane curvature inducing and sensing properties

In previous studies the structure and function of the Ups1/Mdm35 complex was extensively investigated (Watanabe et al., 2015; Yu et al., 2015). It was further revealed that the Ups1/Mdm35 complex is structurally but not on a sequence level similar to the so called START domain (Watanabe et al., 2015) which is present in several LTPs like the phosphatidylinositol transfer protein PITPα (Tilley et al., 2004; Yoder et al., 2001) and the ceramide transport protein CERT (Kudo et al., 2008). In general, the START domain is characterized by a pocket that can accommodate a lipid and a flexible Ω-loop that possesses the role of a lid (Alpy & Tomasetto, 2005). These structural elements were also found and described for Ups1/Mdm35 (Watanabe et al., 2015; Yu et al., 2015). Furthermore, similar to other START domain containing proteins, the Ω-loop in Ups1 is also involved in the lipid transfer activity. A, recent study (Lu et al., 2020) provided greater insight into the mechanism of the Ups1/Mdm35 complex by introducing a model, which shows that the Ω-loop, L2-loop and α3-helix of Ups1 together create a membrane binding interphase. After binding of the complex to the membrane through this membrane binding interphase, Mdm35 dissociates from the complex. Next, the Ω-loop of Ups1 undergoes conformational changes leading to an insertion of W65 and F69 (both residing in the Ω-loop) into the membrane which enables anchoring of Ups1, followed by a PA extraction. After extraction of PA, the Mdm35 re-assembles with Ups1 resulting in a release from the membrane (Lu et al., 2020).

Despite these studies regarding the molecular mechanism of Ups1/Mdm35 mediated membrane binding and lipid transfer, we still wondered how the Ups1/Mdm35 complex decreases the energy barrier to accelerate the extraction of a lipid from a membrane for its transfer through the aqueous IMS compartment? To address this question, we hypothesized that the structural information about the hydrophobic Ω-loop of Ups1/Mdm35 and its insertion into the membrane might already give a hint for its involvement in membrane curvature induction. In other words, the hydrophobic insertion is one possible mechanism that was described for membrane curvature induction where an amphipathic helix or a hydrophobic loop of a protein insert as a wedge into one monolayer of a membrane leading to

a perturbation in the lipid packing that can result in membrane bending (McMahon & Boucrot, 2015; McMahon & Gallop, 2005).

Hence, we suggested that the hydrophobic Ω-loop of Ups1 also inserts into the membrane, hereby creating membrane stress through packing defects that might induce positive membrane curvature. Consequently, the positively curved membrane might provide an energetically favourable condition for lipid extraction. In order to address and confirm this hypothesis, we visualized the morphology of LUVs after incubation with Ups1/Mdm35 through TEM and interestingly observed that the Ups1/Mdm35 complex is indeed able to deform spherical vesicles into tubulated membranes. However, it has to be mentioned here that we used a high protein concentration for our TEM measurements and thus we cannot rule out that the tubulation we observed were also due to or even enhanced by a protein crowding mechanism (Stachowiak et al., 2012). Protein crowding is another mechanism for membrane curvature induction which is mediated by a high local density of protein attached to the membrane that can cause protein collisions and lateral pressure which result in membrane bending (Stachowiak et al., 2013).

Besides membrane curvature induction, membrane curvature sensing has gained more and more attention in the last decade. Theoretically, both mechanisms rely on a synergy model where membrane curvature induction is defined as the deformation of the membrane through a local enrichment of curvature sensing molecules and membrane curvature sensing is defined by the membrane binding affinity of a molecule that depends on the curvature (Baumgart et al., 2011). However, while a clear-cut differentiation of both mechanisms is thus hard to define (Antonny, 2011). For example some amphipathic helices in proteins that contain the so-called ALPS (Amphipathic Lipid Packing Sensor) motifs were found to not induce but rather sense curvature on a membrane (Stachowiak et al., 2013). ALPS motifs were found to sense lipid packing defects in a membrane through their bulky hydrophobic residues. Further ALPS motifs were found to adsorb preferably onto positively curved membranes (Bigay et al., 2003; Drin et al., 2007).

In previous studies a sterol-binding LTP found in yeast, namely Kes1p (or Osh4p) showed structurally a close homology to the previously mentioned START domain (Im et al., 2005). Kes1p carries an α-helix at its N-terminus that acts as a lid to its lipid binding pocket. Interestingly, the lid in Kes1p was further found to function as an ALPS motif that senses membrane curvature (Drin et al., 2007).

To confirm our hypothesis that the Ups1/Mdm35 complex also acts as a curvature sensing LTP, we collaborated with the group of Prof. Dr. Herre Jelger Risselada. Through an *in silico* approach using MD simulations in combination with an umbrella sampling according to a previously published protocol (Stroh & Risselada, 2021) we were able to successfully verify that the Ups1/Mdm35 complex senses positively curved regions on a simulated buckled membrane. In contrast, the Ups1/Mdm35 complex avoided negatively curved regions.

In the following, we hypothesized that the desorption of PA from a positively curved region on the buckled membrane might be energetically favourable over the desorption of PA from regions of zero and negative curvature, which we successfully confirmed *in silico* on a simulated buckled membrane in the absence of any protein. We support our findings by the following explanation, due to its conical shape PA will preferably induce negative curvature on a membrane or localize to negatively curved membrane regions (Thakur et al., 2019). Therefore, extraction of PA might be energetically unfavourable from regions of negative membrane curvature. On the contrary, at positively curved regions, PA desorption might go along with lower energy costs.

Overall, we found an unexpected and novel role of the Ups1/Mdm35 complex as a sensor for positively curved membranes. Further, our results suggest, that the desorption of PA by the Ups1/Mdm35 complex might also occur preferably at positively curved membranes. In order to provide an *in vitro* assay to confirm our results that we observed *in silico*, we performed co-migration assays with the Ups1/Mdm35 complex using liposomes with small and large intrinsic curvature to verify that Ups1/Mdm35 is a curvature sensing LTP. Indeed, we could successfully show that Ups1 preferably bound to liposomes of smaller size and higher intrinsic curvature compared to liposomes of bigger size and lower intrinsic curvature. Moreover, we observed that addition of CL in our liposomes already maximised the binding ability of Ups1 to LUVs. We explain this by the following scenario, that for an enhanced electrostatic interaction of the protein with the membrane, the curvature sensing activity is masked.

Since, Mdm35 hardly bound to liposomes and did not show any curvature sensing ability in our size-dependent flotation assays, we suggest that curvature sensing is exclusively mediated by Ups1. Here, we hypothesized that the curvature sensing ability might be attributed to the Ω-loop of Ups1. Hence, we tested the mutant

Ups1^{L62AW65A}/Mdm35 and confirmed that the double mutation indeed impaired its curvature sensing ability.

All in all, we describe the Ups1/Mdm35 mediated lipid transfer via the following model. The Ups1/Mdm35 complex senses packing defects at positively curved regions on a membrane through its hydrophobic Ω-loop (Figure 5.1). After dissociation of Mdm35, Ups1 inserts into the membrane through hydrophobic residues in the Ω-loop. Hydrophobic membrane insertion might even enhance membrane curvature at these regions accelerating the extraction of PA under low energy costs. Moreover, we conclude from our results that the curvature sensing ability of Ups1 strongly depends on an interplay between specific lipid compositions as well as curvature of the membrane. Conclusively, our study gives a novel insight into the mechanism of the LTP complex Ups1/Mdm35.

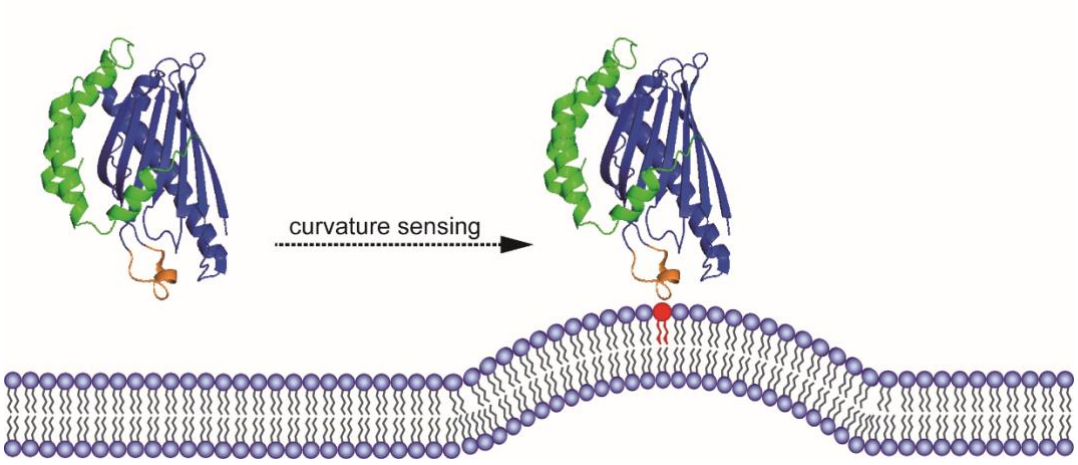

Figure 5.1: Schematic illustration of the membrane curvature sensing of Ups1/Mdm35.

Ups1 (blue) with its Ω-loop (yellow) in a complex with Mdm35 (green). The Ω-loop in Ups1 senses for positively curved regions on a membrane with packing defects. PA is shown in red. The Ups1/Mdm35 complex structure was designed with the PyMOL Version 2.3.1 using the PDB 4XHR by (Yu et al., 2015).

In our study, we provided a possible *in vitro* assay to investigate the curvature sensing ability of the Ups1/Mdm35 complex. Another interesting and different method to analyse curvature sensing of a protein can be obtained by using a GUV which can be attached to a micropipette. Through an optical tweezer a membrane nanotube can be extracted from the GUV while the micropipette can control the tension of the GUV. After addition of the protein in solution, curvature sensing can

be visualized via fluorescence microscopy (Roux et al., 2010). Such experiments for the Ups1/Mdm35 complex must be performed in the future to confirm our findings.

5.3 The Ups1/Mdm35 complex tethers membranes of vesicles by protein oligomerization

In previous studies it was reported that mitochondria of Δ*ups1* showed strong accumulation of PA at membrane contact sites between the OMM and IMM leading to the suggestion that Ups1/Mdm35 mediated lipid transfer of PA occurred most likely at membrane contact sites (Connerth et al., 2012). These contact sites in mitochondria are characterized by an enrichment of negatively charged lipids such as CL (Simbeni et al., 1991) which at the same time might ensure the recruitment of the Ups1/Mdm35 to these regions (Connerth et al., 2012; Scharwey et al., 2013). One interesting observation that we made at a very early stage of our study was that incubation of Ups1/Mdm35 with LUVs led to strong clustering of vesicles which we visualized in our electron micrographs. Strikingly, when we changed our model membrane systems and used GUVs instead, we could obtain similar results that confirmed our findings. Moreover, we found the protein enriched at membrane contact sites in our GUV assays. How is it possible that Ups1/Mdm35 tethers membranes and forms membrane contact sites when it basically contains one membrane binding surface? We had the hypothesis that protein oligomerization might be one possible explanation for our observations. Conclusively, protein oligomerization would provide more binding sites and enable membrane crosslinking.

Previous structural analysis studies by Watanabe et al., showed that the asymmetric unit of the crystal was composed of two Ups1/Mdm35 molecules that had similar conformations while two Ups1 molecules were found to adopt a domain-swapped dimer conformation. The domain-swapped dimer of Ups1 was initially believed to be a crystallization artefact (Watanabe et al., 2015). Interestingly, it was previously reported that this conformation was characterized by a wider opening of the phospholipid binding cavity. Therefore, it cannot be ruled

out that such a dimer of the complex might be an intermediate state that has simply not been found yet in the IMS of mitochondria (Miliara & Matthews, 2016).

We wanted to investigate if our Ups1/Mdm35 meditated membrane tethering and contact site formation results might be due to protein oligomerization. Consequently, we performed a BN-PAGE where we could successfully confirm that Ups1/Mdm35 indeed formed higher molecular complexes. However, in our studies, the western blot after BN-PAGE was only conducted with an antibody against the His-tagged Ups1. Thus, an immunodetection with an antibody against Mdm35 is planned for the future. Moreover, further investigations have to be done to find out about the composition of these complexes (dimer, trimer etc.) and also whether these were only Ups1 homo-oligomers or if Mdm35 was involved (hetero-oligomers). Additionally, we do not know yet which part of the amino acid sequence of Ups1/Mdm35 might promote protein-protein interaction leading to this oligomerization. In order to further investigate and confirm oligomerization of Ups1/Mdm35, we planned to perform FRET (förster resonance energy transfer) measurements in the future.

Interestingly, in some of our flotation assays we detected a protein band at the size of more than 40 kDa on the SDS gels. We suggest that this might correspond in size to a homo-oligomer of two Ups1 molecules. However, in order to verify this observation, we have planned a mass spectrometry as well as a western blot analysis and immunodetection for the future. Overall, our results showed that the tethering abilities of the Ups1/Mdm35 complex are most probably attributed to protein oligomerization.

Lastly, when considering our previously obtained data in these studies showing that Ups1/Mdm35 is a membrane curvature sensor and inducer, the question arises as to how membrane curvature sensing and oligomerization are related to the Ups1/Mdm35 mediated mechanism. In previous studies, oligomerization was shown for other membrane curvature inducing proteins like Mic10, an integral membrane protein which is a core subunit of the MICOS complex (Barbot et al., 2015) or the BAR domain which is a banana-shaped dimer that can induce and sense membrane curvature (Peter et al., 2004). Nevertheless, how the membrane tethering and contact site formation of Ups1/Mdm35 is linked to its role as an LTP and as a curvature sensor remains elusive.

6 Summary and Conclusion

Despite various structural and functional analysis studies of the Ups1/Mdm35 complex, the complete molecular mechanism of action remains elusive.

In this study, we used different *in vitro* assays based on biochemical and biophysical approaches to characterize the binding properties of the Ups1/Mdm35 complex in a pH- and charge-dependent manner. We also determined binding constants for the affinity of the Ups1/Mdm35 complex to artificial supported membranes at different pH values.

In order to confirm our hypothesis that the Ups1/Mdm35 complex possesses membrane curvature inducing abilities we performed electron microscopy studies. Here, we successfully visualized that the Ups1/Mdm35 complex is indeed able to induce membrane curvature by bending artificial membrane vesicles into tubulated shapes *in vitro*. We suggest that the membrane bending ability of the Ups1/Mdm35 complex is allocated to the hydrophobic Ω-loop that might insert as a wedge into the membrane by a combination of a hydrophobic insertion and a protein crowding mechanism.

We further investigated the role of the Ups1/Mdm35 complex to act as a membrane curvature sensor. We confirmed this using molecular dynamics simulations. Here, we discovered that the Ups1/Mdm35 complex indeed senses positively curved regions on a buckled membrane *in silico*. In an *in vitro* flotation assay using artificial membrane vesicles with various intrinsic curvatures, we successfully confirmed that Ups1 but not Mdm35 preferably binds to highly curved liposomes. Moreover, our results strongly suggest that curvature sensing of Ups1 is exclusively attributed to its hydrophobic Ω-loop, since mutations in this lid impaired the sensing ability *in vitro*.

Overall, this study unravels the molecular mechanism of the Ups1/Mdm35 complex as an LTP displaying an unexpected role in membrane curvature induction and sensing. We propose that the hydrophobic Ω-loop of Usp1 not only induces membrane curvature but also senses lipid packing defects in positively curved membranes that might promote and accelerate the extraction of lipids under low energy costs.

In this study, we further discovered that the Ups1/Mdm35 complex tethers artificial membranes of vesicles into clusters which we visualized via electron and

fluorescence microscopy. Additionally, we observed an enrichment of the LTP at membrane contacts sites *in vitro* which led to our hypothesis that the Ups1/Mdm35 complex might form oligomers which we confirmed by blue native PAGE. This would explain its ability to bridge membranes *in vitro*. However, further investigations are planned for the future to find the actual sequence motifs in promoting protein oligomerization *in vitro*. Moreover, it remains elusive how the Ups1/Mdm35 mediated contact site formation and membrane bridging abilities are linked to its role as an LTP.

7 Bibliography

Aaltonen, M. J., Friedman, J. R., Osman, C., Salin, B., di Rago, J. P., Nunnari, J., Langer, T., & Tatsuta, T. (2016). MIC OS and phospholipid transfer by Ups2-Mdm35 organize membrane lipid synthesis in mitochondria. *Journal of Cell Biology*, *213*(5), 525–534. https://doi.org/10.1083/jcb.201602007

AhYoung, A. P., Jiang, J., Zhang, J., Dang, X. K., Loo, J. A., Zhou, Z. H., & Egea, P. F. (2015). Conserved SMP domains of the ERMES complex bind phospholipids and mediate tether assembly. *Proceedings of the National Academy of Sciences of the United States of America*, *112*(25), E3179–E3188. https://doi.org/10.1073/pnas.1422363112

Alpy, F., & Tomasetto, C. (2005). Give lipids a START: The StAR-related lipid transfer (START) domain in mammals. *Journal of Cell Science*, *118*(13), 2791–2801. https://doi.org/10.1242/jcs.02485

Antonny, B. (2011). Mechanisms of membrane curvature sensing. *Annual Review of Biochemistry*, *80*, 101–123. https://doi.org/10.1146/annurev-biochem-052809-155121

Ardail, D., Lerme, F., & Louisot, P. (1991). Involvement of contact sites in phosphatidylserine import into liver mitochondria. *Journal of Biological Chemistry*, *266*(13), 7978–7981. https://doi.org/10.1016/s0021-9258(18)92926-1

Athenstaedt, K. (2021). Phosphatidic acid biosynthesis in the model organism yeast Saccharomyces cerevisiae - a survey. *Biochimica et Biophysica Acta - Molecular and Cell Biology of Lipids*, *1866*(6), 158907. https://doi.org/10.1016/j.bbalip.2021.158907

Athenstaedt, K., & Daum, G. (1999). Phosphatidic acid, a key intermediate in lipid metabolism. *European Journal of Biochemistry*, *266*(1), 1–16. https://doi.org/10.1046/j.1432-1327.1999.00822.x

Athenstaedt, K., & Daum, G. (2000). 1-Acyldihydroxyacetone-phosphate reductase (Ayr1p) of the yeast Saccharomyces cerevisiae encoded by the open reading frame YIL124w is a major component of lipid particles. *Journal of Biological Chemistry*, *275*(1), 235–240. https://doi.org/10.1074/jbc.275.1.235

Athenstaedt, K., Weys, S., Paltauf, F., & Daum, G. (1999). Redundant systems of

phosphatidic acid biosynthesis via acylation of glycerol-3-phosphate or dihydroxyacetone phosphate in the yeast Saccharomyces cerevisiae. *Journal of Bacteriology*, *181*(5), 1458–1463. https://doi.org/10.1128/jb.181.5.1458-1463.1999

Backes, S., & Herrmann, J. M. (2017). Protein translocation into the intermembrane space and matrix of mitochondria: Mechanisms and driving forces. *Frontiers in Molecular Biosciences*, *4*(DEC), 1–11. https://doi.org/10.3389/fmolb.2017.00083

Barbot, M., Jans, D. C., Schulz, C., Denkert, N., Kroppen, B., Hoppert, M., Jakobs, S., & Meinecke, M. (2015). Mic10 Oligomerizes to Bend Mitochondrial Inner Membranes at Cristae Junctions. *Cell Metabolism*, *21*(5), 756–763. https://doi.org/10.1016/j.cmet.2015.04.006

Bassereau, P., Sorre, B., & Lévy, A. (2014). Bending lipid membranes: Experiments after W. Helfrich's model. *Advances in Colloid and Interface Science*, *208*, 47–57. https://doi.org/10.1016/j.cis.2014.02.002

Baumgart, T., Capraro, B. R., Zhu, C., & Das, S. L. (2011). Thermodynamics and Mechanics of Membrane Curvature Generation and Sensing by Proteins and Lipids. *Annual Review of Physical Chemistry*, *62*, 483–506. https://doi.org/10.1146/annurev.physchem.012809.103450.Thermodynamics

Beltrán-Heredia, E., Tsai, F. C., Salinas-Almaguer, S., Cao, F. J., Bassereau, P., & Monroy, F. (2019). Membrane curvature induces cardiolipin sorting. *Communications Biology*, *2*(1), 1–7. https://doi.org/10.1038/s42003-019-0471-x

Benghezal, M., Roubaty, C., Veepuri, V., Knudsen, J., & Conzelmann, A. (2007). SLC1 and SLC4 encode partially redundant acyl-coenzyme A 1-acylglycerol-3-phosphate O-acyltransferases of budding yeast. *Journal of Biological Chemistry*, *282*(42), 30845–30855. https://doi.org/10.1074/jbc.M702719200

Bennett, C. H. (1976). Efficient estimation of free energy differences from Monte Carlo data. *Journal of Computational Physics*, *22*(2), 245–268. https://doi.org/10.1016/0021-9991(76)90078-4

Beranek, A., Rechberger, G., Knauer, H., Wolinski, H., Kohlwein, S. D., & Leber, R. (2009). Identification of a cardiolipin-specific phospholipase encoded by the gene CLD1 (YGR110W) in yeast. *Journal of Biological Chemistry*, *284*(17), 11572–11578. https://doi.org/10.1074/jbc.M805511200

Bigay, J., Gounon, P., Roblneau, S., & Antonny, B. (2003). Lipid packing sensed by ArfGAP1 couples COPI coat disassembly to membrane bilayer curvature. *Nature*, *426*(6966), 563–566. https://doi.org/10.1038/nature02108

Bishop, W. R., & Bell, R. M. (1988). Assembly of phospholipids into cellular membranes: Biosynthesis, transmembrane movement and intracellular translocation. *Annual Review of Cell Biology*, *4*, 579–610. https://doi.org/10.1146/annurev.cb.04.110188.003051

Chabanon, M., Stachowiak, J. C., & Rangamani, P. (2017). Systems biology of cellular membranes: a convergence with biophysics. *Wiley Interdisciplinary Reviews: Systems Biology and Medicine*, *9*(5), 20–22. https://doi.org/10.1002/wsbm.1386

Chacinska, A., Koehler, C. M., Milenkovic, D., Lithgow, T., & Pfanner, N. (2009). Importing Mitochondrial Proteins: Machineries and Mechanisms. *Cell*, *138*(4), 628–644. https://doi.org/10.1016/j.cell.2009.08.005

Chang, S. C., Heacock, P. N., Clancey, C. J., & Dowhan, W. (1998). The PEL1 gene (renamed PGS1) encodes the phosphatidylglycerophosphate synthase of Saccharomyces cerevisiae. *Journal of Biological Chemistry*, *273*(16), 9829–9836. https://doi.org/10.1074/jbc.273.16.9829

Chang, S. C., Heacock, P. N., Mileykovskaya, E., Voelker, D. R., & Dowhan, W. (1998). Isolation and characterization of the gene (CLS1) encoding cardiolipin synthase in Saccharomyces cerevisiae. *Journal of Biological Chemistry*, *273*(24), 14933–14941. https://doi.org/10.1074/jbc.273.24.14933

Chen, Q., Kazachkov, M., Zheng, Z., & Zou, J. (2007). The yeast acylglycerol acyltransferase LCA1 is a key component of Lands cycle for phosphatidylcholine turnover. *FEBS Letters*, *581*(28), 5511–5516. https://doi.org/10.1016/j.febslet.2007.10.061

Connerth, M., Tatsuta, T., Haag, M., Klecker, T., Westermann, B., & Langer, T. (2012). Intramitochondrial transport of phosphatidic acid in yeast by a lipid transfer protein. *Science*, *338*(6108), 815–818. https://doi.org/10.1126/science.1225625

Cullis, P. R., Hope, M. J., & Tilcock, C. P. S. (1979). Lipid polymorphism and the roles of lipids in membranes. *Biochim Biophys Acta.*, *559*(4), 399–420. https://doi.org/10.1016/0304-4157(79)90012-1

Daum, G. (1985). Lipids of mitochondria. *BBA - Reviews on Biomembranes*,

822(1), 1–42. https://doi.org/10.1016/0304-4157(85)90002-4

Daum, G., & Vance, J. E. (1997). Import of lipids into mitochondria. *Progress in Lipid Research*, *36*(2–3), 103–130. https://doi.org/10.1016/S0163-7827(97)00006-4

Dee, C. T., & Moffat, K. G. (2005). A novel family of mitochondrial proteins is represented by the Drosophila genes slmo, preli-like and real-time. *Development Genes and Evolution*, *215*(5), 248–254. https://doi.org/10.1007/s00427-005-0470-4

Dimmer, K. S., Fritz, S., Fuchs, F., Messerschmitt, M., Weinbach, N., Neupert, W., & Westermann, B. (2002). Genetic basis of mitochondrial function and morphology in Saccharomyces cerevisiae. *Molecular Biology of the Cell*, *13*(3), 847–853. https://doi.org/10.1091/mbc.01-12-0588

Dowhan, W. (1997). Molecular basis for membrane phospholipid diversity: Why are there so many lipids? *Annual Review of Biochemistry*, *66*, 199–232. https://doi.org/10.1146/annurev.biochem.66.1.199

Drin, G., Casella, J. F., Gautier, R., Boehmer, T., Schwartz, T. U., & Antonny, B. (2007). A general amphipathic α-helical motif for sensing membrane curvature. *Nature Structural and Molecular Biology*, *14*(2), 138–146. https://doi.org/10.1038/nsmb1194

Elías-Wolff, F., LindénSweden., M., Lyubartsev, A. P., & Brandt, E. G. (2019). Curvature sensing by cardiolipin in simulated buckled membranes. *Soft Matter*, *15*(4), 792–802. https://doi.org/10.1039/c8sm02133c

Endo, T., & Yamano, K. (2009). Multiple pathways for mitochondrial protein traffic. *Biological Chemistry*, *390*(8), 723–730. https://doi.org/10.1515/BC.2009.087

Flis, V. V, & Daum, G. (2013). Lipid Transport between the Endoplasmic. *Cold Spring Harb Perspect Biol*, *5*(6), 1–22.

Gabriel, K., Milenkovic, D., Chacinska, A., Müller, J., Guiard, B., Pfanner, N., & Meisinger, C. (2007). Novel Mitochondrial Intermembrane Space Proteins as Substrates of the MIA Import Pathway. *Journal of Molecular Biology*, *365*(3), 612–620. https://doi.org/10.1016/j.jmb.2006.10.038

Gaigg, B., Simbeni, R., Hrastnik, C., Paltauf, F., & Daum, G. (1995). Characterization of a microsomal subfraction associated with. *Biochimica et Biophysica Acta*, *1234*, 214–220.

Gebert, N., Joshi, A. S., Kutik, S., Becker, T., Guan, X. L., Mooga, V. P., Stroud,

D. A., Kulkarni, G., Wenk, R., Rehling, P., Meisinger, C., Ryan, M. T., Wiedemann, N., Greenberg, L., & Pfanner, N. (2009). Mitochondrial cardiolipin involved in outer membrane protein biogenesis: implications for Barth syndro. *Current Biology*, *19*(24), 2133–2139. https://doi.org/10.1016/j.cub.2009.10.074.Mitochondrial

Genge, M. G., & Mokranjac, D. (2022). Coordinated Translocation of Presequence-Containing Precursor Proteins Across Two Mitochondrial Membranes: Knowns and Unknowns of How TOM and TIM23 Complexes Cooperate With Each Other. *Frontiers in Physiology*, *12*(January). https://doi.org/10.3389/fphys.2021.806426

Gu, Z., Valianpour, F., Chen, S., Vaz, F. M., Hakkaart, G. A., Wanders, R. J. A., & Greenberg, M. L. (2004). Aberrant cardiolipin metabolism in the yeast taz1 mutant: A model for Barth syndrome. *Molecular Microbiology*, *51*(1), 149–158. https://doi.org/10.1046/j.1365-2958.2003.03802.x

Hackenbrock, B. Y. C. R. (1968). CHEMICAL AND PHYSICAL FIXATION OF ISOLATED MITOCHONDRIA IN LOW-ENERGY AND HIGH-ENERGY STATES. *Proc Natl Acad Sci U S A*, *61*(2), 598–605.

Harner, M., Körner, C., Walther, D., Mokranjac, D., Kaesmacher, J., Welsch, U., Griffith, J., Mann, M., Reggiori, F., & Neupert, W. (2011). The mitochondrial contact site complex, a determinant of mitochondrial architecture. *EMBO Journal*, *30*(21), 4356–4370. https://doi.org/10.1038/emboj.2011.379

Helfrich, W. (1973). Elastic properties of lipid bilayers: Theory and Possible Experiments / Helfrich_1973.pdf. *Zeitschrift Für Naturforschung C*, 693–703. https://www.degruyter.com/view/j/znc.1973.28.issue-11-12/znc-1973-11-1209/znc-1973-11-1209.xml

Herrmann, J. M., & Riemer, J. (2012). Mitochondrial disulfide relay: Redox-regulated protein import into the intermembrane space. *Journal of Biological Chemistry*, *287*(7), 4426–4433. https://doi.org/10.1074/jbc.R111.270678

Holthuis, J. C. M., & Levine, T. P. (2005). Lipid traffic: Floppy drives and a superhighway. *Nature Reviews Molecular Cell Biology*, *6*(3), 209–220. https://doi.org/10.1038/nrm1591

Holthuis, J. C. M., & Menon, A. K. (2014). Lipid landscapes and pipelines in membrane homeostasis. *Nature*, *510*(7503), 48–57. https://doi.org/10.1038/nature13474

Hoppins, S., Collins, S. R., Cassidy-Stone, A., Hummel, E., DeVay, R. M., Lackner, L. L., Westermann, B., Schuldiner, M., Weissman, J. S., & Nunnari, J. (2011). A mitochondrial-focused genetic interaction map reveals a scaffold-like complex required for inner membrane organization in mitochondria. *Journal of Cell Biology*, *195*(2), 323–340. https://doi.org/10.1083/jcb.201107053

Horvath, S. E., & Daum, G. (2013). Lipids of mitochondria. *Progress in Lipid Research*, *52*(4), 590–614. https://doi.org/10.1016/j.plipres.2013.07.002

Hovius, R., Lambrechts, H., Nicolay, K., & de Kruijff, B. (1990). Improved methods to isolate and subfractionate rat liver mitochondria. Lipid composition of the inner and outer membrane. *BBA - Biomembranes*, *1021*(2), 217–226. https://doi.org/10.1016/0005-2736(90)90036-N

Im, Y. J., Raychaudhuri, S., Prinz, W. A., & Hurley, J. H. (2005). Structural mechanism for sterol sensing and transport by OSBP-related proteins. *Nature*, *437*(7055), 154–158.

Israelachvili, J. N., Mitchell, D. J., & Ninham, B. W. (1977). Theory of self-assembly of lipid bilayers and vesicles. *BBA - Biomembranes*, *470*(2), 185–201. https://doi.org/10.1016/0005-2736(77)90099-2

Jain, S., Stanford, N. T., Bhagwat, N., Seiler, B., Costanzo, M., Boone, C., & Oelkers, P. (2007). Identification of a novel lysophospholipid acyltransferase in Saccharomyces cerevisiae. *Journal of Biological Chemistry*, *282*(42), 30562–30569. https://doi.org/10.1074/jbc.M706326200

Jarsch, I. K., Daste, F., & Gallop, J. L. (2016). Membrane curvature in cell biology: An integration of molecular mechanisms. *Journal of Cell Biology*, *214*(4), 375–387. https://doi.org/10.1083/jcb.201604003

Jensen, R. E., & Dunn, C. D. (2002). Protein import into and across the mitochondrial inner membrane: Role of the TIM23 and TIM22 translocons. *Biochimica et Biophysica Acta - Molecular Cell Research*, *1592*(1), 25–34. https://doi.org/10.1016/S0167-4889(02)00261-6

Jeong, H., Park, J., & Lee, C. (2016). Crystal structure of Mdm12 reveals the architecture and dynamic organization of the ERMES complex . *EMBO Reports*, *17*(12), 1857–1871. https://doi.org/10.15252/embr.201642706

Jiang, F., Rizavi, H. S., & Greenberg, M. L. (1997). Cardiolipin is not essential for the growth of Saccharomyces cerevisiae on fermentable or non-fermentable carbon sources. *Molecular Microbiology*, *26*(3), 481–491.

https://doi.org/10.1046/j.1365-2958.1997.5841950.x

John, G., Shang, Y., Li, L., Renken, C., Mannella, C., Selker, J., Rangell, L., Bennett, M., & Zha, J. (2005). The Mitochondrial Inner Membrane Protein Mitofilin Controls Cristae Morphology. *Mol Biol Cell*, *15*(December), 5318–5328. https://doi.org/10.1091/mbc.E04

Kawano, S., Tamura, Y., Kojima, R., Bala, S., Asai, E., Michel, A. H., Kornmann, B., Riezman, I., Riezman, H., Sakae, Y., Okamoto, Y., & Endo, T. (2018). Structure-function insights into direct lipid transfer between membranes by Mmm 1-Mdm 12 of ERMES. *Journal of Cell Biology*, *217*(3), 959–974. https://doi.org/10.1083/jcb.201704119

Kay, J. G., & Grinstein, S. (2011). Sensing phosphatidylserine in cellular membranes. *Sensors*, *11*(2), 1744–1755. https://doi.org/10.3390/s110201744

Kopec, K. O., Alva, V., & Lupas, A. N. (2010). Homology of SMP domains to the TULIP superfamily of lipid-binding proteins provides a structural basis for lipid exchange between ER and mitochondria. *Bioinformatics*, *26*(16), 1927–1931. https://doi.org/10.1093/bioinformatics/btq326

Kornmann, B., Currie, E., Collins, S. R., Schuldiner, M., Nunnari, J., Weissman, J. S., & Walter, P. (2009). An ER-mitochondria tethering complex revealed by a synthetic biology screen. *Science*, *325*(5939), 477–481. https://doi.org/10.1126/science.1175088

Kornmann, B., Osman, C., & Walter, P. (2011). The conserved GTPase Gem1 regulates endoplasmic reticulum-mitochondria connections. *Proceedings of the National Academy of Sciences of the United States of America*, *108*(34), 14151–14156. https://doi.org/10.1073/pnas.1111314108

Kuchler, K., Daum, G., & Paltauf, F. (1986). Subcellular and submitochondrial localization of phospholipid-synthesizing enzyme in Saccharomyces cerevisiae. *Journal of Bacteriology*, *165*(3), 901–910. https://doi.org/10.1128/jb.165.3.901-910.1986

Kudo, N., Kumagai, K., Tomishige, N., Yamaji, T., Wakatsuki, S., Nishijima, M., Hanada, K., & Kato, R. (2008). Structural basis for specific lipid recognition by CERT responsible for nonvesicular trafficking of ceramide. *Proceedings of the National Academy of Sciences of the United States of America*, *105*(2), 488–493. https://doi.org/10.1073/pnas.0709191105

Kuroda, T., Tani, M., Moriguchi, A., Tokunaga, S., Higuchi, T., Kitada, S., & Kuge,

O. (2011). FMP30 is required for the maintenance of a normal cardiolipin level and mitochondrial morphology in the absence of mitochondrial phosphatidylethanolamine synthesis. *Molecular Microbiology*, *80*(1), 248–265. https://doi.org/10.1111/j.1365-2958.2011.07569.x

Kutik, S., Rissler, M., Guan, X. L., Guiard, B., Shui, G., Gebert, N., Heacock, P. N., Rehling, P., Dowhan, W., Wenk, M. R., Pfanner, N., & Wiedemann, N. (2008). The translocator maintenance protein Tam41 is required for mitochondrial cardiolipin biosynthesis. *Journal of Cell Biology*, *183*(7), 1213–1221. https://doi.org/10.1083/jcb.200806048

Lev, S. (2010). Non-vesicular lipid transport by lipid-transfer proteins and beyond. *Nature Reviews Molecular Cell Biology*, *11*(10), 739–750. https://doi.org/10.1038/nrm2971

Longen, S., Bien, M., Bihlmaier, K., Kloeppel, C., Kauff, F., Hammermeister, M., Westermann, B., Herrmann, J. M., & Riemer, J. (2009). Systematic Analysis of the Twin Cx9C Protein Family. *Journal of Molecular Biology*, *393*(2), 356–368. https://doi.org/10.1016/j.jmb.2009.08.041

Lu, J., Chan, C., Yu, L., Fan, J., Sun, F., & Zhai, Y. (2020). Molecular mechanism of mitochondrial phosphatidate transfer by Ups1. *Communications Biology*, *3*(1). https://doi.org/10.1038/s42003-020-01121-x

McMahon, H. T., & Boucrot, E. (2015). Membrane curvature at a glance. *Journal of Cell Science*, *128*(6), 1065–1070. https://doi.org/10.1242/jcs.114454

McMahon, H. T., & Gallop, J. L. (2005). Membrane curvature and mechanisms of dynamic cell membrane remodelling. *Nature*, *438*, 590–596.

Merkel, O., Schmid, P. C., Paltauf, F., & Schmid, H. H. O. (2005). Presence and potential signaling function of N-acylethanolamines and their phospholipid precursors in the yeast Saccharomyces cerevisiae. *Biochimica et Biophysica Acta - Molecular and Cell Biology of Lipids*, *1734*(3), 215–219. https://doi.org/10.1016/j.bbalip.2005.03.004

Mesmin, B., Drin, G., Levi, S., Rawet, M., Cassel, D., Bigay, J., & Antonny, B. (2007). Two lipid-packing sensor motifs contribute to the sensitivity of ArfGAP1 to membrane curvature. *Biochemistry*, *46*(7), 1779–1790. https://doi.org/10.1021/bi062288w

Miliara, X., Garnett, J. A., Tatsuta, T., Abid Ali, F., Baldie, H., Pérez-Dorado, I., Simpson, P., Yague, E., Langer, T., & Matthews, S. (2015). Structural insight

into the TRIAP 1/ PRELI -like domain family of mitochondrial phospholipid transfer complexes . *EMBO Reports*, *16*(7), 824–835. https://doi.org/10.15252/embr.201540229

Miliara, X., & Matthews, S. (2016). Structural comparison of yeast and human intra-mitochondrial lipid transport systems. *Biochemical Society Transactions*, *44*(2), 479–485. https://doi.org/10.1042/BST20150264

Miquel, M., & Browse, J. (1992). Arabidopsis mutants deficient in polyunsaturated fatty acid synthesis: Biochemical and genetic characterization of a plant oleoyl-phosphatidylcholine desaturase. *Journal of Biological Chemistry*, *267*(3), 1502–1509. https://doi.org/10.1016/s0021-9258(18)45974-1

Miyata, N., Goda, N., Matsuo, K., Hoketsu, T., & Kuge, O. (2017). Cooperative function of Fmp30, Mdm31, and Mdm32 in Ups1-independent cardiolipin accumulation in the yeast Saccharomyces cerevisiae. *Scientific Reports*, *7*(1), 1–12. https://doi.org/10.1038/s41598-017-16661-2

Miyata, N., & Kuge, O. (2018). Fmp30, Mdm31, and Mdm32 Function in Ups1-Independent Cardiolipin Accumulation Under Low Phosphatidylethanolamine Conditions. *Contact*, *1*, 251525641876404. https://doi.org/10.1177/2515256418764043

Miyata, N., Watanabe, Y., Tamura, Y., Endo, T., & Kuge, O. (2016). Phosphatidylserine transport by Ups2-Mdm35 in respiration-active mitochondria. *Journal of Cell Biology*, *214*(1), 77–88. https://doi.org/10.1083/jcb.201601082

Nagiec, M. M., Wells, G. B., Lester, R. L., & Dickson, R. C. (1993). A suppressor gene that enables Saccharomyces cerevisiae to grow without making sphingolipids encodes a protein that resembles an Escherichia coli fatty acyl-transferase. *Journal of Biological Chemistry*, *268*(29), 22156–22163. https://doi.org/10.1016/s0021-9258(20)80661-9

Nakai, M., Takada, T., & Endo, T. (1993). Cloning of the YAP19 gene encoding a putative yeast homolog of AP19, the mammalian small chain of the clathrin-assembly proteins. *BBA - Gene Structure and Expression*, *1174*(3), 282–284. https://doi.org/10.1016/0167-4781(93)90198-M

Nguyen, T. T., Lewandowska, A., Choi, J. Y., Markgraf, D. F., Junker, M., Bilgin, M., Ejsing, C. S., Voelker, D. R., Rapoport, T. A., & Shaw, J. M. (2012). Gem1 and ERMES Do Not Directly Affect Phosphatidylserine Transport from ER to

Mitochondria or Mitochondrial Inheritance. *Traffic*, *13*(6), 880–890. https://doi.org/10.1111/j.1600-0854.2012.01352.x

Ohlendieck, K., Riesinger, I., Adams, V., Krause, J., & Brdiczka, D. (1986). Enrichment and biochemical characterization of boundary membrane contact sites from rat-liver mitochondria. *Biochimica et Biophysica Acta*, *860*, 672–689.

Osman, C., Haag, M., Potting, C., Rodenfels, J., Dip, P. V., Wieland, F. T., Brügger, B., Westermann, B., & Langer, T. (2009). The genetic interactome of prohibitins: Coordinated control of cardiolipin and phosphatidylethanolamine by conserved regulators in mitochondria. *Journal of Cell Biology*, *184*(4), 583–596. https://doi.org/10.1083/jcb.200810189

Osman, C., Voelker, D. R., & Langer, T. (2011). Making heads or tails of phospholipids in mitochondria. *Journal of Cell Biology*, *192*(1), 7–16. https://doi.org/10.1083/jcb.201006159

Palade, G. (1975). of the Process of Protein Synthesis. *Science*, 347–358.

Pangborn, M. C. (1942). Isolation and Purification of a Serologically Active Phospholipid From Beef Heart. *Journal of Biological Chemistry*, *143*(1), 247–256. https://doi.org/10.1016/s0021-9258(18)72683-5

Peretti, D., Kim, S. H., Tufi, R., & Lev, S. (2020). Lipid Transfer Proteins and Membrane Contact Sites in Human Cancer. *Frontiers in Cell and Developmental Biology*, *7*(January), 1–14. https://doi.org/10.3389/fcell.2019.00371

Peter, B. J., Kent, H. M., Mills, I. G., Vallis, Y., Butler, P. J. G., Evans, P. R., & McMahon, H. T. (2004). BAR Domains as Sensors of Membrane Curvature: The Amphiphysin BAR Structure. *Science*, *303*(5657), 495–499. https://doi.org/10.1126/science.1092586

Pfanner, N., van der Laan, M., Amati, P., Capaldi, R. A., Caudy, A. A., Chacinska, A., Darshi, M., Deckers, M., Hoppins, S., Icho, T., Jakobs, S., Ji, J., Kozjak-Pavlovic, V., Meisinger, C., Odgren, P. R., Park, S. K., Rehling, P., Reichert, A. S., Sheikh, M. S., … Nunnari, J. (2014). Uniform nomenclature for the mitochondrial contact site and cristae organizing system. *Journal of Cell Biology*, *204*(7), 1083–1086. https://doi.org/10.1083/jcb.201401006

Pinot, M., Vanni, S., Pagnotta, S., Lacas-Gervais, S., Payet, L. A., Ferreira, T., Gautier, R., Goud, B., Antonny, B., & Barelli, H. (2014). Polyunsaturated

phospholipids facilitate membrane deformation and fission by endocytic proteins. *Science*, *345*(6197), 693–697. https://doi.org/10.1126/science.1255288

Pomorski, T. G., Nylander, T., & Cárdenas, M. (2014). Model cell membranes: Discerning lipid and protein contributions in shaping the cell. *Advances in Colloid and Interface Science*, *205*, 207–220. https://doi.org/10.1016/j.cis.2013.10.028

Porcelli, A. M., Ghelli, A., Zanna, C., Pinton, P., Rizzuto, R., & Rugolo, M. (2005). pH difference across the outer mitochondrial membrane measured with a green fluorescent protein mutant. *Biochemical and Biophysical Research Communications*, *326*(4), 799–804. https://doi.org/10.1016/j.bbrc.2004.11.105

Potting, C., Tatsuta, T., König, T., Haag, M., Wai, T., Aaltonen, M. J., & Langer, T. (2013). TRIAP1/PRELI complexes prevent apoptosis by mediating intramitochondrial transport of phosphatidic acid. *Cell Metabolism*, *18*(2), 287–295. https://doi.org/10.1016/j.cmet.2013.07.008

Potting, C., Wilmes, C., Engmann, T., Osman, C., & Langer, T. (2010). Regulation of mitochondrial phospholipids by Ups1/PRELI-like proteins depends on proteolysis and Mdm35. *EMBO Journal*, *29*(17), 2888–2898. https://doi.org/10.1038/emboj.2010.169

Racenis, P. V., Lai, J. L., Das, A. K., Mullick, P. C., Hajra, A. K., & Greenberg, M. L. (1992). The acyl dihydroxyacetone phosphate pathway enzymes for glycerolipid biosynthesis are present in the yeast Saccharomyces cerevisiae. *Journal of Bacteriology*, *174*(17), 5702–5710. https://doi.org/10.1128/jb.174.17.5702-5710.1992

Riekhof, W. R., Wu, J., Jones, J. L., & Voelker, D. R. (2007). Identification and characterization of the major lysophosphatidylethanolamine acyltransferase in Saccharomyces cerevisiae. *Journal of Biological Chemistry*, *282*(39), 28344–28352. https://doi.org/10.1074/jbc.M705256200

Roux, A., Koster, G., Lenz, M., Sorre, B., Manneville, J. B., Nassoy, P., & Bassereau, P. (2010). Membrane curvature controls dynamin polymerization. *Proceedings of the National Academy of Sciences of the United States of America*, *107*(9), 4141–4146. https://doi.org/10.1073/pnas.0913734107

Santo-Domingo, J., & Demaurex, N. (2012). Perspectives on: SGP Symposium on

Mitochondrial Physiology and Medicine: The renaissance of mitochondrial pH. *Journal of General Physiology*, *139*(6), 415–423. https://doi.org/10.1085/jgp.201110767

Scharwey, M., Tatsuta, T., & Langer, T. (2013). Mitochondrial lipid transport at a glance. *Journal of Cell Science*, *126*(23), 5317–5323. https://doi.org/10.1242/jcs.134130

Schlame, M., & Haldar, D. (1993). Cardiolipin is synthesized on the matrix side of the inner membrane in rat liver mitochondria. *Journal of Biological Chemistry*, *268*(1), 74–79. https://doi.org/10.1016/s0021-9258(18)54116-8

Schlame, Michael. (2008). Cardiolipin synthesis for the assembly of bacterial and mitochondrial membranes. *Journal of Lipid Research*, *49*(8), 1607–1620. https://doi.org/10.1194/jlr.R700018-JLR200

Schlame, Michael, Brody, S., & Hostetler, K. Y. (1993). Mitochondrial cardiolipin in diverse eukaryotes: Comparison of biosynthetic reactions and molecular acyl species. *European Journal of Biochemistry*, *212*(3), 727–733. https://doi.org/10.1111/j.1432-1033.1993.tb17711.x

Schlame, Michael, & Greenberg, M. L. (2017). Biosynthesis, remodeling and turnover of mitochondrial cardiolipin. *Biochim Biophys Acta Mol Cell Biol*, *1862*(1), 3–7. https://doi.org/10.1016/j.bbalip.2016.08.010.Biosynthesis

Schlame, Michael, & Ren, M. (2009). The role of cardiolipin in the structural organization of mitochondrial membranes. *Biochimica et Biophysica Acta - Biomembranes*, *1788*(10), 2080–2083. https://doi.org/10.1016/j.bbamem.2009.04.019

Schlame, Michael, Rua, D., & Greenberg, M. L. (2000). The biosynthesis and functional role of cardiolipin. *Progress in Lipid Research*, *39*(3), 257–288. https://doi.org/10.1016/S0163-7827(00)00005-9

Sesaki, H., Dunn, C. D., Iijima, M., Shepard, K. A., Yaffe, M. P., Machamer, C. E., & Jensen, R. E. (2006). Ups1p, a conserved intermembrane space protein, regulates mitochondrial shape and alternative topogenesis of Mgm1p. *Journal of Cell Biology*, *173*(5), 651–658. https://doi.org/10.1083/jcb.200603092

Sheetz, M. P., & Singer, S. J. (1974). Biological membranes as bilayer couples. A molecular mechanism of drug erythrocyte interactions. *Proceedings of the National Academy of Sciences of the United States of America*, *71*(11), 4457–4461. https://doi.org/10.1073/pnas.71.11.4457

Shen, H., Heacock, P. N., Clancey, C. J., & Dowhan, W. (1996). The CDS1 gene encoding CDP-diacylglycerol synthase in Saccharomyces cerevisiae is essential for cell growth. *Journal of Biological Chemistry*, *271*(2), 789–795. https://doi.org/10.1074/jbc.271.2.789

Shen, Z., Ye, C., McCain, K., & Greenberg, M. L. (2015). The Role of Cardiolipin in Cardiovascular Health. *BioMed Research International*, *2015*. https://doi.org/10.1155/2015/891707

Shibata, Y., Hu, J., Kozlov, M. M., & Rapoport, T. A. (2009). Mechanisms shaping the membranes of cellular organelles. *Annual Review of Cell and Developmental Biology*, *25*, 329–354. https://doi.org/10.1146/annurev.cellbio.042308.113324

Simbeni, R., Pon, L., Zinser, E., Paltauf, F., & Daum, G. (1991). Mitochondrial membrane contact sites of yeast: Characterization of lipid components and possible involvement in intramitochondrial translocation of phospholipids. *Journal of Biological Chemistry*, *266*(16), 10047–10049. https://doi.org/10.1016/s0021-9258(18)99184-2

Sleight, R. G. (1987). Intracellular lipid transport in eukaryotes. *Annual Review of Physiology*, *Vol. 49*(c), 193–208. https://doi.org/10.1146/annurev.ph.49.030187.001205

Soccio, R. E., & Breslow, J. L. (2003). StAR-related lipid transfer (START) proteins: Mediators of intracellular lipid metabolism. *Journal of Biological Chemistry*, *278*(25), 22183–22186. https://doi.org/10.1074/jbc.R300003200

Stachowiak, J. C., Brodsky, F. M., & Miller, E. A. (2013). A cost-benefit analysis of the physical mechanisms of membrane curvature. *Nature Cell Biology*, *15*(9), 1019-. https://doi.org/10.1038/ncb2832.A

Stachowiak, J. C., Schmid, E. M., Ryan, C. J., Ann, H. S., Sasaki, D. Y., Sherman, M. B., Geissler, P. L., Fletcher, D. A., & Hayden, C. C. (2012). Membrane bending by protein-protein crowding. *Nature Cell Biology*, *14*(9), 944–949. https://doi.org/10.1038/ncb2561

Stenmark, H. (2009). Rab GTPases as coordinators of vesicle traffic. *Nature Reviews Molecular Cell Biology*, *10*(8), 513–525. https://doi.org/10.1038/nrm2728

Stephan, M., Kramer, C., Steinem, C., & Janshoff, A. (2014). Binding assay for low molecular weight analytes based on reflectometry of absorbing molecules in

porous substrates. *Analyst*, *139*(8), 1987–1992. https://doi.org/10.1039/c4an00009a

Stroh, K. S., & Risselada, H. J. (2021). Quantifying Membrane Curvature Sensing of Peripheral Proteins by Simulated Buckling and Umbrella Sampling. *Journal of Chemical Theory and Computation*, *17*(8), 5276–5286. https://doi.org/10.1021/acs.jctc.1c00021

Stroud, D. A., Oeljeklaus, S., Wiese, S., Bohnert, M., Lewandrowski, U., Sickmann, A., Guiard, B., Van Der Laan, M., Warscheid, B., & Wiedemann, N. (2011). Composition and topology of the endoplasmic reticulum-mitochondria encounter structure. *Journal of Molecular Biology*, *413*(4), 743–750. https://doi.org/10.1016/j.jmb.2011.09.012

Tamaki, H., Shimada, A., Ito, Y., Ohya, M., Takase, J., Miyashita, M., Miyagawa, H., Nozaki, H., Nakayama, R., & Kumagai, H. (2007). LPT1 encodes a membrane-bound O-acyltransferase involved in the acylation of lysophospholipids in the yeast Saccharomyces cerevisiae. *Journal of Biological Chemistry*, *282*(47), 34288–34298. https://doi.org/10.1074/jbc.M704509200

Tamura, Y., Endo, T., Iijima, M., & Sesaki, H. (2009). Ups1p and Ups2p antagonistically regulate cardiolipin metabolism in mitochondria. *Journal of Cell Biology*, *185*(6), 1029–1045. https://doi.org/10.1083/jcb.200812018

Tamura, Y., Harada, Y., Nishikawa, S. I., Yamano, K., Kamiya, M., Shiota, T., Kuroda, T., Kuge, O., Sesaki, H., Imai, K., Tomii, K., & Endo, T. (2013). Tam41 is a CDP-diacylglycerol synthase required for cardiolipin biosynthesis in mitochondria. *Cell Metabolism*, *17*(5), 709–718. https://doi.org/10.1016/j.cmet.2013.03.018.Tam41

Tamura, Y., Harada, Y., Yamano, K., Watanabe, K., Ishikawa, D., Ohshima, C., Nishikawa, S. I., Yamamoto, H., & Endo, T. (2006). Identification of Tam41 maintaining integrity of the TIM23 protein translocator complex in mitochondria. *Journal of Cell Biology*, *174*(5), 631–637. https://doi.org/10.1083/jcb.200603087

Tamura, Y., Iijima, M., & Sesaki, H. (2010). Mdm35p imports Ups proteins into the mitochondrial intermembrane space by functional complex formation. *EMBO Journal*, *29*(17), 2875–2887. https://doi.org/10.1038/emboj.2010.149

Tamura, Y., Sesaki, H., & Endo, T. (2014). Phospholipid transport via mitochondria.

Traffic, *15*(9), 933–945. https://doi.org/10.1111/tra.12188

Tarasenko, D., & Meinecke, M. (2021). Protein-dependent membrane remodeling in mitochondrial morphology and clathrin-mediated endocytosis. *European Biophysics Journal*, *50*(2), 295–306. https://doi.org/10.1007/s00249-021-01501-z

Tatsuta, T., Scharwey, M., & Langer, T. (2014). Mitochondrial lipid trafficking. *Trends in Cell Biology*, *24*(1), 44–52. https://doi.org/10.1016/j.tcb.2013.07.011

Thakur, R., Naik, A., Panda, A., & Raghu, P. (2019). Regulation of membrane turnover by phosphatidic acid: Cellular functions and disease implications. *Frontiers in Cell and Developmental Biology*, *7*(JUN), 1–14. https://doi.org/10.3389/fcell.2019.00083

Tilley, S. J., Skippen, A., Murray-Rust, J., Swigart, P. M., Stewart, A., Morgan, C. P., Cockcroft, S., & McDonald, N. Q. (2004). Structure-Function Analysis of Phosphatidylinositol Transfer Protein Alpha Bound to Human Phosphatidylinositol. *Structure*, *12*(2), 317–326. https://doi.org/10.1016/j.str.2004.01.013

Tuller, G., Hrastnik, C., Achleitner, G., Schiefthaler, U., Klein, F., & Daum, G. (1998). YDL142c encodes cardiolipin synthase (Clslp) and is non-essential for aerobic growth of Saccharomyces cerevisiae. *FEBS Letters*, *421*(1), 15–18. https://doi.org/10.1016/S0014-5793(97)01525-1

Van Den Brink-Van Der Laan, E., Antoinette Killian, J., & De Kruijff, B. (2004). Nonbilayer lipids affect peripheral and integral membrane proteins via changes in the lateral pressure profile. *Biochimica et Biophysica Acta - Biomembranes*, *1666*(1–2), 275–288. https://doi.org/10.1016/j.bbamem.2004.06.010

Van Meer, G. (1989). Lipid traffic in animal cells. *Annual Review of Cell Biology*, *5*, 247–275. https://doi.org/10.1146/annurev.cb.05.110189.001335

Van Meer, Gerrit, Voelker, D. R., & Feigenson, G. W. (2008). Membrane lipids: Where they are and how they behave. *Nature Reviews Molecular Cell Biology*, *9*(2), 112–124. https://doi.org/10.1038/nrm2330

Vance, J. E. (1990). Phospholipid synthesis in a membrane fraction associated with mitochondria. *Journal of Biological Chemistry*, *265*(13), 7248–7256. https://doi.org/10.1016/s0021-9258(19)39106-9

Vanni, S., Hirose, H., Barelli, H., Antonny, B., & Gautier, R. (2014). A sub-

nanometre view of how membrane curvature and composition modulate lipid packing and protein recruitment. *Nature Communications*, *5*. https://doi.org/10.1038/ncomms5916

von der Malsburg, K., Müller, J. M., Bohnert, M., Oeljeklaus, S., Kwiatkowska, P., Becker, T., Loniewska-Lwowska, A., Wiese, S., Rao, S., Milenkovic, D., Hutu, D. P., Zerbes, R. M., Schulze-Specking, A., Meyer, H. E., Martinou, J. C., Rospert, S., Rehling, P., Meisinger, C., Veenhuis, M., … van der Laan, M. (2011). Dual Role of Mitofilin in Mitochondrial Membrane Organization and Protein Biogenesis. *Developmental Cell*, *21*(4), 694–707. https://doi.org/10.1016/j.devcel.2011.08.026

Watanabe, Y., Tamura, Y., Kawano, S., & Endo, T. (2015). Structural and mechanistic insights into phospholipid transfer by Ups1-Mdm35 in mitochondria. *Nature Communications*, *6*, 1–12. https://doi.org/10.1038/ncomms8922

White, T., Bursten, S., Federighi, D., Lewis, R. A., & Nudelman, E. (1998). High-resolution separation and quantification of neutral lipid and phospholipid species in mammalian cells and sera by multi-one-dimensional thin-layer chromatography. *Analytical Biochemistry*, *258*(1), 109–117. https://doi.org/10.1006/abio.1997.2545

Whyte, J. R. C., & Munro, S. (2002). Vesicle tethering complexes in membrane traffic. *Journal of Cell Science*, *115*(13), 2627–2637. https://doi.org/10.1242/jcs.115.13.2627

Wirtz, K. W. A., Schouten, A., & Gros, P. (2006). Phosphatidylinositol transfer proteins: From closed for transport to open for exchange. *Advances in Enzyme Regulation*, *46*(1), 301–311. https://doi.org/10.1016/j.advenzreg.2006.01.020

Wirtz, K. W., & Zilversmit, D. B. (1968). Exchange of phospholipids between liver mitochondria and microsomes in vitro. *Journal of Biological Chemistry*, *243*(13), 3596–3602. https://doi.org/10.1016/s0021-9258(19)34182-1

Yoder, M. D., Thomas, L. M., Tremblay, J. M., Oliver, R. L., Yarbrough, L. R., & Helmkamp, G. M. (2001). Structure of a multifunctional protein: Mammalian phosphatidylinositol transfer protein complexed with phosphatidylcholine. *Journal of Biological Chemistry*, *276*(12), 9246–9252. https://doi.org/10.1074/jbc.M010131200

Yu, F., He, F., Yao, H., Wang, C., Wang, J., Li, J., Qi, X., Xue, H., Ding, J., & Zhang,

P. (2015). Structural basis of intramitochondrial phosphatidic acid transport mediated by U ps1- M dm35 complex . *EMBO Reports*, *16*(7), 813–823. https://doi.org/10.15252/embr.201540137

Zheng, Z., & Zou, J. (2001). The initial step of the glycerolipid pathway: Identification of glycerol 3-phosphate/dihydroxyacetone phosphate dual substrate acyltransferases in Saccharomyces cerevisiae. *Journal of Biological Chemistry*, *276*(45), 41710–41716. https://doi.org/10.1074/jbc.M104749200

Zimmerberg, J., & Kozlov, M. M. (2006). How proteins produce cellular membrane curvature. *Nature Reviews Molecular Cell Biology*, *7*(1), 9–19. https://doi.org/10.1038/nrm1784

Zinser, E., Sperka-Gottlieb, C. D. M., Fasch, E. V., Kohlwein, S. D., Paltauf, F., & Daum, G. (1991). Phospholipid synthesis and lipid composition of subcellular membranes in the unicellular eukaryote Saccharomyces cerevisiae. *Journal of Bacteriology*, *173*(6), 2026–2034. https://doi.org/10.1128/jb.173.6.2026-2034.1991

Zinser, Erwin, & Daum, G. (1995). Isolation and biochemical characterization of organelles from the yeast, Saccharomyces cerevisiae. *Yeast*, *11*(6), 493–536. https://doi.org/10.1002/yea.320110602